CONSTRAINING THE PHYSICS OF GALAXY FORMATION AND EVOLUTION USING GALAXY CLUSTERING

By

Douglas F. Watson

Dissertation

Submitted to the Faculty of the

Graduate School of Vanderbilt University

in partial fulfillment of the requirements

for the degree of

DOCTOR OF PHILOSOPHY

in

PHYSICS

May, 2012

Nashville, Tennessee

Approved:

Dr. Andreas A. Berlind

Dr. Kelly Holley-Bockelmann

Dr. Robert J. Scherrer

Dr. Thomas J. Weiler

Dr. David A. Weintraub

Dr. Will E. Johns

DEDICATION

This thesis is dedicated to my mother and father for their unwavering support in all of my endeavors.

ACKNOWLEDGMENTS

Thank you....

First and foremost, I am thankful for the supervision of Dr. Andreas Berlind. This thesis would not be possible without your mentorship and guidance. I would also like to thank the rest of the members of my committee as they have all been crucial in my development as a scientist.

Patricia, I am forever grateful for your self-sacrifice and loving support.

My brother Drew, for being my role model, inspiration and best friend.

Cameron McBride and Andrew Zentner, I am extremely thankful for all of the vibrant science discussions and insightful advice throughout my graduate career.

To the 9th floor crew, a Ph.D. is never possible without the support and friendship of fellow graduate students.

Finally, I would like to thank my mother and father to whom this thesis is dedicated. You have always been a constant source of support and love throughout all of my pursuits in life. Thank you for being there to walk this path with me.

Table of Contents

DEDICATION ii

ACKNOWLEDGMENTS iii

LIST OF TABLES vii

LIST OF FIGURES viii

Chapter Page

I. INTRODUCTION 1

1.1. ΛCDM Cosmology & the Homogeneous Universe 3
1.2. Dark Matter & The Growth of Structure 6
1.3. Halo Formation & Mergers 8
1.3.1. The Halo Mass Function 10
1.3.2. Halo Structure 11
1.4. Connecting the Dark and Light Sectors 12
1.4.1. The Formation of Galaxies 13
1.4.2. Subhalos & Galaxies 14
1.4.3. Spatial Clustering 16
1.4.4. Galaxy Surveys 19
1.4.5. Redshift Space Distortions 21
1.4.6. Dark Matter & Galaxies on Extremely Small Scales 24

II. THE GALAXY CORRELATION FUNCTION CONSPIRACY . . . 26

2.1. Introduction 27
2.2. A Modern Restatement of the Problem in Halo Model Language 32
2.2.1. Halo Model Basics 32
2.2.2. The Battle of the 1- Halo and 2- Halo Terms 37
2.3. Overview of Halo Substructure Modeling 40
2.4. Effects of Subhalo Dynamics on the Galaxy Correlation Function 44
2.4.1. Halo Occupation Distribution Statistics 44
2.4.2. Constructing the Correlation Function 50
2.5. Mass and Redshift Dependence of the Correlation Function 54
2.5.1. Dependence on Mass 54

2.5.2. Dependence on Redshift 56
2.5.3. The Balance Between Accretion and Destruction . . 63
2.6. Achieving a Power-Law Correlation Function 66
2.7. Discussion & Primary Conclusions 79

III. CONSTRAINING SATELLITE GALAXY STELLAR MASS LOSS AND PREDICTING INTRAHALO LIGHT 86

3.1. Introduction 87
3.2. Motivation 90
3.3. The Subhalo Evolution Model 94
3.4. Models for Satellite Galaxy Stellar Mass Loss 98
3.4.1. Model 1 100
3.4.2. Model 2 105
3.5. Constraining Satellite Galaxy Stellar Mass Loss Using Galaxy Clustering 108
3.5.1. The Effect of Scatter in the Stellar-to-Halo Mass Relation 115
3.6. Luminosity Dependence of Satellite Galaxy Stellar Mass Loss 117
3.7. Predictions for Intrahalo Light at Varying Scales 120
3.8. Summary & Discussion 128

IV. MODELING THE VERY SMALL-SCALE CLUSTERING OF LUMINOUS RED GALAXIES 134

4.1. Introduction 135
4.2. Data 137
4.3. Method 139
4.3.1. The Halo Occupation Distribution 139
4.3.2. The Galaxy Number Density 141
4.3.3. The Galaxy 2-point Correlation Function 142
4.3.4. Probing the Parameter Space 144
4.4. Results 145
4.4.1. Varying $P(N|M)$ 145
4.4.2. Varying the Concentration of Satellite Galaxies . . 146
4.4.3. Varying the Density Profile 148
4.5. Discussion 152

V. THE EXTREME SMALL SCALES: DO SATELLITE GALAXIES TRACE DARK MATTER? 154

5.1. Introduction 155
5.2. Data 157

5.3. Review of the Method 160
5.3.1. The HOD and the Galaxy 2PCF 160
5.3.2. The PNM and PNMCG Models 165
5.4. Results 168
5.5. Summary & Discussion 181

VI. CONCLUSIONS 187

List of Tables

Table Page

V.1. 162

List of Figures

Figure		Page
1.1.	The Evolution of Structure Over Cosmic Time	8
1.2.	The Galaxy Correlation Function	18
1.3.	The Galaxy Distribution in Galaxy Redshift Surveys and Mock Catalogs	20
1.4.	The Correlation Function in Redshift Space	23
2.1.	The Correlation Function of Galaxies vs. Dark Matter	33
2.2.	Effects of Non-linear Dynamics on the HOD and $\xi(r)$	47
2.3.	Mass Dependence of $\xi(r)$	55
2.4.	Redshift Dependence of $\xi(r)$	58
2.5.	Departures From a Power Law	60
2.6.	The Accretion and Destruction Rate of Subhalos	64
2.7.	Exploration of the HOD Parameter Space Yielding a Power-Law $\xi(r)$ as a Function of Number Density and Redshift	69
2.8.	Exploration of the HOD Parameter Space Yielding a Power-Law $\xi(r)$ as a Function of $M_{\rm min}, M_1, M^*$ and Redshift	76
3.1.	Average Fractional Subhalo Dark Matter Mass Loss as a Function of Redshift	97
3.2.	Schematic of How Satellite Galaxy Stellar Mass Loss Occurs	99
3.3.	The Stellar-to-Halo Mass Relation	102
3.4.	Clustering Predictions for Model 1	111
3.5.	Clustering Predictions for Model 2	114
3.6.	The Effect of Scatter on the SHMR	116

3.7. The Luminosity Dependence of Satellite Galaxy Stellar Mass Loss . 118

3.8. IHL Predictions from the Extreme Cases of Model 1 121

3.9. IHL Predictions of Model 1 and Model 2 124

4.1. Model Fits to the Projected Correlation Function of LRGs 147

4.2. Allowed Density Profiles for LRG Satellite Galaxies 151

5.1. Model Fits to $w_p(r_p)$ for Luminosity Thresholds Spanning $M_r < -18$ to LRGs 166

5.2. $\xi(r)$ Residuals from an r^{-2} Power Law from the PNMCG Best-Fit Models 170

5.3. The Radial Profile of Satellite Galaxies as a Function of Luminosity 174

5.4. The Slope and Concentration of the Inner Density Profile of Satellite Galaxies as a Function of Galaxy Luminosity 175

5.5. The $\gamma - f_{\rm gal}$ Parameter Space as a Function of Luminosity 177

5.6. $M_{1/10}$: A More Physically Useful Definition of Satellite Galaxy Concentration 180

Chapter I

INTRODUCTION

Our Universe has evolved from being nearly homogeneous at a time shortly after the Big Bang to the present epoch which is permeated with complex structures. Perturbations in the matter density field of the early Universe, seeded by the enhancement of quantum fluctuations during the epoch of inflation, resulted in areas of slight over-densities of matter which coalesce via gravity. Over time, massive bound systems emerge in the form of dark matter called dark matter halos. These halos are natural sites for the baryonic structures we can observe, such as galaxies, galaxy clusters and superclusters.

While our theoretical picture of how the dark matter density field has evolved over cosmic time has progressed significantly, our understanding of how galaxies form and evolve with respect to the dark matter background remains elusive. Our observational capabilities over the last decade have advanced at an astonishing rate, transforming the field of observational cosmology into a precision science. Large-scale galaxy surveys have mapped the 3-dimensional distribution of galaxies revealing a rich and intricate organization. Making the connection between the dark and light sides of the Universe is a principal goal of astrophysical cosmology and being able to accurately map galaxies to the "dark sector" of the Universe is a vital bridge between theory

and observation.

One of the fundamental tools at the Astronomer's disposal for propelling our understanding of galaxy formation is *galaxy clustering*. Galaxy clustering describes the spatial distribution of galaxies. Measuring how galaxies cluster has given us a window into the cosmic evolution of our Universe. It can be used to probe a broad range of physical phenomena on vast cosmological scales. On scales of individual galaxy clusters and smaller, on the order of a few Mpc, galaxy clustering probes the manner in which galaxies interact and merge, and allows us to investigate complex physical processes (Masjedi et al., 2006; Watson et al., 2010, 2011a). On intermediate scales, $\sim 0.5 - 50$Mpc, galaxy clustering can be used primarily to investigate the relationship between galaxies and the dark matter density field (Zehavi et al., 2005a). On the very largest scales, $\gtrsim 100$Mpc, clustering can be used to constrain cosmological parameters (Tegmark et al., 2004; Eisenstein et al., 2005; Percival et al., 2009; Reid et al., 2009) and to test fundamental properties of the Universe, such as flatness (Eisenstein et al., 2005) and homogeneity (Hogg et al., 2005).

Using theoretical approaches driven by recent observational results, the scope of this work is to explore ways to constrain fundamental physics pertaining to galaxy formation in a cosmological context by using galaxy clustering.

1.1 ΛCDM Cosmology & the Homogeneous Universe

There is now an established concordance cosmological model known as ΛCDM. It is dictated by two components pertaining to the dark sector of the Universe: Cold Dark Matter (CDM), a yet-to-be-determined, non-relativistic particle which most likely only interacts with itself and baryonic matter through gravity [1], and *dark energy* (Λ); the negative pressure associated with the vacuum of space causing the accelerated expansion of the Universe.

The fact that the Universe is expanding had been established in the 1920's, observationally by Edwin Hubble (Hubble, 1929) and mathematically by Alexander Friedmann. However, it has been only a little over a decade since the discovery that the expansion of the Universe is *accelerating*. If we assume that our Universe is simply composed of ordinary baryonic matter and radiation, then we would be lead to believe that gravity would slow this expansion. Astonishingly, observations of distant type Ia Supernovae (SNe Ia) revealed that the expansion of the Universe was accelerating (Riess et al., 1998; Perlmutter et al., 1999). In the ΛCDM cosmological model, $\sim 72\%$ of the energy density of the Universe exists in the form of dark energy, responsible for the accelerated expansion, yet the precise physical origin of dark energy remains a mystery. The rest of the mass budget in the Universe is comprised of $\sim 24\%$ dark matter and $\sim 4\%$ baryonic matter.

[1] It should be noted that recent studies have shown that some Self-Interacting Dark Matter (SIDM) models, which agree with the gross properties of CDM models, may also able to relieve the tension between the brightest Milky Way satellites and the dense subhalos found in CDM simulations (e.g., Boylan-Kolchin et al., 2011a,b; Vogelsberger et al., 2012)

We know the expansion history of the Universe through the field equations specified by Einstein's theory of General Relativity. Under the assumption that the Universe is homogeneous and isotropic on very large scales (Einstein's so-called Cosmological Principle), the field equations can be simplified to the Friedmann Equations:

$$\frac{\ddot{a}}{a} = -\frac{4}{3}\pi G\Big(\rho + \frac{3p}{c^2}\Big) + \frac{\Lambda}{3} \tag{1.1}$$

and

$$H^2 = \Big(\frac{\dot{a}}{a}\Big)^2 = \frac{8\pi G}{3}\rho - \frac{kc^2}{R_0^2 a^2} + \frac{\Lambda}{3} \tag{1.2}$$

where Λ is the Cosmological Constant, and ρ, p, R_0 and k are the mass density, pressure, present day radius of curvature and the curvature parameter of the Universe, respectively. Specifically, $k = -1, 0, +1$ depending on the shape of the Universe. k is believed to be zero, describing a spatially flat Universe. H is the *Hubble parameter*, and represents the expansion of the Universe given by Hubble's Law, $v = H \times d$, which says that the recession velocity v of an object is proportional to its proper distance d, with $H(t) = \frac{\dot{a}}{a}$. a is the *scale factor* and is a function of time (it is defined such that $a = 1$ today, and it is related to redshift $z = \frac{a(t_0)}{a(t)} - 1$). H is typically normalized to its present day value $H_0 = H(t_0) = 100h\text{km s}^{-1}\text{Mpc}^{-1}$, where h is a dimensionless parameter denoting the fact that we do not know H_0 to perfect accuracy.

It can be advantageous to consider the expansion of the Universe in terms of

densities, thus we simplify Equation 1.2:

$$\frac{\dot{a}}{a} = H_0\sqrt{\Omega_m(1+z)^3 + \Omega_r(1+z)^4 + \Omega_k(1+z)^2 + \Omega_\Lambda} \tag{1.3}$$

with

$$\Omega_m = \frac{\rho_m}{\rho_c},\ \Omega_r = \frac{\rho_r}{\rho_c},\ \Omega_\Lambda = \frac{\rho_\Lambda}{\rho_c} \tag{1.4}$$

representing the matter, radiation and dark energy densities, respectively, in units of the critical density, $\rho_c = \frac{3H^2}{8\pi G}$ (Ω_k is assumed to be zero). The critical density is defined as the density required to make the Universe spatially flat. Non-relativistic matter evolves as $\rho_m \propto (1+z)^3$ (this matter component also considers the baryonic contribution Ω_b along with the more dominant dark matter component). Radiation is relativistic and wavelengths will be redshifted due to the expansion of the Universe, making $\rho_r \propto (1+z)^4$. ρ_Λ is assumed to be constant here. The very early Universe was dominated by radiation, and hence, relativistic species, whose tremendous pressure stifled the growth of structure. When the age of the Universe was $\sim 100,000$ years, matter became the dominant component propelling the growth of structure through the gravitational collapse of matter. However, the Universe was still tremendously hot and dense, retarding structure growth. It was not until $\sim 300,000$ years after the Big Bang that the Universe had sufficiently expanded and cooled such that radiation and matter became decoupled (an epoch known as "recombination") allowing for further collapse. Structure formation has been persistent ever since, evolving over $\sim$ 13Gyr.

1.2 Dark Matter & The Growth of Structure

The spatial clustering of galaxies is thought to be directly related to that of dark matter, since dark matter comprises $\sim 85\%$ of the matter content in the Universe. Although we do not know the explicit nature of dark matter, we have a solid understanding of its behavior. We have good reason to believe that it is cold – moves with velocities much less than the speed of light, dissipationless – does not cool via radiating photons, and it is collisionless – only interacts through the force of gravity. If we can model the behavior of dark matter in the Universe, we can make the initial assumption that the less ubiquitous observable matter (i.e., galaxies) traces the dark matter. This affords us an excellent starting point to predict galaxy clustering.

The most powerful achievement of the ΛCDM model is its ability to predict the structures we observe in the Universe. As alluded to previously, fluctuations in the early Universe plasma resulted in slight areas of over-density of matter. While the fluctuations in the primordial density field are quantum in nature, they become amplified during inflation. Structure formation is "seeded" by exiguous perturbations in the matter density field that are expanded to cosmological scales due to inflation and the subsequent Hubble expansion. Dark matter, the dominant form of matter in the Universe, is believed to have zero pressure, which results in gravitational collapse ultimately leading to the growth of perturbations.

We can characterize the local matter density fluctuation about the mean density

of the Universe, $\bar{\rho}$, such that,

$$\delta(\overrightarrow{\mathbf{r}}) = \frac{\rho(\overrightarrow{\mathbf{r}}) - \bar{\rho}}{\bar{\rho}}. \tag{1.5}$$

$\delta(\overrightarrow{\mathbf{r}})$ is expected to have a distribution that is nearly Gaussian (with mean zero). The fluctuations are not randomly distributed throughout space, rather they are correlated with each other. This is the foundation for the understanding of the observed clustering of galaxies, discussed in § 1.4.3.

At early times linear theory provides a good description of the evolution of these density perturbations. Specifically, perturbations grow through a simple relation,

$$\delta(\overrightarrow{\mathbf{r}}, t) = \delta_0(\overrightarrow{\mathbf{r}}) \times \mathrm{D}(t) \tag{1.6}$$

where $\delta_0(\overrightarrow{\mathbf{r}})$ is the density at the present epoch and $\mathrm{D}(t)$ is the "growth factor". Linear theory is a good approximation for structure growth in the regime where $|\delta(\overrightarrow{\mathbf{r}})| \ll 1$ everywhere. However, after sufficient time has elapsed, perturbations become non-linear ($|\delta(\overrightarrow{\mathbf{r}})| > 1$), and their evolution is substantially more complex. Since linear theory breaks down for high density regions, analytic formalisms (which will be discussed in 1.3), or more accurate, dark matter numerical N-body simulations which compute the fully non-linear calculation can be employed. Figure 1.1 shows the evolution of the dark matter density field as a function of time in an N-body simulation. Each panel is color-coded according to density, with red regions

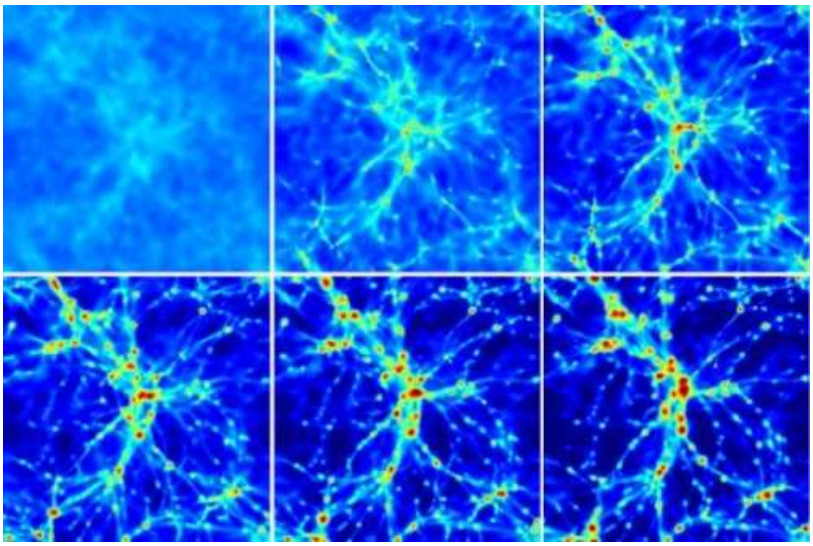

Figure 1.1: The evolution of the dark matter density field as a function of time. The Universe evolved from being very smooth (upper left panel) to the present time, which exhibits rich structure. Panels are color-coded according to density, with red regions representing the most over-dense regions. Image courtesy of Craig Booth and the VIRGO Consortium.

representing the most over-dense regions. In the early Universe, the density field is quite smooth (upper left panel). As we arrive at the current epoch (top left panel to the bottom right panel), structure evolves into a complex "cosmic web" with areas of large over-density, thin filaments and under-dense "voids". I will now focus on this non-linear regime and the formation of dark matter halos.

1.3 Halo Formation & Mergers

Gravitational coalescence of dark matter will lead to the formation of gravitationally bound structures called *dark matter halos*. The formation of halos is complex, though a heuristic description comes from the spherical collapse model (Gunn, 1977). A density fluctuation can become so dense that that the pull from its own self-gravity

wins out over the expansion of the Universe. If we approximate this small fluctuation as a sphere, then at a "turn around" point where the sphere has reached a critical radius at which its own self-gravity dominates, then the density fluctuation will collapse to form a dark matter halo. Ultimately, total collapse will never occur due to the fact that the kinetic energy associated with collapse is converted into random particle motions. In this model, when the sphere will collapse to half its critical radius, the halo will be in virial equilibrium - the kinetic energy K associated with random motions of the dark matter particles is equal to half the gravitational potential U of the particles ($K = -\frac{1}{2}U$). In essence, this means that virialization occurs when the density contrast between the halo and the background density reaches some critical value, $\Delta_{\rm vir}$. The spherical collapse model predicts this to occur at $\Delta_{\rm vir} = 1 + \delta_{\rm vir} = \frac{\rho}{\bar{\rho}} \cong 200$. $\Delta_{\rm vir}$ can be written more generally as a function of time, $\Delta_{\rm vir}(z) = \Omega_m^{-1} \times [18\pi^2 + 82(\Omega_m - 1) - 39(\Omega_m - 1)^2]$ (Bryan & Norman, 1998).

Unfortunately, halo formation is not as simple as the spherical collapse model. In nature, halos do not always form in isolation, rather they can grow through the accretion of smaller halos. Since halos are believed to be the natural sites for galaxies to reside, knowing the merger history of halos is crucial for understanding how galaxies evolve and assemble.

1.3.1 The Halo Mass Function

The *Halo Mass Function* describes the abundance of halos in the Universe and can be approximated by an extension of the spherical collapse model. Press & Schechter (1974) used simple Gaussian random field statistics to derive a halo mass function, since the assumption is that halos form in the peaks in the Gaussian random density field of dark matter. The number of halos per unit volume in the mass range M to $M + \delta M$ is $(\frac{\mathrm{d}n}{\mathrm{d}M}) \times \delta M$, where,

$$\frac{\mathrm{d}n}{\mathrm{d}M}(M,t) = \Big(\frac{2}{\pi}\Big)^{1/2} \frac{\bar{\rho}}{M^2} \frac{\delta_c(t)}{\sigma(M)} \Big| \frac{d\ \ln\ \sigma}{d\ \ln\ M} \Big| \times \exp\Big[- \frac{\delta_c^2(t)}{2\sigma^2(M)} \Big]. \tag{1.7}$$

$\sigma(M)$ is the variance of the density field (smoothed on a mass scale $M = \frac{4\pi}{3}\bar{\rho}R^3$) and $\delta_c(t)$ is the critical density for a halo to collapse at time t (Eke et al., 1996).

It is important to note that there is a characteristic mass scale, $M_*(z)$, associated with the halo mass function. $M_*(z)$ is the typical mass scale (at a given redshift) for a halo to collapse ($M_*(z) \approx 10^{12} M_\odot$ today). The halo mass function has an intrinsic shape where the number density of halos at the low-mass end is a decreasing power-law function ($\frac{\mathrm{d}n}{\mathrm{d}M} \propto M^{-\alpha}, \alpha \approx 1.8$), because the initial power spectrum predicts that small fluctuations are very abundant. Conversely, very large fluctuations are rare, hence, large mass halos will be uncommon. As a result, the halo mass function begins to turn over and exponentially drop off at masses greater than $M_*(z)$. Though this analytic formalism does not provide an extremely accurate description of results from dark matter N-body simulations (e.g., Zentner, 2007; Robertson et al., 2009), it

is nonetheless a remarkably elegant and useful picture for halo formation.

1.3.2 Halo Structure

Halos are characterized by their large over-densities, which correspond, roughly, to virialized regions of dark matter. Again, utilizing the spherical collapse model, we can define a virial radius that is related to this density contrast ($\Delta_{\rm vir}$),

$$R_{\rm vir} = \Big(\frac{3M}{4\pi\bar{\rho}\Delta_{\rm vir}}\Big)^{1/3} \tag{1.8}$$

A fascinating result measured from N-body simulations is a universal spherically-averaged density profile for dark matter within halos. This is especially surprising given the chaotic, non-linear processes within halos. This density profile was introduced by Navarro, Frenk, & White (1997, NFW) and it has a unique functional form,

$$\rho(r) = \frac{\rho_s}{\Big(\frac{r}{r_s}\Big)\Big(1+\frac{r}{r_s}\Big)^2} \tag{1.9}$$

Recent studies have shown that halo density profiles may be better described by the three-parameter Einasto profile (Einasto, 1965), which includes a parameter α that controls how the logarithmic slope will vary with radius to accurately account for the fact that halo profiles seem to not be self-similar (Gao et al., 2008; Navarro et al., 2010; Ludlow et al., 2010). However, on average, the simpler, two-parameter NFW model is accurate to within $10-20\%$ (Benson, 2010), and the largest discrepancies

arise very close to halo centers where baryonic physics are expected to affect the dark matter profile. The NFW profile implies that at small radii the slope of the density profile (in log space) decreases as r^{-1}, transitions to r^{-2} at a characteristic scale radius that weakly depends on halo mass, $r_{\rm s}$, then drops off as r^{-3} at large radii. The ratio of the scale radius to a halo's virial radius is defined through the *concentration parameter*

$$C = \frac{r_{\rm s}}{R_{\rm vir}} \tag{1.10}$$

which is a strong reflection of a halo's assembly history (Wechsler et al., 2002), with halos that formed earlier being more concentrated (Prada et al., 2011). It has also been found that more massive halos are less concentrated (e.g., Bullock et al., 2001; Macciò et al., 2008), though there is large scatter in this $C-$Mass relation.

1.4 Connecting the Dark and Light Sectors

Dark matter halos set the backdrop for the formation of the luminous structures that we can observe. Knowing key ingredients of this dark sector, such as halo formation and merging, the halo mass function, and the internal structure of halos, we can take on the formidable problem of how galaxies are connected to these virialized structures they reside in.

Galaxies are the "lighthouses" of the Universe, informing us about the overall distribution of matter in the Universe. I now turn to an introduction to the complex nature of how galaxies form and how we can use their spatial clustering to tackle

several unsolved problems relating to their formation and evolution, which constitutes the crux of this work.

1.4.1 The Formation of Galaxies

Dark matter is $\sim 6\times$ more prevalent than the ordinary baryonic that comprises galaxies. Thus, it is plausible that the distribution of baryons may trace the underlying dark matter density field. Shortly after recombination, as the primordial density fluctuations began to collapse, so too did the pristine gas that resided in these regions of over-density. The hot gas in halos cools and condenses as it sinks towards the potential well minimum (White & Rees, 1978; Blumenthal et al., 1986). Therefore, the density fluctuations that gravitationally attracted dark matter and gas seeded the formation of halos and galaxies.

The first "proto-galaxies" consisted primarily of neutral hydrogen and, to a lesser extent, helium. Unlike the formation of halos which is governed by the simple, collisionless, dissipative nature of dark matter, the proto-galactic gas can collide and lose energy, causing it to collapse. These collisions of clumps of gas induce shock fronts of extremely high density and the heated gas will then sufficiently cool to become a nursery for star formation. Continual collapse will cause the gas to settle into a rotating disk. The galactic ecosystem involves the recycling of available gas due to the life-cycle of stars. Older generations of stars will deposit gas back into the surrounding environment, enriching the intergalactic medium resulting in a new generation

of stars to be formed. However, this re-processing can not last forever and the gas reservoir may be quenched. Additionally, energy feedback from supernovae or a massive central black hole (AGN) can blow out available gas, inhibiting star formation. Hence, galaxies that formed very early may no longer exhibit signs of star formation and are typically red (and elliptical in shape due to morphological disruptions as a result of galaxy mergers) due to the dimming of the stellar populations, while more recently forming galaxies are typically blue (and disk-shaped).

As discussed in § 1.3, dark matter halos can grow through the accretion of smaller halos, and this process is naturally extended to galaxies. When a galaxy merges into a larger halo it will experience intense gravitational processes. For example, the tidal field of the larger halo can act to shred the galaxy apart. Also, dynamical friction causes the merged galaxy to spiral towards the halo potential well minimum. Thus, the larger, central galaxy can grow by cannibalizing smaller galaxies. These ideas are expounded upon in detail in Chapters II and III. Ultimately, galaxy formation is extremely complex and requires a complete understanding of gas/stellar dynamics (collisional processes), star formation, and feedback mechanisms.

1.4.2 Subhalos & Galaxies

When a smaller halo merges into a larger one, it can retain its integrity as a self-bound, orbiting dark matter entity. These accreted objects are dubbed "subhalos" or "substructure" (Ghigna et al., 2000; Klypin et al., 1999a; Moore et al., 1999; Diemand

et al., 2004; Kravtsov et al., 2004a). When a halo is accreted by a larger halo, thus becoming a subhalo, the galaxy within it becomes a "satellite" galaxy within a galaxy group or cluster. Understanding the detailed relationship between (satellite) galaxies and (sub) halos is a long-standing focus of galaxy formation theory.

In the hierarchical paradigm, these smaller objects, upon merging, become victims of intense tidal fields within their "parent" or "host" halo. The dark matter mass associated with a subhalo may be rapidly stripped upon infall. But what happens to the galaxy residing in the subhalo? Does it change color and/or morphology? How is the gas component affected? How is star formation altered? Do some, none, or all of the stars associated with the galaxy become unbound as well? These are challenging questions to answer and predominantly remain unresolved. In this thesis I look to shed light on this final question of satellite galaxy stellar mass loss.

Tidal stripping acts on the periphery of the subhalo first, causing dark matter mass loss. This suggests that the luminous galaxy, residing deep in the potential well of the subhalo, may be unharmed. However, after enough time has elapsed, stripping of stars may begin to occur as well. Massive halos are known to have unbound, diffuse stellar material unassociated with any particular satellite galaxy (or the central galaxy) of the system. These liberated stars that are ripped from satellite galaxies are the likely source of "intrahalo light" (IHL: e.g., Gallagher & Ostriker, 1972; Mihos et al., 2005; Gonzalez et al., 2007). In Chapter III, I constrain the liberation of stars from satellite galaxies by connecting stellar mass loss to subhalo

dark matter mass loss using galaxy clustering (which I describe in detail in § 1.4.3) and IHL observations (this work has been submitted for publication in Watson et al. 2011c).

1.4.3 Spatial Clustering

The principal strategy of this work is to use the *spatial clustering* of galaxies to gain insight into fundamental aspects of galaxy formation. To quantify the degree of clustering, we consider two infinitesimally small spheres centered on two objects, located at $\overrightarrow{\mathbf{r_1}}$ and $\overrightarrow{\mathbf{r_2}}$ in space. If the spheres have volume V_1 and V_2 respectively, then the joint probability of finding these two objects at a separation $\overrightarrow{\mathbf{r}} = \overrightarrow{\mathbf{r_1}} - \overrightarrow{\mathbf{r_2}}$ is,

$$dP_{12} = \bar{n}^2[1 + \xi(\overrightarrow{\mathbf{r}})]dV_1dV_2 \tag{1.11}$$

where $\bar{n}$ is the mean number density of objects in space, and $\xi(\overrightarrow{\mathbf{r}})$ is the two-point correlation function. The two-point correlation function is the *excess* probability of finding a pair of objects at a given separation $\overrightarrow{\mathbf{r}}$ relative to a random distribution. The full series of n-point correlation functions will completely describe the distribution of large-scale structure. However, due to observational limitations, most work exploits the two-point correlation function (which I will just refer to as the correlation function throughout the remainder of the Introduction), though powerful new galaxy surveys (see § 1.4.4) have now made it possible to measure higher moments, such as the the three-point correlation function (McBride et al., 2011).

The correlation function is defined to be in the range $[-1 \leq \xi(\overrightarrow{\mathbf{r}}) \leq \infty\ ]$, such that,

1. $\xi(\overrightarrow{\mathbf{r}}) > 0 \rightarrow$ objects are correlated

2. $\xi(\overrightarrow{\mathbf{r}}) = 0 \rightarrow$ objects are randomly distributed

3. $\xi(\overrightarrow{\mathbf{r}}) < 0 \rightarrow$ objects are anti-correlated

Given our definition for $\delta(\overrightarrow{\mathbf{r}})$ from Equation 1.5,

$$\xi(\overrightarrow{\mathbf{r}}) = \langle \delta(\overrightarrow{\mathbf{r_1}}) \delta(\overrightarrow{\mathbf{r_2}}) \rangle \tag{1.12}$$

$\xi(r)$ is a vital statistic to quantify the spatial clustering of structures in the Universe and it can be used to describe any class of objects being correlated. For instance, the clustering of galaxies, $\xi_{\rm gg}(\overrightarrow{\mathbf{r}})$, of (dark) matter, $\xi_{\rm mm}(\overrightarrow{\mathbf{r}})$, or of dark matter halos, $\xi_{\rm hh}(\overrightarrow{\mathbf{r}})$. An important quantity to note is the *bias* parameter, b, which relates the correlation function of a certain class of objects to the correlation function of dark matter. It is thus a useful definition for the "biased" relation between, for instance, galaxies and dark matter: $b = \sqrt{\xi_{\rm gg}(\overrightarrow{\mathbf{r}}) / \xi_{\rm mm}(\overrightarrow{\mathbf{r}})}$.

From an observational standpoint, different estimators can be used to compare galaxy distributions to random ones (Peebles & Hauser, 1974; Davis & Peebles, 1983; Hamilton, 1993; Landy & Szalay, 1993) which are based on the counts of neighbors of galaxies at a given scale. They all need to address complications that can arise from underestimating the number of neighbors near the boundary of the survey sample.

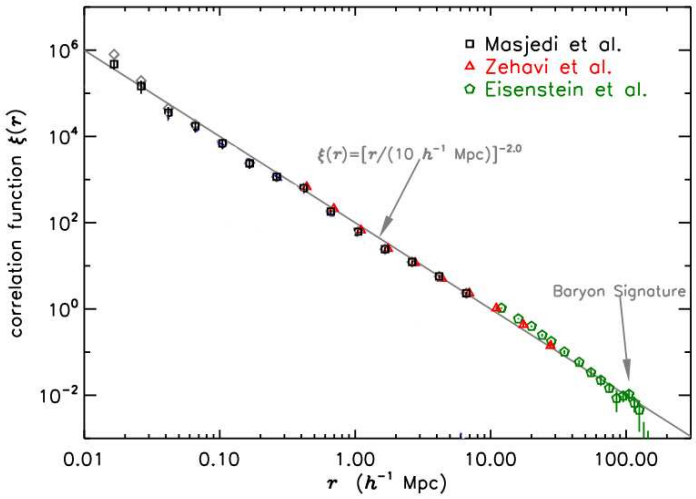

Figure 1.2: The galaxy two-point correlation function of luminous red galaxies (LRGs) from the Sloan Digital Sky Survey. An $\sim r^{-2}$ power-law slope spans roughly four orders of magnitude in LRG-LRG separation scales. Image (modified) from Masjedi et al. (2006).

One of the more common estimators is from Landy-Szalay (Landy & Szalay, 1993),

$$\xi = \frac{DD - 2DR + RR}{RR} \tag{1.13}$$

where DD, DR and RR are the normalized numbers of weighted data-data, data-random and random-random pairs in each bin of radial separation. Figure 1.2 is the measured correlation function of luminous red galaxies (massive, bright elliptical galaxies) from the Sloan Digital Sky Survey (see § 1.4.4). Nature has provided a rather simple approximate power-law form for galaxies, $\xi_{\rm gg}(\overrightarrow{\mathbf{r}}) = (\frac{\vec{\mathbf{r}}}{\vec{\mathbf{r}}_0})^{-\gamma}$, where $\overrightarrow{\mathbf{r}}_0$ (an intrinsic correlation length that depends on the objects being correlated) and γ (the slope of the power-law) are fit to a given galaxy sample. Here, $\gamma = 2$ over an enormous range of scales spanning $\sim$ 4 orders of magnitude. The $\xi(r) \propto r^{-2}$

power-law form has been known for over four decades, though the physical processes governing this simple shape was an unsolved problem. As a result of the explosion of high quality data over the last decade mapping the spatial distribution of galaxies, I confront this long-standing conundrum from a theoretical standpoint in Chapter II with the aim of revealing the physics behind the power-law nature of $\xi_{\rm gg}(\overrightarrow{\mathbf{r}})$ (the results of which have been published in Watson et al. 2011b).

1.4.4 Galaxy Surveys

The Center for Astrophysics Redshift Surveys (CfA: Davis et al. 1982, CfA2: Huchra et al. 1983) were the first surveys to attempt to map the 3-dimensional large-scale structure of the Universe. The aim was to measure the radial velocities of a large sample of galaxies in the northern sky. CfA provided us with the first ever mapping of the local Universe, as well as the first measurements of galaxy clustering properties. CfA2 was started several years later, and measured the redshifts to nearly 18,000 galaxies. These surveys clearly demonstrated that the galaxy distribution is far from random. Galaxies were seen to be highly clustered and surrounded by voids.

The Two Degree Field Galaxy Redshift Survey (2dFGRS: Colless et al. 2001) drastically extended the number of galaxies observed by probing a significantly larger volume. 2dFGRS used a 4-meter telescope with a two degree field of view, mapping $\sim 2,000$ square degrees. They retrieved spectra of $\sim 250,000$ galaxies. This allowed for a high precision determination of the large-scale galaxy distribution in the local

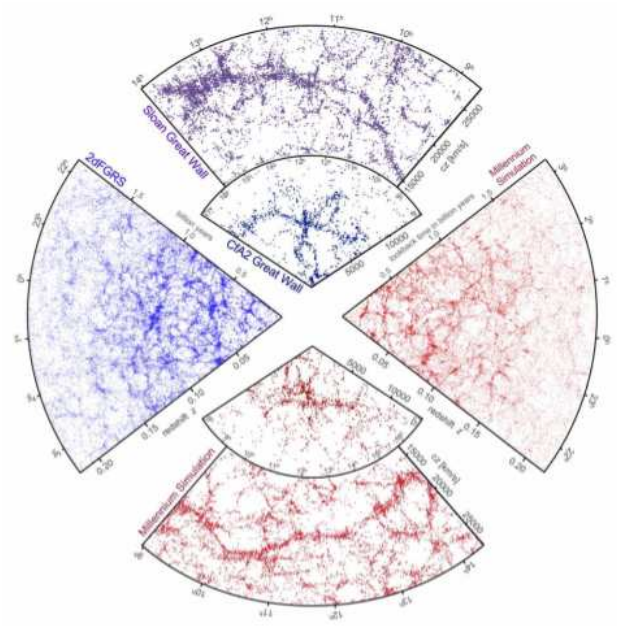

Figure 1.3: The galaxy distribution in galaxy redshift surveys and mock catalogs. Every point in a given slice represents one galaxy. The small, foreground slice at the top shows results from CfA2 and the background section is from SDSS. The cone on the left shows one-half of 2dFGRS. At the bottom and on the right, mock galaxy surveys constructed from the Millennium simulation. Image from Springel et al. (2006)

Universe.

We are now in the midst of one of the most ambitious undertakings in astronomy. The Sloan Digital Sky Survey (SDSS:York et al. 2000) has produced the largest ever spectroscopic sample of galaxies. Due to the enormous volume probed, SDSS has provided 3D maps of distant galaxies yielding precise clustering measurements. It has allowed astronomers to place powerful constraints on the nature and origin of the primordial density fluctuations that seeded the growth of structure, as well as the matter and energy contents of the Universe.

Figure 1.3 combines results from all three of the aforementioned surveys. The

upper two slices show results from SDSS and CFA2 and the left slice is from 2dFGRS (each point represents a galaxy). At the bottom and on the right are mock galaxy surveys constructed using semi-analytic techniques to model the distribution of galaxies within the dark matter distribution in the Millennium simulation (Springel et al., 2005). Rich structure is evident with highly clustered regions of galaxies surrounded by large under-dense voids.

1.4.5 Redshift Space Distortions

Distance measures are a common thorn in the side of astronomers. Simply having spectroscopic redshifts of galaxies will not give a true 3-dimensional picture. This is because an important signature of gravitational instability is that collapsing structures will generate *peculiar velocities*. By definition, redshift compares the observed wavelength to the intrinsic wavelength. How the observed wavelength is shifted can arise from two separate effects when considering cosmological scales. First, there is the redshift associated with objects moving with the Hubble flow (as discussed in § 1.1). Second, there is the redshift contribution due to the intrinsic line-of-sight motions of the objects observed (the doppler effect),

$$z_{\rm doppler} \simeq \frac{\overrightarrow{\mathbf{v}}_{\rm pec}}{c} \tag{1.14}$$

where $\overrightarrow{\mathbf{v}}_{\rm pec}$ is the peculiar (line-of-sight) velocity relative to the Hubble flow (c is the speed of light). Therefore, redshift as defined for large-scale structure is the product

of the cosmological and doppler contributions,

$$1 + z = (1 + z_{\rm cosmo})(1 + z_{\rm doppler}) \tag{1.15}$$

A measured redshift combines Hubble's law with the radial component of $\overrightarrow{\mathbf{v}}_{pec}$, such that $cz \simeq H_0 r + \overrightarrow{\mathbf{v}}_{\rm pec}$. If structure forms via gravitational collapse, there should be coherent infall velocities on large scales where $\overrightarrow{\mathbf{v}}_{\rm pec}$ can be small compared to the size of the associated structure. In other words, consider an enormous supercluster (like the "Sloan Great Wall" Gott et al. 2005) of size R_0. If $R_0 \times H > \overrightarrow{\mathbf{v}}_{pec}$ then there is an observed squashing or flattening of structure in redshift-space, known as the "Kaiser Effect" (Kaiser, 1987). Conversely, in the case of a galaxy cluster, peculiar velocities associated with the random orbital motions of galaxies are much larger than $R_0 \times H$. This produces what is known as the "finger-of-God" effect, where structures appear highly elongated in redshift space. Since galaxy redshift is not a "true" distance, we decompose the separation r between galaxies into perpendicular, r_p, and parallel, line-of-sight, π, components to encapsulate these redshift distortions. Perpendicular separations are true measures of distance, but the radial separations are distorted by $\overrightarrow{\mathbf{v}}_{\rm pec}$. In Figure 1.4, both effects can be clearly seen in the 2-dimensional correlation function, $\xi(r_p, \pi)$, as measured in the 2dFGRS (Peacock et al., 2001). Here, r_p is denoted as σ and the upper-right quadrant has been mirrored along both axes to illustrate deviations from circular symmetry. In the absence of redshift space distortions, the contours would be isotropic. However, for small-scale

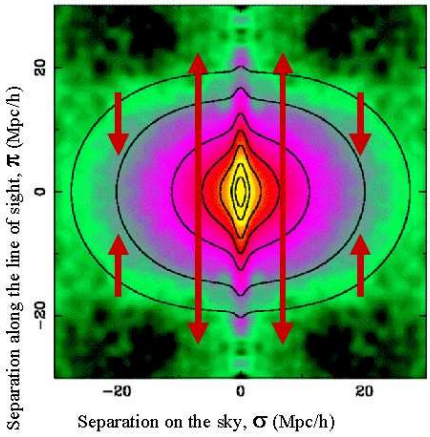

Figure 1.4: The 2-dimensional correlation function as measured in the 2dF Galaxy Redshift Survey (Peacock et al., 2001). The separation r between galaxies is decomposed into perpendicular, r_p, and parallel, π, components. Coherent infall velocities on large scales where peculiar velocities can be small compared to an associated large structure (such as the "Sloan Great Wall") produce an observed "flattening" of structure. Conversely, for smaller regions such as galaxy clusters, peculiar velocities associated with the random orbital motions of galaxies are much larger than the cluster they reside in resulting in structures appearing highly elongated in redshift space (flattening and elongation are highlighted by the red arrows). The upper-right quadrant has been mirrored along both axes to highlight deviations from circular symmetry. In the absence of redshift space distortions, the contours would be isotropic.

projected separations, the contours are elongated from the finger-of-God effect, while compression from the Kaiser effect is evident on large scales (as highlighted by the red arrows).

To compensate for redshift distortions it is common practice to compute the *projected* correlation function, $w_p(r_p)$, by integrating along the line of sight (Davis & Peebles, 1983; Zehavi et al., 2004):

$$w_{\rm p}(r_{\rm p}) = 2\int_0^\infty \xi(r_p,\pi)d\pi. \tag{1.16}$$

For a typical galaxy sample, the line-of-sight component is integrated to $\pi_{\rm max} \sim$

$50h^{-1}$Mpc to incorporate most correlated pairs (e.g., Zehavi et al., 2011).

1.4.6 Dark Matter & Galaxies on Extremely Small Scales

This thesis revolves strongly around modeling of observational measurements of the projected correlation function of galaxies. The galaxy correlation function on scales smaller than the virial radii of the largest dark matter halos ($r \lesssim 1$Mpc) is dictated by the *radial distribution* of galaxies. Therefore, the measured galaxy correlation function itself is a powerful tool for shedding light on how galaxies trace the underlying dark matter within halos since the radial distribution of dark matter is fairly well pinned down. Chapters II and III involved modeling of the correlation function on scales $\sim 100\text{kpc} - 20\text{Mpc}$ to glean information on galaxy formation and evolution. But what about on scales much deeper within individual halos, $r <$ 100kpc?

Galaxies, being massive and extended, are subject to dynamical mechanisms such as dynamical friction and mass loss. These processes become more chaotic towards the centers of halos where the tidal field is strongest, and should affect large and massive (and hence, very luminous) objects more than small ones. Therefore, the very small-scale correlation function can be used to investigate the luminosity dependence of the radial distribution of satellite galaxies and the degree to which it differs from an NFW distribution. I take advantage of recent precision measurements of projected correlation functions from SDSS to perform such a study and this is addressed in

Chapters IV and V (the results have been published in Watson et al. 2010, 2011a).

Chapter II

THE GALAXY CORRELATION FUNCTION CONSPIRACY

Abstract

We model the evolution of galaxy clustering through cosmic time to investigate the nature of the power-law shape of $\xi(r)$, the galaxy two-point correlation function. While $\xi(r)$ on large scales is set by primordial fluctuations, departures from a power law are governed by galaxy pair counts on small scales, subject to non-linear dynamics. We assume that galaxies reside within dark matter halos and subhalos. Therefore, the shape of the correlation function on small scales depends on the amount of halo substructure. We use a semi-analytic substructure evolution model to study subhalo populations within host halos. We find that tidal mass loss and, to a lesser extent, dynamical friction dramatically deplete the number of subhalos within larger host halos over time, resulting in a $\sim 90\%$ reduction by $z = 0$ compared to the number of distinct mergers that occur during the assembly of a host halo. We show that these non-linear processes resulting in this depletion are essential for achieving a power-law $\xi(r)$. We investigate how the shape of $\xi(r)$ depends on subhalo mass (or luminosity) and redshift. We find that $\xi(r)$ breaks from a power law at high masses, implying that only galaxies of luminosities $\lesssim L^*$ should exhibit power-law clustering. Moreover, we demonstrate that $\xi(r)$ evolves from being far from a power law at high redshift, toward

a near power-law shape at $z = 0$. We argue that $\xi(r)$ will once again evolve away from a power law in the future. This is in large part caused by the evolving competition between the accretion and destruction rates of subhalos over time, which happen to strike just the right balance at $z \approx 0$. We then investigate the conditions required for $\xi(r)$ to be a power law in a general context. We use the halo model along with simple parametrizations of the halo occupation distribution (HOD) to probe galaxy occupation at various masses and redshifts. We show that key ingredients determining the shape of $\xi(r)$ are the fraction of galaxies that are satellites, the relative difference in mass between the halos of isolated galaxies and halos that contain a single satellite on average, and the rareness of halos that host galaxies. These pieces are intertwined and we find no simple, universal rule for which a power-law $\xi(r)$ will occur. However, we do show that the physics responsible for setting the galaxy content of halos do not care about the conditions needed to achieve a power law $\xi(r)$ and these conditions are met only in a narrow mass and redshift range. We conclude that the power-law nature of $\xi(r)$ for L^* and fainter galaxy samples at low redshift is a cosmic coincidence.

2.1 Introduction

The two-point correlation function of galaxies was measured four decades ago and found to be consistent with a $\xi(r) \propto r^{-2}$ power law (Totsuji & Kihara, 1969; Peebles, 1973; Hauser & Peebles, 1973; Peebles & Hauser, 1974; Peebles, 1974). Since that time, successively larger galaxy redshift surveys (e.g., Huchra et al., 1983; da

Costa et al., 1988; Santiago et al., 1995; Shectman et al., 1996; Saunders et al., 2000; Colless et al., 2001; York et al., 2000) have mapped the distribution of galaxies with ever increasing precision and confirmed correlation functions consistent with power laws over a large range of scales (e.g., de Lapparent et al., 1988; Marzke et al., 1995; Hermit et al., 1996; Tucker et al., 1997; Jing et al., 1998, 2002; Norberg et al., 2002; Zehavi et al., 2002). The scales on which a single power-law description is valid span a range from large regions exhibiting mild density fluctuations ($r \gtrsim 10$ Mpc), to smaller regions with large density fluctuations experiencing rapid non-linear evolution ($r \sim 1-10$ Mpc), to collapsed and virialized galaxy groups and clusters ($r \lesssim 1$ Mpc). It has long been noted that the lack of any feature delineating the transitions among these scales is surprising (e.g., Peebles, 1974; Gott & Turner, 1979; Hamilton & Tegmark, 2002; Masjedi et al., 2006; Li & White, 2010). This is especially true given that the matter correlation function in the now well-established concordance cosmological model differs significantly from a power law. In this paper, we return to this long-standing problem and address the origin of a power-law galaxy correlation function in the context of our modern paradigm for the growth of cosmic structure.

This conundrum can be refined within the contemporary framework in which galaxies live within virialized halos of dark matter (White & Rees, 1978; Blumenthal et al., 1984). In such a model, galaxy clustering statistics can be modeled as a combination of dark matter halo properties and a halo occupation distribution (HOD) that specifies how galaxies occupy their host halos (e.g., Peacock & Smith, 2000;

Scoccimarro et al., 2001; Berlind & Weinberg, 2002; Cooray & Sheth, 2002). In this *halo model* approach, the galaxy correlation function is a sum of two terms: On small scales, pairs of galaxies reside in the same host dark matter halo (the "one-halo" term), whereas on large scales, the individual galaxies of a pair reside in distinct halos (the "two-halo" term). These two terms depend on the HOD in different ways, requiring delicate tuning in order to spawn an unbroken power law (e.g., Berlind & Weinberg, 2002). Consequently, a feature in $\xi(r)$ at scales corresponding to the radii of the typical, virialized halos that host luminous galaxies is expected.

In a dramatic success for the halo model, Zehavi et al. (2004) first detected a statistically-significant departure from a power law due to the high precision measurements of the Sloan Digital Sky Survey, and demonstrated that the halo model provides an acceptable fit to the data. Zehavi et al. (2005b) confirmed this result, adding that power-law departures grow stronger with galaxy luminosity (see also Blake et al., 2008; Ross et al., 2010). $\xi(r)$ has since been shown to deviate from a power law at high redshifts (Ouchi et al., 2005; Lee et al., 2006; Coil et al., 2006; Wake et al., 2011). Nevertheless, it remains a fact that deviations from a power law at low redshifts are small and the galaxy correlation function is roughly a power law over an enormous range of galaxy-galaxy separations. Deviations have been revealed only through ambitious observational efforts.

Halos are known to be replete with self-bound structures, dubbed "subhalos" (Ghigna et al., 1998; Klypin et al., 1999b; Moore et al., 1999), and both halos and

subhalos are thought to be the natural sites of galaxy formation. Subhalos were isolated halos in their own right, hosting distinct galaxies before merging into a larger group or cluster halo[1]. Remarkably, the clustering of host halos along with their associated subhalos is very similar to that of observed galaxies (Kravtsov & Klypin, 1999; Colín et al., 1999; Kravtsov et al., 2004a), suggesting a simple correspondence of galaxies with host halos and subhalos. This was clearly demonstrated by Conroy et al. (2006) who compared the correlation functions of hosts and subhalos to that of galaxies over a broad range of luminosities and redshifts ($z \sim 0-4$), finding excellent agreement. These results indicate that an understanding of the physics governing the subhalo populations within host halos may provide insight into the physics of galaxy clustering and the near power-law form of the galaxy two-point correlation function.

In this paper, we examine the causes of the observed power-law correlation function by studying the mergers, survival, and/or destruction of dark matter subhalos. Our focus in this paper is on the gross features of the galaxy two-point function and *not* on detailed comparisons to specific data sets. We explore more sophisticated galaxy-halo assignments and statistical comparisons with data in a forthcoming follow-up study (Watson et al. in prep.).

We argue that the nearly power-law, low-redshift galaxy correlation function is a coincidence. The correlation function of common $L \lesssim L^*$ galaxies evolves from

[1] *Satellites* or *subhalos* are used throughout the paper to refer to self-bound entities lying within the virial radius of a larger halo. Those that do not lie within a larger system are designated as *centrals*, *host halos* or simply *hosts*.

relatively strong small-scale clustering at early times, through a power-law at the present epoch, and most likely toward relatively weak small-scale clustering in the future. The origin of the present-day power law, in turn, relies on the tuning of several disconnected ingredients, at least three of which are: the normalization of primordial density fluctuations determined by early Universe physics; a halo mass scale for efficient galaxy formation determined largely by atomic physics, stellar physics, and the physics of compact objects; and relative abundances of baryonic matter, dark matter, and dark energy in the Universe.

Our paper is organized as follows. In § 2.2 we review the halo model and restate the problem in terms of this framework. In § 2.3 we give an overview of our primary modeling technique. In § 2.4 we investigate the individual roles of merging, dynamical friction, and mass loss in shaping the halo occupation statistics of subhalos, as well as the resulting halo correlation function. In § 2.5 we show how $\xi(r)$ depends on host halo mass and redshift. In § 2.6 we explore a standard parametrization of the HOD to see what is required to get a power-law $\xi(r)$, and we predict the masses and redshifts at which a power-law $\xi(r)$ can be constructed. In § 2.7 we give a summary of our results and our primary conclusions. Throughout this paper, we work within the standard, vacuum-dominated, cold dark matter (ΛCDM) cosmological model with $\Omega_{\rm m} = 0.3$, $\Omega_{\Lambda} = 0.7$, $\Omega_{\rm b} = 0.04$, $h_0 = 0.7$, $\sigma_8 = 0.9$, and $n_{\rm s} = 1.0$. These values differ slightly form the WMAP best-fit values, however this has little effect on our general results and was chosen in order to compare to previous work that used similar

cosmological models.

2.2 A Modern Restatement of the Problem in Halo Model Language

Though the observed galaxy correlation function is nearly a power law, the matter correlation function predicted by the concordance cosmological model is not. This is evident in Figure 2.1. On scales corresponding to collapsed objects, the dark matter correlation function exceeds the values that would be obtained by extrapolating the larger-scale power law to small scales. However, galaxies are biased with respect to dark matter in such a way as to counteract this excess. We can examine this discrepancy in terms of the halo model. If the reader is familiar with the halo model formalism, he or she may wish to skip to § 2.2.2

2.2.1 Halo Model Basics

Assuming that all galaxies live within virialized dark matter halos, the galaxies comprising any pair can come either from within the same halo (the *one-halo term*) or from two separate halos (the *two-halo term*). The correlation function is then given as the sum of these two terms

$$\xi(r) = \xi(r)^{\rm 1halo} + \xi(r)^{\rm 2halo} + 1, \tag{2.1}$$

(e.g., Cooray & Sheth 2002; for this particular form of the equation see Zheng 2004). The probability distribution $P(N|M)$ that a halo of mass M contains N galaxies

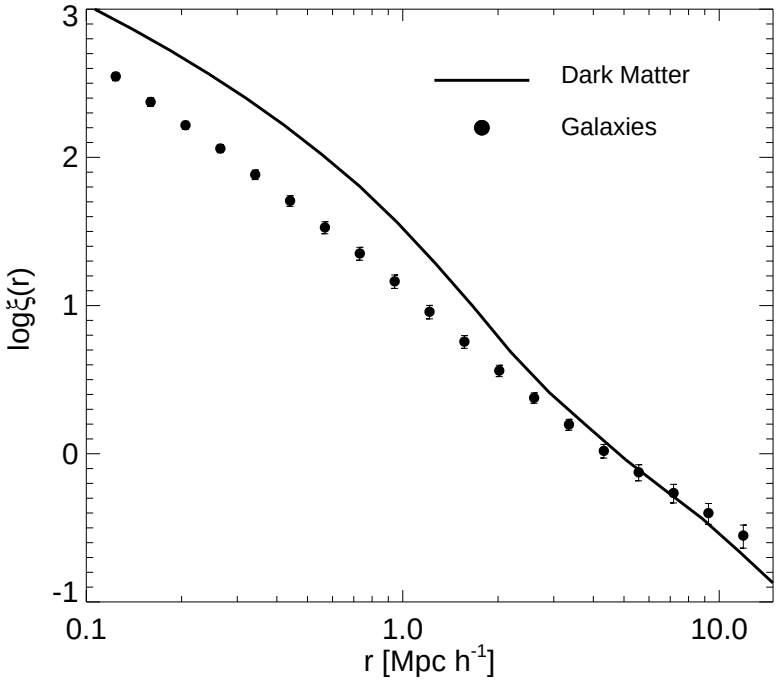

Figure 2.1: Correlation function of galaxies compared to dark matter. Points show the correlation function of galaxies from the APM survey, estimated from deprojecting the angular correlation function (Maddox et al., 1990; Baugh, 1996). The curve shows the correlation function of dark matter measured from the LCDM GIF simulation run by the Virgo collaboration (Jenkins et al., 1998).

together with the spatial distribution of galaxies within their host halos constitute the *halo occupation distribution* (HOD). We denote the first and second moments of $P(N|M)$ at a specific mass M as $\langle N \rangle_M$ and $\langle N(N-1) \rangle_M$, respectively. The one-halo term can be computed by counting the average number of galaxy pairs of a given separation in a common halo and averaging over all halos. We write the one-halo

term as (Berlind & Weinberg, 2002)

$$1+\xi(r)^{\rm 1halo} = \frac{1}{2\pi r^2 \bar{n}_{\rm g}^2}\int dM \frac{dn}{dM} \times \frac{\langle N(N-1)\rangle_M}{2} F(r|M) \tag{2.2}$$

where dn/dM is the halo mass function, $\langle N(N-1)\rangle_M/2$ is the mean number of galaxy pairs within a halo of mass M, and $F(r|M)$ is the distribution of separations between these pairs[1]. If the average spatial distribution of galaxies within their host halos is $\lambda(r|M)$, then the pair separation distribution $F(r|M)$ is the convolution of $\lambda(r|M)$ with itself. The quantity $\bar{n}_{\rm g}$ is the mean density of galaxies in the Universe,

$$\bar{n}_{\rm g} = \int dM \frac{dn}{dM} \langle N\rangle_M. \tag{2.3}$$

Motivated by theoretical considerations (e.g., Berlind et al., 2003; Kravtsov et al., 2004a; Zheng et al., 2005), the HOD of galaxies is usually considered separately for central galaxies that live near the centers of their host halos and satellite galaxies that orbit within the host halo potential. Each halo above some mass threshold should contain one central galaxy and possibly one or more satellites, depending on the host mass and the HOD. In this framework it is useful to consider contributions to the one-halo term separately for central-satellite and satellite-satellite pairs. Therefore,

[1]This notation is slightly different from that used in Berlind & Weinberg (2002), in which $F(r)$ denoted the *cumulative* pair distribution.

we rewrite the one-halo term as (Berlind & Weinberg, 2002)

$$\begin{aligned} 1+\xi(r)^{\rm 1halo} &= \frac{1}{2\pi r^2 \bar{n}_{\rm g}^2}\int dM \frac{dn}{dM} \\ \times \Big[\langle N_{\rm cen}N_{\rm sat}\rangle_M F_{\rm cs}(r|M) &+ \frac{\langle N_{\rm sat}(N_{\rm sat}-1)\rangle_M}{2} F_{\rm ss}(r|M)\Big], \end{aligned} \tag{2.4}$$

where $\langle N_{\rm cen}N_{\rm sat}\rangle_M$ and $\langle N_{\rm sat}(N_{\rm sat}-1)\rangle_M/2$ are the mean number of central-satellite and satellite-satellite pairs in hosts of mass M, and $F_{\rm cs}(r|M)$ and $F_{\rm ss}(r|M)$ are the pair separation distributions of central-satellite and satellite-satellite pairs, respectively. If the central galaxies always reside very close to the center of the host halo and the average distribution of satellite positions within the host halo is $\lambda_{\rm s}(r|M)$, then $F_{\rm cs} = \lambda_{\rm s}(r|M)$ and $F_{\rm ss}(r|M)$ is the convolution of $\lambda_{\rm s}(r|M)$ with itself. In practical cases there is at most one central galaxy and satellites are only present in halos with a central, so that $\langle N_{\rm cen}N_{\rm sat}\rangle_M = \langle N_{\rm sat}\rangle_M$. The total fraction of galaxies that are satellites in a sample is then

$$\begin{aligned} f_{\rm sat} &= \bar{n}_{\rm g}^{-1}\int dM\,\frac{dn}{dM}\langle N_{\rm sat}\rangle_M \\ &= \frac{\int dM\,\frac{dn}{dM}\langle N_{\rm sat}\rangle_M}{\int dM\,\frac{dn}{dM}(\langle N_{\rm cen}\rangle_M + \langle N_{\rm sat}\rangle_M)}. \end{aligned} \tag{2.5}$$

The satellite fraction, $f_{\rm sat}$, will prove an important quantity in determining the shape of the galaxy correlation function.

On scales significantly larger than individual halos, the two-halo term dominates the clustering strength. It is most simply written in Fourier space as (Cooray & Sheth

2002; for this particular form of the equation see Tinker et al. 2005)

$$P^{\rm 2halo}(k) = P_{\rm m}(k)\Bigg[\bar{n}_{\rm g}^{-1}\int dM \frac{dn}{dM}\langle N\rangle_M \times b_h(M,r)\tilde{\lambda}(k|M)\Bigg]^2, \tag{2.6}$$

where $P_{\rm m}(k)$ is the matter power spectrum, $b_h(M,r)$ is a (possibly scale-dependent) halo bias function, and $\tilde{\lambda}(k|M)$ is the Fourier transform of the spatial number density of galaxies within their host halos. We can invert the Fourier transform of the two-halo power spectrum to recover the two-halo term of the correlation function. In the limit that the galaxy pair separation is larger than any halo of interest, the two-halo term becomes

$$\begin{aligned}\xi^{\rm 2halo}(r) &\simeq \left[\bar{n}_{\rm g}^{-1}\int b_h(M,r)\,\langle N\rangle_M \frac{dn}{dM}\,{\rm d}M\right]^2 \xi_m, \\ &= b_{\rm g}^2\ \xi_m,\end{aligned} \tag{2.7}$$

where $\xi_m(r)$ is the matter correlation function. Equation (2.7) explicitly shows that the large-scale galaxy correlation function is essentially the halo correlation function except halos of different masses are weighted by $\langle N\rangle_M$. The galaxy bias describing the relative clustering of galaxies to dark matter $b_{\rm g} = \sqrt{\xi/\xi_m}$ is the quantity in square brackets in Equation (2.7).

2.2.2 The Battle of the 1- Halo and 2- Halo Terms

Berlind & Weinberg (2002) showed that maintaining a power-law correlation function requires a careful balance between the one-halo and two-halo terms and is thus quite difficult to achieve. This is because the one-halo term generally changes by a larger amount than the two-halo term in response to changes to the HOD. A close examination of Equations (2.3), (2.4), (2.6) and (2.7) reveals why this is the case.

Consider first the two-halo term as it is the simplest. On large scales, the two-halo term is just a weighted average of the clustering of host halos. For simplicity, assume (albeit incorrectly) the halo bias to be a constant function of halo mass. Increasing $\langle N \rangle_M$ increases both the number of two-halo pairs at a given separation (the square of the integral in Eqs. [2.6] and [2.7]) and the number of random pairs $\bar{n}_{\rm g}^2/2$, by the same amount. The reason the two-halo term is at all sensitive to the HOD is that the bias of halos does depend on mass and so changing the relative number of galaxies in high-mass vs. low-mass halos changes the weight in the average of the halo bias in Equation (2.7). For example, assigning a large number of satellite galaxies to high-mass halos increases $\xi^{\rm 2halo}(r)$ by weighting highly-biased, high-mass halos more heavily. The possible range in the amplitude of the two-halo term is limited by the variation of the halo bias function $b_h(M)$, within the mass range relevant to galaxies, $10^{11} \lesssim M/M_\odot \lesssim 10^{15}$. At low masses, the halo bias is $b_h \sim 0.65$ while, in the cluster regime ($M \sim 10^{14} h^{-1} M_\odot$), it grows to values of $b_h \sim 2$ (Tinker et al., 2005). Bias continues to grow with mass, but more massive halos are rare and do not contribute

much to the weighted average because dn/dM is minuscule. The two-halo term scales like the square of the average bias $b_{\rm g}$ in Equation (2.7), so the possible dynamic range $\xi^{\rm 2halo}$ can display is, at most, a factor of ~ 9 and is usually significantly smaller. Simply put, the two-halo term depends weakly on the HOD because on large scales it is not possible to make galaxies significantly more or less clustered than the host halos they occupy.

On small scales, the one-halo term dominates and the situation is different. The number of galaxy pairs within an individual halo scales with $\langle N(N-1)\rangle_M$ while the number of random pairs scales with $\bar{n}_{\rm g}^2$, or $\langle N\rangle_M^2$. It is instructive to break the HOD into central and satellite galaxies. In the regime where there is one central galaxy per halo, the mean number of central-satellite pairs is $\langle N_{\rm cen}N_{\rm sat}\rangle_M = \langle N_{\rm sat}\rangle_M$, whereas the mean number of satellite-satellite pairs is $\langle N_{\rm sat}(N_{\rm sat}-1)\rangle_M/2$. Assuming a Poisson distribution for the number of satellite galaxies (Kravtsov et al., 2004a), $\langle N_{\rm sat}(N_{\rm sat}-1)\rangle_M = \langle N_{\rm sat}\rangle_M^2$. The mean number of random pairs scales like $(1+\langle N_{\rm sat}\rangle)_M^2$. In the limit $\langle N_{\rm sat}\rangle_M \gg 1$, the number of satellite-satellite pairs dominates the number of central-satellite pairs, but in this limit both the number of one-halo pairs and the square of the mean galaxy number density scale as $\langle N_{\rm sat}\rangle_M^2$ so the one-halo term saturates to a maximum value and is insensitive to the number of satellite galaxies per halo.

In most practical cases, the fraction of satellite galaxies in an observational sample is $f_{\rm sat} \lesssim 0.25$, so samples tend to be dominated by halos with satellite galaxy

populations in the opposite limit, $\langle N_{\rm sat}\rangle_M \ll 1$. This is due to the fact that very massive host halos are rare, so halos with $\langle N_{\rm sat}\rangle_M > 1$ are rare. With $\langle N_{\rm sat}\rangle_M \ll 1$, the central-satellite term dominates and the number of such pairs scales as $\langle N_{\rm sat}\rangle_M$ while the mean number density $\bar{n}_{\rm g}$ is approximately constant. Examination of Equations (2.4) and (2.5) reveals that in this regime $\xi^{\rm 1halo}$ scales *in proportion to the fraction of satellite galaxies and in inverse proportion to the number of host halos.* Host halo mass is largely fixed by requiring the galaxies in any sample to have an appropriate average number density (this is why rare galaxies exhibit strong small-scale clustering). Therefore, the one-halo term describing any given sample varies approximately linearly with $\langle N_{\rm sat}\rangle_M$ until $\langle N_{\rm sat}\rangle > 1$, at which point it saturates. It is interesting that nearly all the sensitivity of the correlation function to the HOD comes from central-satellite galaxy pairs in host halos where satellite galaxies are uncommon!

In this work, we aim to understand the origin of the nearly power-law galaxy correlation function. The relevant question is why is it that the number of galaxies (or satellite galaxies to be more specific) per halo is set just so that the one-halo and two-halo terms in the galaxy correlation function match smoothly, leaving only small deviations from a single power law over several orders of magnitude in scale? We confront this problem by studying the properties and evolution of subhalo populations. We now turn to some of the details of our modeling methods.

2.3 Overview of Halo Substructure Modeling

Our approach is to study the evolution of subhalos within virialized host halos as a method to understand satellite galaxies and, in turn, the evolution of galaxy clustering. We focus our attention on the relative strengths of small-scale and large-scale clustering. We study subhalo populations using the approximate semi-analytic model of Zentner et al. (2005, hereafter Z05). In this section, we briefly review the fundamental aspects of the model that are of immediate relevance and we refer the reader to Z05 for details and validation. The subhalo model is based on Zentner & Bullock (2003) and is similar to the independent models of Taylor & Babul (2004, 2005a,b) and Peñarrubia & Benson (2005), while sharing many features with other approximate treatments of halo substructure (Oguri & Lee, 2004; van den Bosch et al., 2005; Faltenbacher & Mathews, 2005; Purcell et al., 2007; Giocoli et al., 2008, 2009).

Semi-analytic models are an approximation to the calculations of large N-body simulations, yet such models offer many advantages: (1) semi-analytic calculations are computationally inexpensive; (2) they have no inherent resolution limits; (3) they enable the statistical study of subhalos within very large numbers of host halos; (4) they allow the growth and mass-loss histories of particular subhalos to be tracked without significant post-processing and analysis; (5) they make studies of model parameter space tractable; and (6) semi-analytic models facilitate parsing complex physical phenomena so that the relative importance of different physical effects may be understood. Our goal is to quantify the relative importance of merging, which increases

subhalo abundances, and dynamical friction and mass loss, which decrease subhalo abundances. We also aim to explore predictions for subhalo populations and galaxy correlation functions from high redshift to several Hubble times in the future. Z05 extensively tested the model we use in this paper and showed that the model produces subhalo mass functions, occupation statistics, and radial distributions within hosts that are in good agreement with a number of high-resolution N-body simulations (see the recent comparison in Koushiappas et al., 2010, as well).

The analytic model proceeds in several steps. For a host halo of a given mass M, observed at a given redshift z, we generate a halo merger tree using the mass-conserving implementation of the excursion set formalism (Bond et al., 1991; Lacey & Cole, 1993, 1994) developed by Somerville & Kolatt (1999, see Zentner 2007 for a review). This yields a complete history of the masses and redshifts of all halos that merged to form the final, target halo of mass M at redshift z. The host halo is the largest halo at each point in the merger tree. We model the density distributions of all halos as Navarro et al. (1997, hereafter NFW) profiles with concentrations determined by their merger histories according to Wechsler et al. (2002). At the time of each merger, we assign the subhalo initial orbital parameters drawn from distributions measured in N-body simulations (Z05, see Benson 2005 for similar formalisms). We then integrate each subhalo orbit within the host halo gravitational field, taking into account dynamical friction and mass loss. We estimate dynamical friction with an updated form of the Chandrasekhar (1943) approximation (Hashimoto et al.,

2003; Zentner & Bullock, 2003), account for internal heating so that scaling relations describing the internal structures of subhalos are obeyed (Hayashi et al., 2003; Kazantzidis et al., 2004; Kravtsov et al., 2004b), and allow for loss of material beyond the tidal radius on a timescale comparable to the local dynamical time. The details of each ingredient are given in Z05.

The correlation function of halos and subhalos and their associated galaxies is sensitive to the abundance of subhalos that survive both possible mergers with the central, host galaxy due to dynamical friction as well as mass loss and thus remain as distinct objects in orbit within their host halos with their galaxies intact. Therefore, it is necessary to specify conditions under which the galaxy within a subhalo may be "destroyed" and removed from our samples. In this work, we consider the clustering of mass-threshold samples of halos and subhalos as a proxy for luminosity-threshold samples of galaxies, so significant mass loss will lead to a galaxy that is either destroyed or dropped out of our sample. We assume such a scaling between halo mass and galaxy luminosity *solely for the sake of simplicity*. Our primary points are qualitative in nature, but we note that this is similar to other schemes that have described data successfully (e.g., Kravtsov & Klypin, 1999; Colín et al., 1999; Kravtsov et al., 2004a; Tasitsiomi et al., 2004; Conroy et al., 2006) and our calculations with similar, but more sophisticated assignments do not alter any of our basic results or conclusions. In rare cases, subhalos may survive close encounters with the center of their host halo potentials. We remove all subhalos that have orbital apocenters $r_{\rm apo} < 5$ kpc. This

choice is physically motivated because the galaxies within such subhalos would likely have merged with the central galaxy, or at least be observationally indistinguishable from the central galaxy. This choice is relatively conservative in that galaxies on larger orbits would also likely be influenced and it only affects the results of calculations in which tidal mass loss is not permitted (see below). The net result of evolving orbits for each subhalo in the merger tree is a catalog of all surviving subhalos in the final host halo at the time of observation. In some cases, a halo that merges into a larger host contains subhalos of its own. These subs-of-subs are only abundant inside very large host masses and are present in our model.

One of our aims is to study the individual roles of halo merging, dynamical friction, and mass loss on the clustering of halos. Therefore, we compute subhalo populations in four different sets of circumstances:

No Effects - a "bare-bones" model that does not allow satellite galaxies to be modified by dynamical friction or mass loss. In this case, any infalling subhalo remains intact, and we assume that this subhalo harbors a galaxy that will survive forever. This is tantamount to assuming that galaxies form in all sufficiently-large peaks in the primordial density field and survive until today.

Fric. Only - a model that only considers the effects of halo merging and dynamical friction. Subhalos never lose mass and can only be destroyed by sinking to the very centers of their hosts.

Strip. Only - a model that only considers halo merging and mass loss and assumes

no dynamical friction or central merging. Subhalos can lose mass and drop out of a mass threshold sample, but they cannot lose orbital energy and sink to the center of the host potential.

Full - our full model treating halo merging, dynamical friction, and mass loss. This is the model that was developed in Z05 and validated against N-body simulations.

We run our models for host masses[2] in the range from $\log(M_{\rm host}/h^{-1}M_{\odot}) = 11.0$ to 15.0 in steps of $\Delta(\log M_{\rm host}) = 0.1$. For each of these masses, we run 1000 statistical model realizations representing different realizations of the local density field and different halo merger histories. In this way, we sample the statistical properties of subhalo populations over the entire range of host halo masses relevant to galaxy-galaxy correlations. We repeat this process for host masses at $z = 0$ as well as two past redshifts, $z = 3$ and $z = 1$, and two future redshifts, $z = -0.6$, and $z = -0.9$.

2.4 Effects of Subhalo Dynamics on the Galaxy Correlation Function

2.4.1 Halo Occupation Distribution Statistics

The galaxy correlation function may be considered primarily a function of the galaxy HOD (e.g., Berlind & Weinberg, 2002). The prevailing cosmological model is now stringently constrained and may be considered fixed for our purposes. Moreover, theoretical predictions of the abundances, clustering, and structures of host dark

[2]We note that we use the "virial" definition of a halo in which a halo is defined as a spherical region of mean density equal to $\Delta_{\rm vir}$ times the mean background density. For our cosmological model, $\Delta_{\rm vir} = 337$ at $z = 0$ and approaches 178 at high z.

matter halos in the concordance cosmology are now well established. Consequently, we focus on the properties of the HOD and the manner in which the HOD determines galaxy clustering.

We expect that each host halo of sufficient size contains one dominant, central galaxy associated with the host itself, as well as additional satellite galaxies that are associated with relatively large subhalos. Thus, the HOD of galaxies should resemble the HOD of all halos (hosts plus their subhalos), and such a model is bolstered by significant empirical support (Kravtsov & Klypin, 1999; Colín et al., 1999; Kravtsov et al., 2004a; Tasitsiomi et al., 2004; Conroy et al., 2006). As a result, we concentrate on the insight that can be gleaned about the development of the HOD of all halos, paying particular attention to the separate effects of halo mergers, dynamical friction, and mass loss.

The left column of Figure 2.2 shows the mean occupation number of host halos and subhalos as a function of host halo mass $\langle N \rangle_M$, at $z = 0$. The three panels give results for halo samples defined by different mass thresholds. In the interest of simplicity, we assume that all host halos and surviving subhalos with masses $M \geq M_{\rm min}$ harbor an observable galaxy. This assignment is simpler than those supported by detailed comparisons to data, which typically assume that all host halos and surviving subhalos with masses $M \geq M_{\rm min}$ (or some maximum circular velocity) *at the epoch of accretion* harbor an observable galaxy. We proceed in this manner because the subtleties discussed in the aforementioned literature do not influence our primary points

and may serve to obscure them. This is primarily because any mass threshold chosen at the epoch of accretion will have a second "destruction" threshold due to the finite resolution of a given N-body simulation. This can alter clustering measurements, and since the aim of this paper is to present the qualitative trends responsible for the low-redshift correlation function, we use the simpler final mass approximation. We have confirmed that using mass at accretion with our model reproduces the same general results. In a forthcoming paper we consider more sophisticated models to compare with data. In the top, middle, and bottom panels we show samples with $\log(M_{\rm min}/h^{-1}M_{\odot}) = 11.4,\ 11.7$, and 12.3, respectively. These particular mass thresholds result in average galaxy number densities (see Eq. [2.3]) equal to those in observed SDSS samples with r-band luminosity thresholds of $M_r < -18.5,\ -19.5,$ and -20.5 (Zehavi et al., 2005b). The four curves in each panel represent the four model modes described in § 2.3, and we calculate each curve from the mean of the 1000 model realizations.

First, the black dot-dashed curves represent the *No Effects* model. As explained in § 2.3, this model assumes that any halo that merges into a larger host system (and becomes a subhalo of that system) is thereafter unaltered by dynamical effects in the host halo environment. Physically, this corresponds to the simple (and observationally untenable) assumption that each subhalo above $M_{\rm min}$ brings with it an observable galaxy upon merging into the host and that this galaxy is not destroyed or dimmed by dynamical evolution within the host halo. In effect, each local peak of sufficient

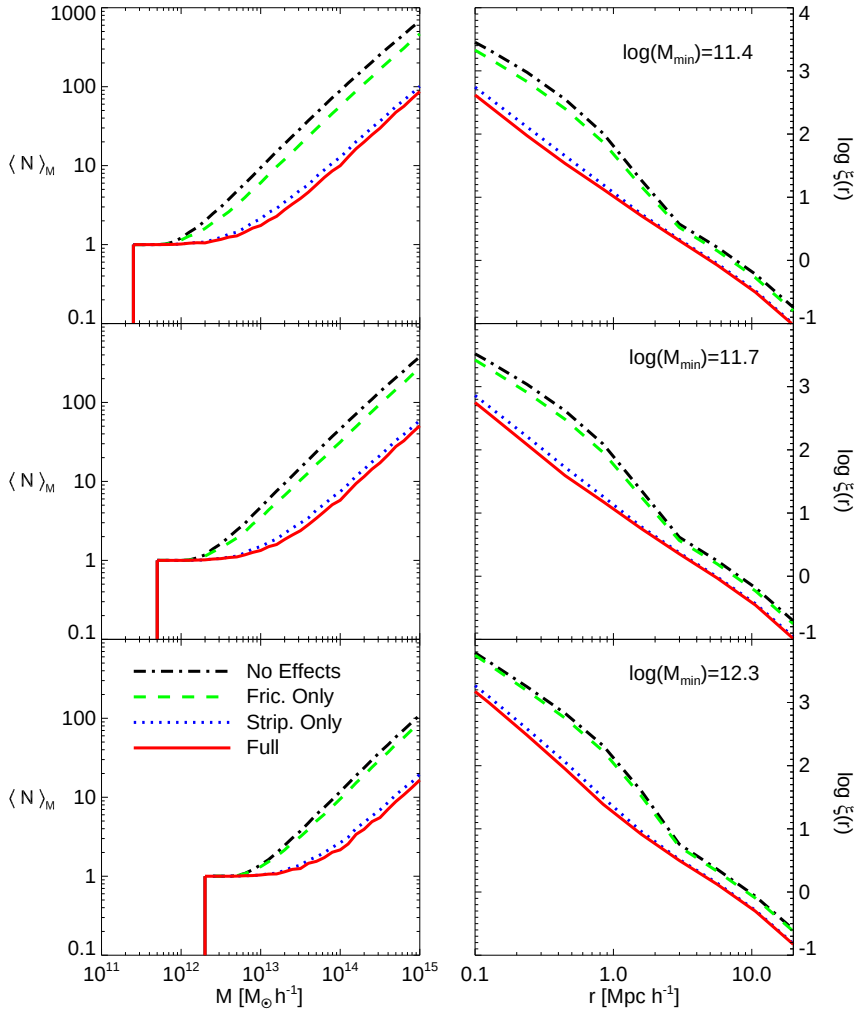

Figure 2.2: *Left Panels*: Mean number of all halos (hosts plus subhalos) predicted by our subhalo model as a function of host halo mass, at redshift $z = 0$. The three panels show results for three mass threshold values: $\log(M_{\rm min}/h^{-1}M_\odot) = 11.4, 11.7$, and 12.3. The four curves in each panel correspond to the four models described in § 2.3: *No Effects* considers no gravitational effects on subhalos as they orbit inside their host halos (black dot-dashed curve); *Fric. Only* considers only the effects of dynamical friction (green dashed curve); *Strip. Only* considers only the effects of mass loss (blue dotted curve); *Full* considers both dynamical friction and mass loss (solid red curve). *Right Panels*: The correlation function of all halos predicted by our subhalo model. $\xi(r)$ is computed from the halo model using the occupation statistics shown in the left panels. The figure shows that dynamical effects (especially mass loss) are needed in order to reduce the number of subhalos sufficiently and produce a power-law correlation function.

mass in the smoothed density distribution forms a galaxy and the galaxy can not be destroyed. Of course, we expect the mean halo occupation in this model to be high for all host masses as compared to the other models.

Next, we turn to the curves depicting the individual effects of dynamical friction (*Fric. Only*, green dashed curves) and mass loss (*Strip. Only*, blue dotted curves). These dynamical mechanisms can destroy subhalos, but they cannot affect the host halo or central galaxy. This is why all the curves converge to the value $\langle N \rangle_M = 1$ at low host masses. As a convenient shorthand, we refer to any subhalo that fell into its host system with a mass $M_{\rm sub} \geq M_{\rm min}$, but then merged with the central host galaxy or lost sufficient mass to fall below this threshold, as *destroyed*. This does not mean that the subhalo has become unbound, but merely that it has either merged or no longer has a bound mass above some minimum mass threshold.

Dynamical friction acting alone destroys subhalos by causing them to sink to the centers of their hosts and "merge" with it. This mechanism alone causes a 20-35% decrease in the mean number of surviving satellites for all host masses as compared to the *No Effects* model. The fractional decrease in subhalos depends only weakly on host mass, but a comparison of the different mass threshold panels shows a modest dependence on subhalo mass, with smaller mass subhalos being depleted more. These trends are counter-intuitive because the dynamical friction force is an increasing function of $M_{\rm sub}/M_{\rm host}$, the mass ratio between the subhalo and its host (Binney & Tremaine, 2008). One might expect the depletion of subhalos to be larger for smaller

host masses at fixed subhalo mass or for larger subhalo masses at fixed host mass. Our results differ from this expected behavior for two reasons. First and foremost, low-mass-ratio mergers tend to occur at higher redshifts than high-mass-ratio mergers. At higher redshifts, host halos are significantly smaller than they are at present, so high-redshift mergers probe only the dense interiors of contemporary host halos and evolve approximately according to the subhalo-host mass ratio at the redshift of the merger. These early-merging subhalos also have a longer period of time during which to evolve. Second, our models include subhalos-of-subhalos. As we move to larger host masses at fixed subhalo mass or smaller subhalo masses at fixed host mass, more subhalos are subs-of-subs that have much higher mass ratios with their immediate hosts. These effects result in the trends we see in Figure 2.2.

Mass loss is significantly more effective at "erasing" subhalos than dynamical friction. Mass loss processes can effectively "destroy" subhalos because many lose sufficient mass to fall below the threshold of a sample. This mechanism typically drives an 80-85% decrease in the number of objects above a given mass threshold compared to the *No Effects* model. Again, the fractional decrease in subhalos is nearly independent of host mass, but it shows a slight dependence on subhalo mass, with smaller mass subhalos being destroyed more efficiently.

Finally, the *Full* model (red, solid curves) includes the effects of both subhalo mass loss and orbital decay by dynamical friction. These processes do not simply sum together. As a subhalo sinks deeper into its host potential well due to dynamical

friction, it experiences a stronger tidal field and is thus more efficiently stripped of its mass. Conversely, less massive subhalos are less susceptible to orbital decay via dynamical friction. A comparison of the *Full* model to the *Strip. Only* model shows that including dynamical friction causes an additional $\sim$ 15% depletion of substructure. Mass loss is by far the dominant cause of subhalo destruction. Overall, Figure 2.2 shows that dynamical effects reduce the number of subhalos by $\sim$ 90% compared to the number of distinct mergers that occur during the formation of a host halo.

2.4.2 Constructing the Correlation Function

We use the halo model outlined in § 2.2 to compute the correlation function predicted by our subhalo model. Specifically, we use the Jenkins et al. (2001) mass function and we follow Tinker et al. (2005) in using the Smith et al. (2003) formula for the non-linear matter power spectrum and the Tinker et al. (2005) scale-dependent halo bias relative to the non-linear power spectrum. We derive HOD statistics from our subhalo models as exemplified by the previous section, and we compute the pair separation distributions by assuming that the radial distributions of satellites follows an NFW profile for simplicity. In actuality, the subhalo distributions in both our models and N-body simulations are slightly shallower than NFW (see Z05 for model and simulation results). We adopt the NFW profile for analytical convenience as deviations from NFW are small and only influence correlation functions notably on

scales significantly smaller than $r \sim 100h^{-1}$kpc (e.g., Z05; also see Watson et al. 2010 for a demonstration of this point regarding satellite galaxies).

The right column of Figure 2.2 shows the host+subhalo correlation functions computed in this manner from the HODs predicted by our subhalo model. In the *No Effects* case, where no subhalos are destroyed, $\xi(r)$ is very different from a power law, having a one-halo term that is too large relative to the two-halo term so that a distinct feature is present in $\xi(r)$ on scales $r \sim 2$ Mpc. In fact, comparing this to Figure 2.1, we see that it is very similar to the dark matter correlation function. This is perhaps not surprising because subhalos in this model behave as massive test particles that cannot be altered. As dynamical effects are included and substructure is consequently depleted, $\xi(r)$ drops on all scales. Recall that only subhalos (hosting satellite galaxies) can be destroyed and the number of host galaxies remains unaltered. The fraction of all objects that are satellites therefore decreases. As we discussed in § 2.2, for a fixed population of central galaxies, the one-halo term drops in approximate proportion to the number of satellite galaxies. So as the number of satellites declines, so does the number of pairs within halos relative to the total number of pairs and the one-halo term declines.

Large-scale clustering is less sensitive to changes in the satellite galaxy population. The two-halo term drops because subhalos tend to populate more massive hosts (as in the left column of Figure 2.2), so the average host halo mass of a sample decreases as subhalos are depleted. The large-scale clustering strength of halos increases with

halo mass, so this depletion results in weaker large-scale clustering. The variability of the two-halo term is relatively mild because the halo bias is not a rapidly-varying function of halo mass near $M \sim M_{\rm min}$ (Tinker et al., 2005).

With enough depletion of substructure, the one- and two-halo terms align and result in a nearly power-law shape. This is exactly what happens in Figure 2.2. In our *Full* subhalo model the correlation function is roughly a power law. To obtain a nearly power-law galaxy correlation function, it is necessary that a majority of early galaxies and proto-galaxies that merge to form a massive system at low redshift be destroyed through either central mergers or mass loss. Our results suggest that mass loss is mainly responsible for this depletion, while dynamical friction and central galaxy mergers play a comparably small, supporting role. Incidentally, this picture implies that infalling satellite galaxies lose significant stellar mass so that they provide an important source of the diffuse intracluster light observed in galaxy groups and clusters and this picture is consistent with observations (Purcell et al., 2007, 2008). Comparing our correlation function results for the three different mass thresholds, we note that $\xi(r)$ is closer to a power law for lower-mass samples. We revisit this point in the next section.

We now return to the mean occupation statistics shown in the left panels of Figure 2.2. The so-called "plateau" region of the HOD is the flat region at $\langle N \rangle_M = 1$, where host halos are more massive than $M_{\rm min}$, but not yet massive enough to host

subhalos above our mass threshold [3]. As substructure is depleted, the prominence of this plateau increases. The "length" of the plateau in the HOD can be expressed as the ratio between the mass of a halo that hosts a single satellite on average, M_1, to the minimum mass required to host a central galaxy, $M_{\rm min}$. Zehavi et al. (2005b) fit an HOD model to the measured correlation function of SDSS galaxies and found that a ratio $M_1/M_{\rm min} \sim 23$ is consistent with clustering data, nearly independent of galaxy luminosity. In other words, a consistent picture is one in which the entire HOD shifts to higher masses in a self-similar manner, with $M_1/M_{\rm min}$ fixed, in order to accommodate higher-luminosity samples. Remarkably, Kravtsov et al. (2004a) studied this for subhalos in a high-resolution N-body simulation and found that $M_1/M_{\rm min} \sim 20$, regardless of $M_{\rm min}$ as well. Meanwhile, Tinker et al. (2005) fit a slightly more complex HOD model to the SDSS data and found that $M_1/M_{\rm min} \sim 25$ for galaxy samples with luminosities less than L^*, but decreases to $M_1/M_{\rm min} \lesssim 5$ to accommodate the highest-luminosity samples (absolute r-band magnitudes $M_r \leq -21$). The new analysis by Zehavi et al. (2011) also finds this trend with $M_1/M_{\rm min} \sim 17$ for $M_r \geq -20.5$ and much lower values for higher luminosity galaxies. For the purpose of comparison, the *Full* subhalo model shown in Figure 2.2 predicts $M_1/M_{\rm min} \sim 40$ for the low-mass samples of $\log(M_{\rm min}/h^{-1}M_\odot) = 11.4$ and $\log(M_{\rm min}/h^{-1}M_\odot) = 11.7$, and $M_1/M_{\rm min} \sim 30$ for the higher-mass sample of $\log(M_{\rm min}/h^{-1}M_\odot) = 12.3$.

[3]Roughly speaking, the most massive subhalo within any host is a few percent of the mass of the host halo (e.g., Z05). This is the case with, for example, the Large Magellanic Cloud within the halo of the Milky Way (Busha et al., 2010).

These results suggest that getting the length of the HOD plateau right may be a key ingredient needed to establish a power-law correlation function and this has been part of the interpretation in the literature. The importance of $M_1/M_{\rm min}$ stems from the fact that most one-halo pairs reside in halos with average satellite numbers $\langle N_{\rm s}\rangle_M \lesssim 1$, so modeling the HOD at relatively low satellite occupation numbers is critical (see Conroy et al., 2006). We investigate this further in § 2.6.

2.5 Mass and Redshift Dependence of the Correlation Function

2.5.1 Dependence on Mass

While dynamical processes act in a manner to deplete substructure and push $\xi(r)$ toward a power law at all mass thresholds, it is evident that deviations from a power law are stronger with increasing host mass. Figure 2.3 shows the correlation functions predicted by our *Full* subhalo model for four different mass thresholds, ranging from $\log(M_{\rm min}/h^{-1}M_\odot) = 13.5$, corresponding to bright galaxies such as Luminous Red Galaxies (LRGs), down to $\log(M_{\rm min}/h^{-1}M_\odot) = 10.5$, corresponding to dwarf galaxies. While the correlation function of the "dwarf" sample is a near power law, that of the "LRG" sample exhibits strong departures from power-law behavior. This trend has been detected with SDSS galaxies by Zehavi et al. (2005b) who found evidence that a power-law model provides a better fit to low-luminosity galaxies than high-luminosity galaxies. Halo and subhalo clustering exhibits the same trend. More massive halos contain slightly more of their bound masses in substructure relative to less massive

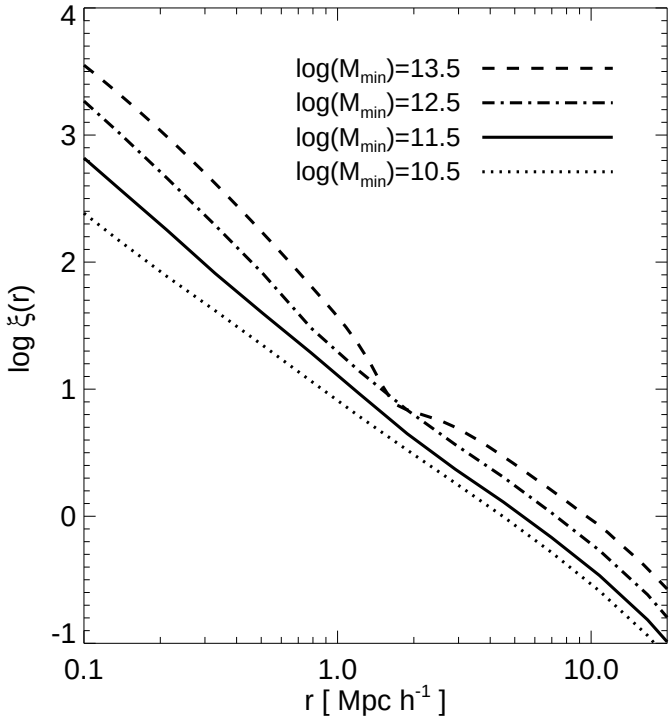

Figure 2.3: Correlation function of all halos (hosts plus subhalos) predicted by our subhalo model at redshift $z = 0$. The four curves show $\xi(r)$ for four mass threshold samples and the threshold values $M_{\rm min}$ (in units of $h^{-1}M_{\odot}$) are listed in the panel. The figure shows that $\xi(r)$ breaks more and more from a power law for higher mass halo samples, which correspond to higher luminosity galaxy samples.

halos, but this is a comparably small effect (Z05) and drives only $\sim$ 30% of the mass-dependence of the one-halo term in Figure 2.3. At *fixed redshift*, the departure from a power-law at high mass (high luminosity) is caused by the relative rareness of high-mass host halos (see § 2.2.2 for interpretive discussion).

2.5.2 Dependence on Redshift

Substructure abundances vary with time. Infall of new subhalos acts as a "source" of halo substructure. The rate of mergers of halos into larger systems is a function of redshift that typically peaks at redshifts $z \sim 1 - 3$ in the halo mass range of interest and declines thereafter (Z05; Zentner 2007). Once a subhalo merges into a larger host halo, dynamical friction shrinks its orbit and the subhalo loses mass. Given enough time, the subhalo will eventually lose enough mass to fall below $M_{\rm min}$ or merge with the central galaxy and lose its identity. The balance between the halo merger rate and the rates of destructive processes (which occur on a halo dynamical time) determine the redshift dependence of halo substructure.

Figure 2.4 shows the redshift evolution of the mean halo occupation number and resulting correlation functions. The layout of Figure 2.4 is similar to that of Figure 2.2, with $\langle N \rangle_M$ shown in the left panels, $\xi(r)$ shown in the right panels. However, in Figure 2.4 all results are for the *Full* subhalo model, and the various lines denote quantities evaluated at different redshifts, $z = 3,\ 1,\ 0,\ -0.6,\ -0.9$ (where negative redshifts correspond to *future* epochs). Moreover, in each panel the correlation functions are scaled by a power law to better highlight departures from a power-law shape.

The left-hand panels of Figure 2.4 show that the average number of subhalos within hosts of a given mass starts out high at early times and begins to decrease after $z = 3$, as merger rates decline. By the present epoch ($z = 0$), the number of

subhalos has dropped by $\sim 25-30\%$ relative to what it was at $z = 3$. One Hubble time into the future ($z = -0.6$), the abundance of substructure has dropped by $\sim 60\%$. This is because the rate of merging as a source for new subhalos declines rapidly. This decrease in the merger rate is dictated in large part by the quenching of structure growth by the cosmological constant (Carroll et al., 1992), but also because most halos of interest are below the typical collapsing mass, which approaches $M^* \simeq 10^{14}\, h^{-1}\mathrm{M}_\odot$ in the future (Zentner, 2007). Meanwhile, destructive processes continue to operate on orbiting halo substructure for several additional dynamical times. Three Hubble times into the future ($z = -0.9$) the average halo occupation has dropped by $\sim 90\%$. As with our previous results, the fractional decrease in subhalo abundance appears to be roughly independent of host mass, meaning that the slope of the HOD in the high-$\langle N \rangle_M$ limit is not significantly altered by evolution. The amplitude of $\langle N \rangle_M$ declines considerably, resulting in increasing $M_1/M_{\rm min}$, or a "lengthening" of the HOD plateau with time. This behavior is strikingly similar to that seen in Figure 2.2 in the sense that turning on dynamical effects at a fixed redshift has a qualitatively similar impact as evolving forward in time, and the effects on the correlation function are similar.

Turning to the right panels, $\xi(r)$ is shown at each redshift scaled by an $r^{-1.7}$ power law in order to emphasize features in the correlation function. Starting at $z = 3$ (long dashed curves), $\xi(r)$ is very far from a power-law, with a slope that is much steeper on small scales. At $z = 1$ (short dashed curves) the break from a power law is less pronounced, but it is still significant. These results are qualitatively consistent with

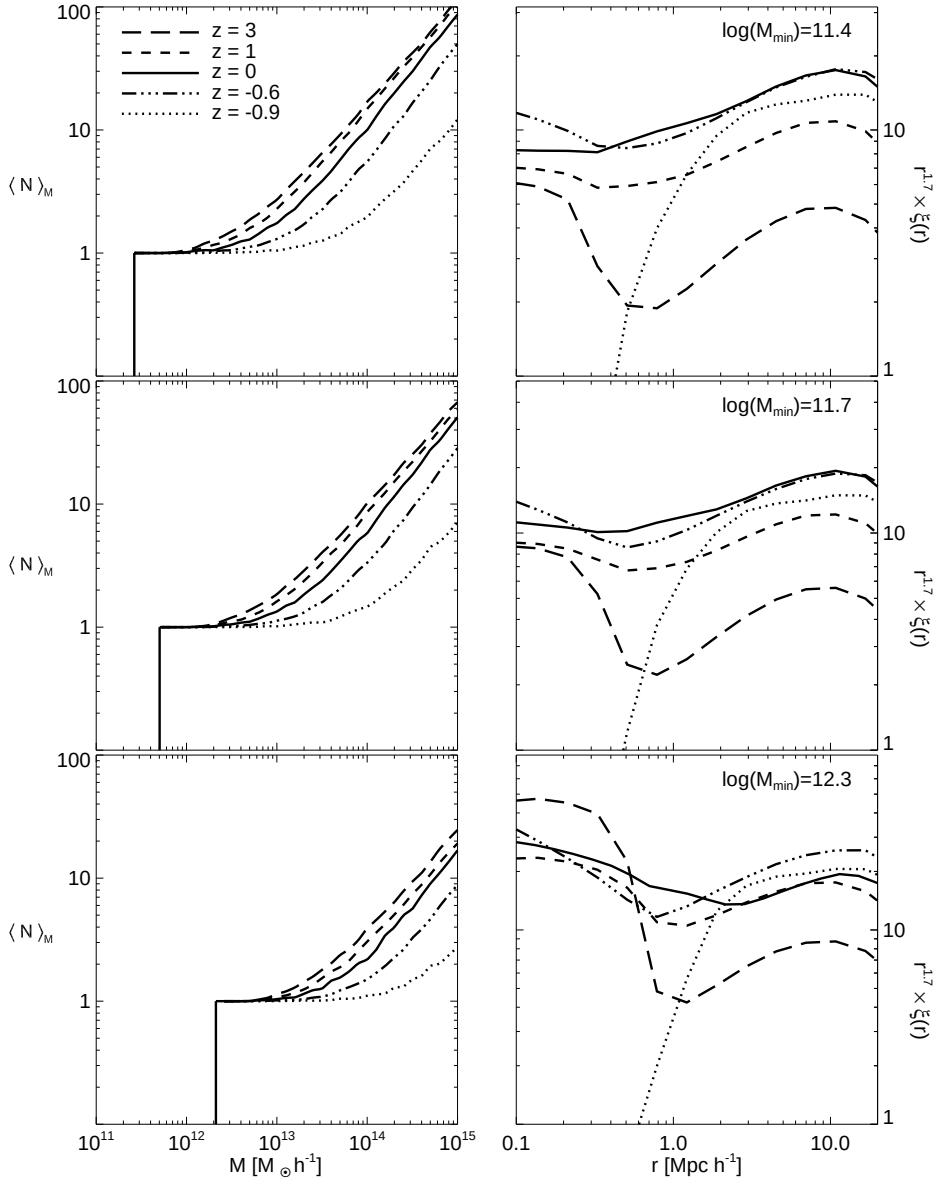

Figure 2.4: *Left panels*: Mean number of all halos (hosts plus subhalos) predicted by our *Full* subhalo model as a function of host halo mass, at five different redshifts. The three panels show results for three mass threshold values: $\log(M_{\rm min}/h^{-1}M_\odot) = 11.4$, 11.7, and 12.3. The five curves in each panel correspond to the redshifts $z = 3, 1, 0, -0.6, -0.9$ (negative redshifts correspond to future epochs). *Right panels*: Correlation functions corresponding to the halo samples shown in the left panels. In each case, $\xi(r)$ has been scaled by a power law in order to clearly show departures from a power-law shape. The figure shows that the number of subhalos steadily decreases from high to low redshift, causing the correlation function to evolve from not being a power law at high redshift, towards having a nearly power-law shape at the present epoch, and once again deviating from a power law at future epochs.

clustering measurements at high redshifts (Coil et al., 2006; Ouchi et al., 2005; Lee et al., 2006). At $z = 0$ (solid curves), the correlation function is approximately a power law, though there is still a mild, discernible feature at the transition scale between the one- and two-halo terms. In the future, $\xi(r)$ once again breaks from a power law. At $z = -0.6$ (dot-dashed curves), departures from a power-law shape are about as strong as they were at $z = 1$. Three Hubble times into the future, at $z = -0.9$ (dotted curves), the departures from a power law are significant and represent a dramatic reduction in the relative contribution of the one-halo term.

Figure 2.5 focuses on the $\log(M_{\rm min}/h^{-1}M_{\odot}) = 12.3$ threshold sample and shows the correlation function at four different redshifts, while also showing the one-halo and two-halo terms explicitly. Figure 2.5 clearly demonstrates how a delicate balance is needed between the two terms in order for $\xi(r)$ to achieve a power-law shape. The two-halo term exhibits modest variations from panel to panel, with a range of about a factor of ~ 3. The decreased large-scale clustering at $z \gtrsim 0$ is due to the linear growth of perturbations with time, but this is always kept modest because the increasing bias of halos of fixed mass with redshift (see Zentner, 2007) compensates for large-scale structure growth. At $z < 0$, the slight decrease in two-halo clustering is due to the decay of halo bias once halo growth slows (Fry, 1996).

The variation in the one-halo term is significantly larger, as our earlier discussions suggest, and changes by a factor of $\sim 45 - 150$ (depending on scale), equivalent to $\sim 15 - 50$ times the variation in the two-halo term. At high redshift, the relative

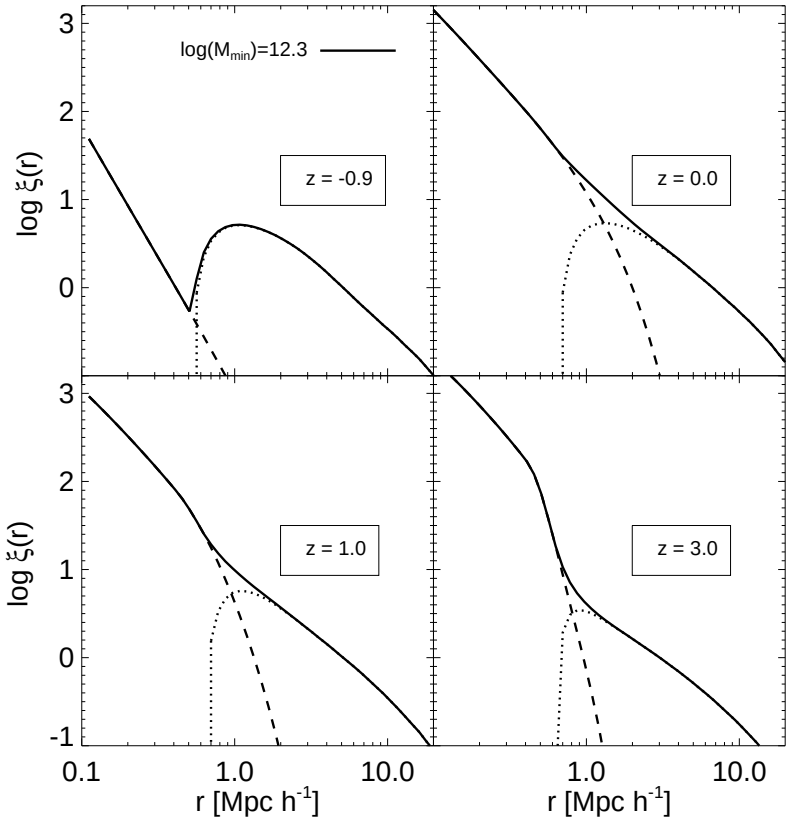

Figure 2.5: The correlation function of all halos (hosts plus subhalos) predicted by our *Full* subhalo model as a function of redshift, for a single mass threshold sample $\log(M_{\rm min}/h^{-1}M_\odot) = 12.3$. Each panel shows $\xi(r)$ for a different redshift (solid curve), as well as the one-halo (dashed curve) and two-halo (dotted curve) terms. The figure shows that the one-halo term evolves strongly with redshift and only at $z = 0$ strikes the right balance with the two-halo term to result in a power law.

rareness of host halos and the large amount of substructure cause $\xi(r)$ to be boosted significantly in the one-halo regime as shown in the $z = 3$ panel of Figure 2.5. At $z = 0$, just the right amount of substructure has been depleted to strike a near balance between the one-halo and two-halo contributions. In the future, the continual destruction of subhalos suppresses the one-halo term, driving $\xi(r)$ away from a power law again. By $z = -0.9$, the depression in small-scale clustering is striking.

Some of the evolution of $\xi(r)$ on small-scales comes from the fact that halos large enough to host luminous galaxies become increasingly rare as redshift increases. The characteristic collapsing mass is a rapidly decreasing function of redshift and is only $M^* \approx 10^9\, h^{-1}\mathrm{M}_\odot$ at $z = 3$. In the relevant regime, the strength of the one-halo term grows in approximate proportion to the number of satellite galaxies and in inverse proportion to the number of host halos of appropriate size (see § 2.2), so the relative paucity of host halos at high redshift also drives strong one-halo clustering because Fig. 2.5 describes samples of fixed absolute mass threshold. However, it is subhalo abundance that has the larger influence on the redshift dependence of clustering. We have computed the correlations of Figure 2.5 using samples in which $M_{\rm min}$ varies with redshift so as to maintain a *constant number density* of halos. These samples are less subject to the gross evolution of the halo mass function. We find all of the same qualitative results for this case, though the two-halo term varies by a factor of ~ 4, while the variation in the one-halo term is limited to a factor of $\sim 12 - 80$ (again, depending on scale), resulting in a variation in the one-halo term that is $\sim 3-20$ times larger than that of the two-halo term. Moreover, we have re-computed correlation functions using a combination of the predicted low-redshift HODs alongside the high-redshift mass functions in order to isolate the contribution due to the mass function and HOD evolution. The majority the redshift dependence of $\xi(r)$ on small scales is due to the evolution of subhalo abundance. To maintain a power-law correlation function at high-redshift would require fewer subhalos per host than at $z = 0$ in order

to compensate for the relative rareness of host halos at high-redshift. In fact, hosts at high redshift have a *larger* number of subhalos of any given mass so these effects *reinforce one another*, leading to a strong deviation from a power-law $\xi(r)$ at high redshift.

We have already described the reasons that the one-halo and two-halo terms behave so differently under changes in the HOD. To reiterate, on large scales, $\xi(r)$ is essentially a weighted average of the clustering of host halos, where $\langle N \rangle_M$ provides the weighting (see the integral in Eqs. [2.6] and [2.7], note that $\tilde{\lambda}(k, M) \approx 1$ for $k < 1/R_{\rm vir}$). The possible variability in $\xi(r)$ on large scales is limited because it is always bound by the limited variation in the clustering of host halos. As we discussed in § 2.2, the difference in the large-scale bias of the largest relative to the smallest halos is at most a factor of ~ 3 (e.g., Tinker et al. 2005). Significant variations in large-scale clustering require dramatic variations in the HOD at high mass, which are not expected on theoretical grounds and are not mandated by data. However, on scales smaller than the size of individual host halos, $\xi(r)$ can vary dramatically depending on the HOD. For example, in the extreme case of only one object per host halo, there will be zero pairs within halos and the one-halo term will vanish. For large numbers of satellites, the one-halo term will be significantly larger than a power-law extrapolation of the two-halo term to small scales.

The sensitivity of the one-halo term to the HOD, coupled with the relative insensitivity of the two-halo term, means that achieving a power-law correlation function

requires fine-tuning in the number of satellite galaxies per halo. The satellite galaxy abundance naturally evolves with redshift, so $\xi(r)$ can only be a power law during those epochs when substructure has evolved to join the one-halo term to the two-halo term. Of course, it may be possible for features in the host halo mass function or bias relations to conspire to compensate for substructure evolution, but such features would somehow need to be coordinated with low-redshift structure growth. A different way to state this is that the halo mass function and halo bias depend on the statistics of the linear density field, and do not "know" about the non-linear galaxy formation and gravitational processes that occur within halos. It would be quite strange if their evolution were somehow connected with the evolution of satellite galaxies in virialized hosts. It seems to be a coincidence that the epoch of near power-law clustering of typical galaxies lies near $z = 0$.

2.5.3 The Balance Between Accretion and Destruction

We have just seen how the depletion of substructure over time leads to evolution in the correlation function such that it becomes a power law at the present epoch. However, what drives substructure depletion? We expect that most subhalos will lose significant amounts of mass or merge with the central galaxy given sufficient time. However, this will be compensated to some degree by the infall of new subhalos. If the rate at which satellites are accreted is greater than the rate at which they are destroyed, then the net amount of substructure will grow with time. The evolution in

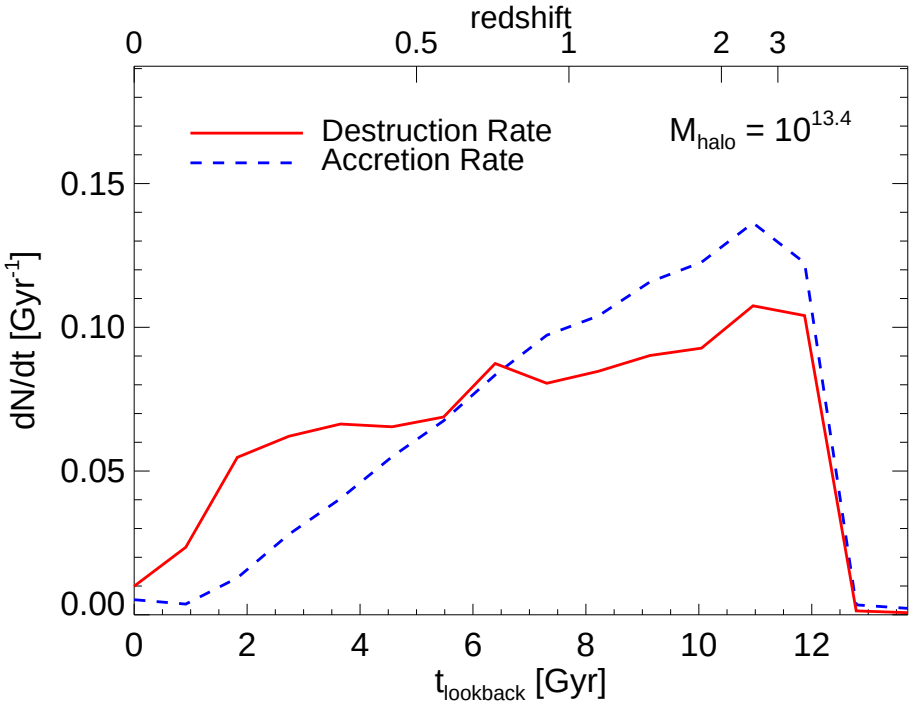

Figure 2.6: The accretion versus destruction rate of subhalos over cosmic time, as predicted by our full subhalo model. The accretion rate shown is the number of subhalos per Gyr that merge into a host halo of mass $\log(M/h^{-1}M_\odot) = 13.4$. The destruction rate is the number of these same subhalos per Gyr that are destroyed (i.e., their mass drops below some threshold value). The two rates equalized when the Universe was $\sim$ 6Gyr old (at $z \sim 1$). Before $z = 1$, the net number of subhalos increased with time, whereas at later times the net number decreased with time. The figure shows how the balance between accretion and destruction changes with redshift, which explains why the correlation function can only be a power law at a single epoch.

the number of subhalos (and hence the correlation function) depends on the balance between accretion and destruction. Z05 give a related discussion of accretion and destruction in their § 4.4 and the perspective we adopt here complements Z05.

In Figure 2.6 we illustrate the competition between accretion and destruction in host halos of mass $M = 10^{13.4}\ h^{-1}\mathrm{M}_\odot$. To measure the accretion rate (dashed curve), we count all subhalos with masses greater than $10^{11}h^{-1}M_\odot$ that accrete onto

these hosts in finite time intervals. For the destruction rate (solid curve), we count the number of these same subhalos that drop below $10^{11}h^{-1}M_{\odot}$ during the time intervals. The accretion rate minus the destruction rate will then give us the net rate of change in the number of subhalos per unit time.

Figure 2.6 shows that the accretion rate quickly grew and reached a peak at $z \sim 2-3$. Since this peak, the accretion rate has been steadily declining and is close to zero at the present epoch. The decline in merger rates is partly due to the shape of the power spectrum (see Lacey & Cole, 1993; Somerville & Kolatt, 1999; Zentner, 2007), but the driving force for the recent fast decline in the merger rate of halos is the reduced rate of structure growth caused by accelerated cosmic expansion. The destruction rate also peaked at $z \sim 2-3$ and lags the accretion rate because most destruction happens over a period of several dynamical times. Figure 2.6 clearly shows that the accretion rate has been dropping faster than the destruction rate since their peaks, with accretion and destruction roughly balancing just below $z \sim 1$ (see also Stewart et al., 2009). This means that the number of subhalos in hosts that grow to a mass of $M = 10^{13.4}\ h^{-1}\mathrm{M}_{\odot}$ by $z = 0$ increased until $z \approx 1$ and has been declining ever since, despite the fact that the virial masses of these halos have been growing. The general trend toward reduced substructure at low redshift explains the behavior exhibited in Figure 2.4. The correlation function is close to a power law at the present epoch because the balance between accretion and destruction over time has led to the requisite abundance of substructure today.

2.6 Achieving a Power-Law Correlation Function

We now step back from making predictions using our specific subhalo model and undertake a general exploration of the properties of the HOD that yield nearly power-law correlation functions at different masses and redshifts. The HOD characterizes the number and spatial distribution of galaxies within dark matter halos. It is typically specified with a handful of parameters that are constrained using galaxy clustering measurements (e.g., Magliocchetti & Porciani, 2003; Zehavi et al., 2005b; Tinker et al., 2005; Zheng et al., 2007). We choose an HOD model that is motivated by theoretical predictions from hydrodynamic simulations, semi-analytic models, and high-resolution N-body simulations (Berlind et al., 2003; Kravtsov et al., 2004a; Zheng et al., 2005). According to this model, halos above some threshold mass contain a single "central" galaxy plus a number of "satellite" galaxies. The number of satellites in any given halo is drawn from a Poisson distribution whose mean is a power-law function of host halo mass. The central galaxy is placed at the center of the host halo, while the satellites are spatially distributed according to an NFW density profile. Specifically, we adopt an HOD parametrization that is similar to the one used by Tinker et al. (2005). This is a simple, yet powerful model in which the number of central galaxies is modeled as a step function,

$$N_{\rm cen} = \begin{cases} 1 & \text{if } M \geq M_{\rm min} \\ 0 & \text{if } M < M_{\rm min} \end{cases} , \tag{2.8}$$

while the mean number of satellites follows a power-law with an exponential cutoff at low mass,

$$\langle N_{\rm sat}\rangle_M = \left(\frac{M}{M_1}\right)^{\alpha} \exp\left(\frac{-M_0}{M}\right). \tag{2.9}$$

The parameters in the model are as follows.

1. $M_{\rm min}$ is the minimum host halo mass to contain a central galaxy.

2. M_0 is the host halo mass below which satellite galaxies are exponentially suppressed.

3. M_1 is the host halo mass to contain, on average, one satellite galaxy.

4. α is the index of the power-law relation between the mean number of satellite galaxies and halo mass.

Previous studies have shown that the power-law index $\alpha \approx 1$ for subhalos and simulated galaxies (Kravtsov et al., 2004a; Zheng et al., 2005; Zentner et al., 2005), as well as observed galaxies dimmer than L^* (Zehavi et al., 2005b), leading Tinker et al. (2005) to set $\alpha = 1$ throughout their analysis. However, we allow α to vary because the correlation function is sensitive to it and, although it may be near unity when modeling observed data, it may need to deviate from unity to yield a power-law correlation function at high redshifts. On the other hand, $\xi(r)$ is not sensitive to M_0, consequently we fix its value by adopting the Conroy et al. (2006) $M_0 - M_1$ relation,

$$\log(M_0/h^{-1}M_\odot) = 0.76\ \log(M_1/h^{-1}M_\odot) + 2.3. \tag{2.10}$$

The result is an HOD model with only three free parameters: $M_{\rm min}$, M_1, and α.

The two-halo term of $\xi(r)$ depends on the mean occupation $\langle N \rangle_M = \langle N_{\rm cen} + N_{\rm sat} \rangle_M$, which is equal to $1 + \langle N_{\rm sat} \rangle_M$ for $M > M_{\rm min}$. The one-halo term also requires the second moment of the occupation distribution $\langle N_{\rm sat}(N_{\rm sat} - 1) \rangle_M$, so characterizing the mean occupation is not sufficient. We assume that the number of satellites follows a Poisson distribution, for which $\langle N_{\rm sat}(N_{\rm sat} - 1) \rangle_M \equiv \langle N_{\rm sat} \rangle_M^2$. Our *Full* model deviates mildly from a pure Poisson distribution (see Fig. 7 of Z05, and recent simulations of Boylan-Kolchin et al., 2010, that find similar deviations from a Poisson distribution), but the effect of this deviation on $\xi(r)$ is minor (Fig. 16 of Z05). We also note that there are any number of possible parametrizations for $\langle N_{\rm sat} \rangle_M$ to choose from besides the one adopted here. We have found that mildly different parametrizations that exhibit the same basic features and are consistent with contemporary data (e.g., the one used by Zehavi et al. 2005b) yield similar conclusions.

We consider the HOD parameter space that yields a power-law correlation function for three galaxy samples of fixed number density $\bar{n}_{\rm g}$, at three different redshifts $z = 0, 1, 3$. Fixing number density is a way to compare similar samples at different redshifts because the high-redshift sample is more likely to represent the progenitors of the low-redshift sample than it would in the case of mass threshold samples. We choose number densities equal to $\bar{n}_{\rm g} = 0.02$, 0.01, and 0.003 $h^3{\rm Mpc}^{-3}$, which correspond to three $z \simeq 0$, volume-limited, r-band threshold samples in the SDSS: $M_r < -18.5$, -19.5, and -20.5 (Zehavi et al., 2005b).

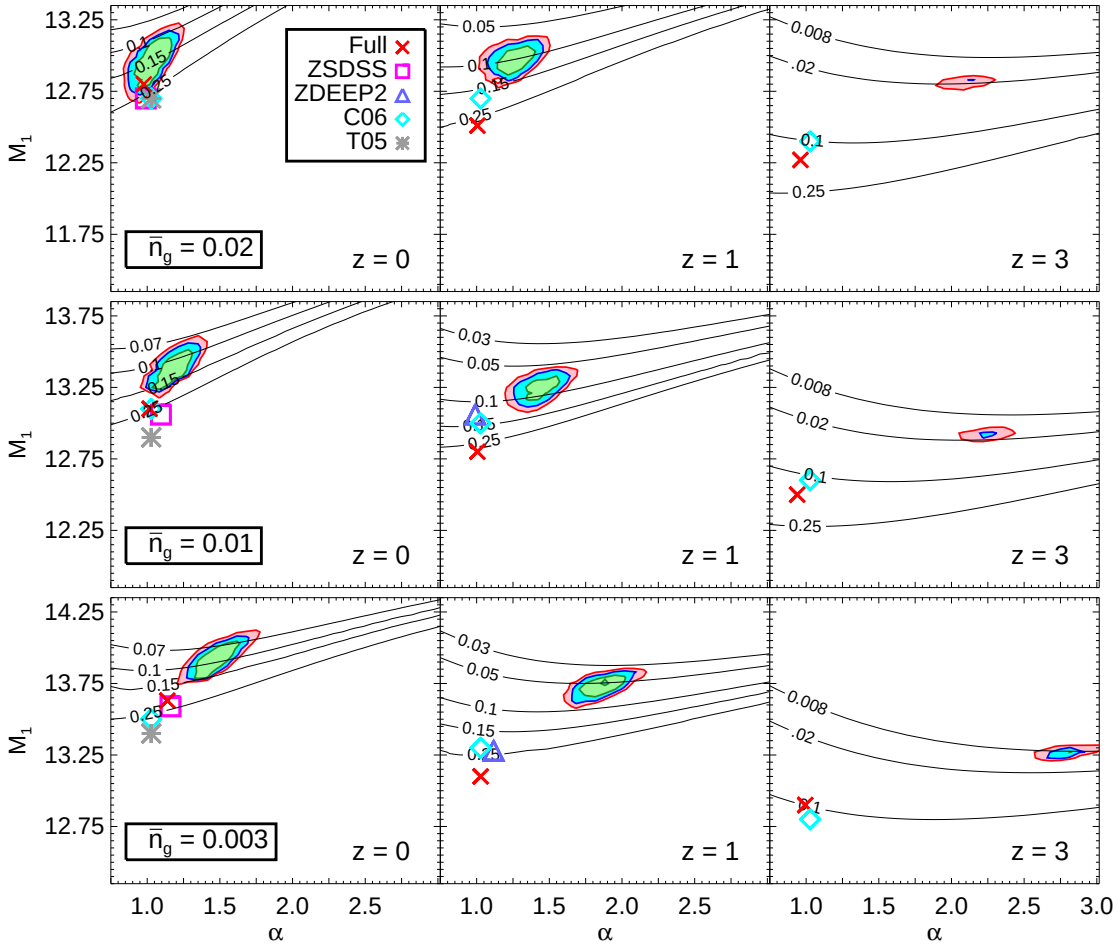

Figure 2.7: Exploration of the HOD parameter space that yields a power-law $\xi(r)$, as a function of redshift and sample number density. Each column of panels shows results for a different redshift ($z = 0, 1, 3$). Each row of panels shows results for a different sample number density ($\bar{n}_g = 0.02, 0.01, 0.003 h^3\mathrm{Mpc}^{-3}$). We adopt the four-parameter HOD model shown in equations 2.8, 2.9, and 2.10. Each panel shows the parameter space probed by α, the slope of the mean occupation number of satellites, and M_1, the halo mass that contains on average one satellite galaxy. For each pair of α and M_1 values, we find the value of $M_{\rm min}$ that yields the desired galaxy number density. We then use the halo model to compute $\xi(r)$ for that set of HOD parameters. We do this on a 50×50 grid of $\alpha - M_1$ parameter combinations. We fit each correlation function to a power law, and the shaded contours represent the 68.3%, 95% and 99.6% power-law likelihood (green, blue, red contours). Also shown are contours of constant satellite fraction (solid black curves). The red X in each panel shows the HOD parameters predicted by our *Full* subhalo model. For comparison, we also show results from HOD modeling of real galaxy samples from the SDSS at $z = 0$ (Zheng et al. 2007, T05 - magenta boxes and grey asterisks); and DEEP2 at $z = 1$ (Zheng et al. 2007 - purple triangles). Finally, we show the simulation results of Conroy et al. (2006) that are designed to model SDSS, DEEP2, and Lyman-break galaxies at $z = 0$, 1, and 3, respectively (cyan diamonds).

For a given number density and redshift combination (e.g., $\bar{n}_{\rm g} = 0.02\,h^3{\rm Mpc}^{-3}$ at $z = 1$), we create a 50×50 grid of $M_1 - \alpha$ parameter combinations. For each pair of M_1 and α on this grid, we use Equation (2.3) to find the value of $M_{\rm min}$ that is needed to enforce the desired number density. In this manner, the 2,500 HOD models on the grid represent galaxy samples with the same number densities, but different HODs. We then compute the first and second moments of the mean galaxy occupation using equations (2.8) and (2.9), and use the halo model described in § 2.2 to construct $\xi(r)$. We assign 10% errors on all scales to $\xi(r)$, as such errors are roughly consistent with jackknife re-sampling errors in current clustering measurements (Zehavi et al., 2005b), and we fit a power-law function to all 2,500 correlation functions. We perform our fits using a Markov Chain Monte Carlo (MCMC) analysis in which we vary the slope and correlation length of the fitted power-law. We then find the minimum χ^2 value for a power-law fit to $\xi(r)$ for any given $M_1 - \alpha$ combination. This allows us to approximate the HOD parameter space in which $\xi(r)$ is consistent with a power law at a level similar to contemporary observations. For two free parameters, the 68.3% (1σ), 95% (2σ), and 99.6% (3σ) likelihood regions correspond to values of reduced $\chi^2 \leq 1.15,\ 1.61$, and 2.06, respectively.

Figure 2.7 shows the contours generated from the aforementioned procedure. Each row in the figure represents a different $\bar{n}_{\rm g}$ value and each column corresponds to a different redshift. The "satellite fraction" ($f_{\rm sat}$, the fraction of all galaxies that are satellites, see Eq. [2.5]) is relevant to the shape of the galaxy two-point correla-

tion function. Therefore, over-plotted in each panel are curves of constant $f_{\rm sat}$ (the labeled, solid, black curves). To compare these results with measurements from observed galaxies, in each panel we also show best-fit M_1 and α values from published halo model fits to measurements of $\xi(r)$ using galaxy samples with the same number densities at the same redshifts. Squares and triangles represent the best-fit parameter values from Zheng et al. (2007) who fit SDSS ($z = 0$) and DEEP2 ($z = 1$) data (ZSDSS, ZDEEP2) and asterisks represent the best-fit Tinker et al. (2005) values for SDSS data (T05). Diamonds represent the Conroy et al. (2006) values for SDSS, DEEP2, and the $z = 3$ Subaru data of Lyman-break galaxies (C06).

The best-fit parameter combinations should be regarded as best-fit "regions", because there are errors associated with the derived parameters (e.g., the Zheng et al. (2007) SDSS α and M_1 errors at each luminosity are of order 10%). We note that Tinker et al. (2005) considered several possible values of σ_8, but we show their results for $\sigma_8 = 0.9$ to be consistent with the cosmological model used in the other studies. Finally, in each panel we show the HOD parameters predicted by our *Full* subhalo model (marked by an "X") for samples with mass thresholds that yield the desired number density. The *Full* model gives $\langle N_{\rm sat}\rangle_M$ and we fit this with Equation (2.9) to obtain best-fit values of M_1 and α.

Several interesting conclusions can be drawn from this figure.

1. The region of HOD parameter space that yields a power-law $\xi(r)$ drifts to lower values of both M_1 and α with increasing number density. These trends

increase the satellite fraction as number density increases to compensate for the relative reduction in the one-halo term compared to the two-halo term induced by moving to a lower-mass, more abundant halo sample.

2. The values of α that result in the best power laws drift higher with increasing redshift in an effort to boost the two-halo term by placing galaxies in massive, highly-biased halos. In general, it is difficult to arrange a power law at $z \geq 3$ for these three number densities.

3. As might be expected from our previous discussions, there is a relatively narrow range of $f_{\rm sat}$ for the best-fit power-law space at each redshift. At $z = 0$, the space that is consistent with a power-law with 10% errors on the data lie near $f_{\rm sat} \sim 0.1 - 0.15$. The direct fits to observational data lie near $f_{\rm sat} = 0.2 - 0.3$. At $z = 1$, the power-law region is shifted to $f_{\rm sat} \sim 0.05 - 0.1$, while at $z = 3$ the power-law region is even lower, $f_{\rm sat} \sim 0.01 - 0.02$. Note that the power-law regions are not precisely aligned along constant-$f_{\rm sat}$ contours, particularly at low redshift and low number density, indicating that other factors, such as host halo abundances and the physical sizes of host halos, contribute to the power-law nature of $\xi(r)$. However, at high redshift and low number density, the power-law regions become more nearly co-linear with contours of constant $f_{\rm sat}$ over a range of α values.

4. The SDSS ($z \sim 0$) best-fit points lie near the power-law contours, but not within these likelihood regions. This is not surprising as the SDSS measurement is more precise over a wide range of scales than the $\sim 10\%$ errors we have assumed and the observed $\xi(r)$ is now known to exhibit very small, but statistically-significant deviations from a power law (Zehavi et al., 2004).

5. As predicted from Figure 2.3, the fits to observational data lie further from the power-law regions as we move to lower $\bar{n}_{\rm g}$ (higher luminosity) samples. At fixed redshift, this is driven largely because the host halos of these galaxies become increasingly rare. However, it is worth noting that the growth of the one-halo term with increasing $M_{\rm min}$ is reinforced by an increase in satellite abundance at fixed scaled mass $M_{\rm sub}/M_{\rm host}$ as $M_{\rm host}$ increases, accounting for $\sim 30\%$ of the rise. This increase satellite abundance with $M_{\rm host}$ arises because more massive host halos assemble more recently, leaving less time for the evolution of substructure and less satellite destruction (Z05). The relative time available for satellite evolution is an important part of determining the power-law nature of the correlation function.

6. The fits to observational data lie near the power-law regions at $z = 0$, but grow more distinctly separated with increasing redshift. This evolution is driven by satellite fractions at high-z that are too large to be consistent with power-law clustering. This supports our basic picture that satellite destruction over cosmic time is needed to achieve a power law $\xi(r)$, and that the observed low-luminosity,

low-redshift $\xi(r)$ is a coincidence.

7. The HOD values predicted by our *Full* subhalo model are similar to all of the observed data fits at all redshifts. This is a remarkable result considering our model treats only subhalos and not galaxies explicitly. We explore more complicated associations of galaxies and subhalos in a follow-up study.

8. Our subhalos, as well as all observational data, reveal values of $\alpha \simeq 1$ for all redshifts, in accord with previous theoretical results (Kravtsov et al., 2004a; Zheng et al., 2005; Zentner et al., 2005; Conroy et al., 2006). Moreover, at each redshift, they have fixed satellite fractions, independent of $\bar{n}_{\rm g}$. At $z = 0$, $z = 1$, and $z = 3$, our model and the observational data cluster near $f_{\rm sat} \approx 0.25$, $f_{\rm sat} \approx 0.2$, and $f_{\rm sat} \approx 0.1$, respectively. We note that the lower satellite fractions at high redshift are *not* due to HOD evolution. Figure 2.4 shows that $\langle N_{\rm sat} \rangle$ is higher at high z. Instead, satellite fractions are lower at high z because all relevant host halos have $M_{\rm host} > M^*$ and lie on the exponentially-decreasing portion of the halo mass function, so the relative number of M_1-mass host halos to $M_{\rm min}$-mass halos decreases with redshift. Nevertheless, these satellite fractions at high redshift are too high to support a power-law galaxy correlation function.

9. Figure 2.7 implies that the physical mechanisms that dictate the HOD of galaxies operate to maintain α and $f_{\rm sat}$ approximately fixed and *not* to achieve a

power-law correlation function.

We have established that the observed power-law correlation function at low masses and low redshifts should not persist at higher masses or redshifts for simple, physical reasons. However, exploring the HOD parameter space has not revealed a single simple property that yields a power-law shape for $\xi(r)$. In an effort to better understand the factors that drive a power-law $\xi(r)$ at high precision, we continue to explore the HOD parameter space in a different way. Specifically, we investigate the two mass scales in the standard HOD models, $M_{\rm min}$ and M_1, relative to the characteristic non-linear collapse mass, M^*. To complement our previous analysis and to be consistent with gross theoretical predictions, we fix $\alpha = 1$ and take our two parameters to be $M_{\rm min}/M^*$ and $M_1/M_{\rm min}$. The first ratio specifies roughly the host masses that galaxies occupy relative to the exponential regime of the halo mass function, and the second ratio sets the length of the "plateau" in the HOD.

Figure 2.8 probes the power-law $\xi(r)$ space as a function of the ratios $M_{\rm min}/M^*$ and $M_1/M_{\rm min}$. For this analysis we switch from fixed number density samples to fixed mass thresholds, and we choose four values of minimum mass that correspond to a range of sub-L^* galaxies ($M_{\rm min} = 10^{10.0}, 10^{10.5}, 10^{11.0}, 10^{11.5} h^{-1} M_\odot$), showing results for each in a distinct panel. In each panel, we sample redshifts from $z = -0.9$ to $z = 2.9$ in steps of $\Delta z = 0.08$ (labeled on the right vertical axis). Each redshift value also corresponds to a $M_{\rm min}/M^*$ ratio, which we label on the left vertical axis. At each redshift, we also loop over $M_1/M_{\rm min}$ ratios from 1 to 100 in steps of $\Delta(M_1/M_{\rm min}) = 2$.

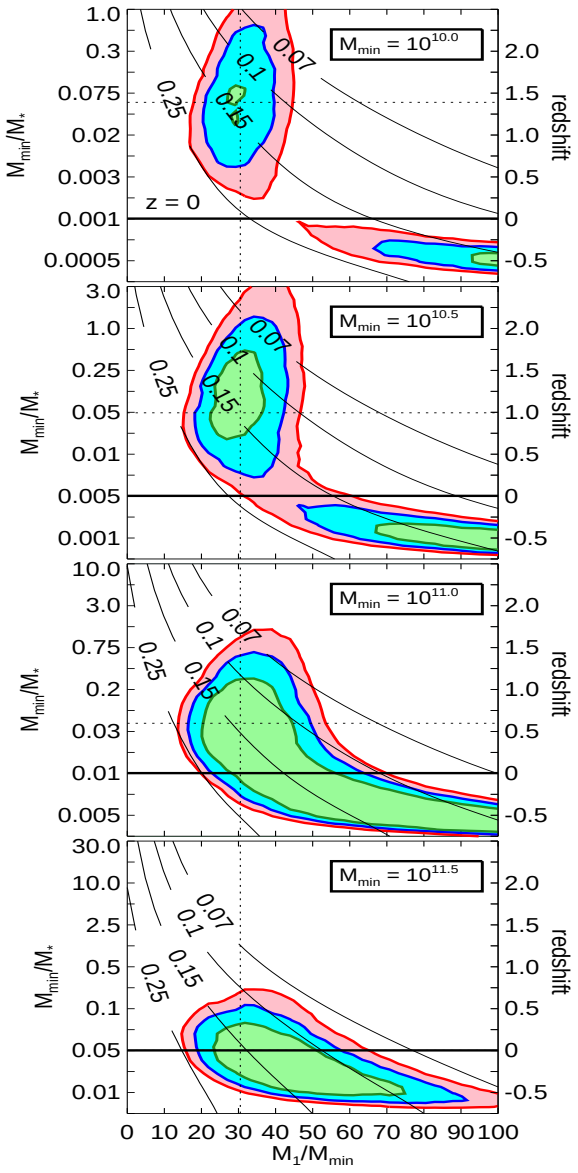

Figure 2.8: Exploration of the HOD parameter space that yields a power-law $\xi(r)$. Each panel corresponds to a different mass threshold $M_{\rm min}$ (in units of $h^{-1}M_{\odot}$). The y-axis shows redshift (right-hand side), which also corresponds directly to the ratio $M_{\rm min}/M^*$ (left-hand side), since the characteristic non-linear mass M^* depends directly on redshift. The horizontal axis shows the ratio $M_1/M_{\rm min}$. We fix the slope of the satellite mean occupation function to be $\alpha = 1$ and we set the fourth HOD parameter M_0 using equation 2.10. Each point on the horizontal axis therefore corresponds to a specific set of HOD parameters, while moving along the vertical axis shifts the HOD to different redshifts. As in Fig. 2.7, shaded contours represent the 68.3%, 95% and 99.6% power-law likelihood spaces and thin solid curves show contours of constant satellite fraction. The horizontal and vertical dotted lines correspond to fixed values of $M_{\rm min}/M^* = 0.05$ and $M_1/M_{\rm min} = 30$, which bisect the best-fit power-law space in all four panels. Solid black horizontal lines denote $z = 0$, below which the parameter space corresponds to future epochs.

For every pair of $M_{\rm min}/M^*$ and $M_1/M_{\rm min}$ values, we compute $\xi(r)$ using the halo model and fit a power-law function in the same fashion as described previously. As before, we show the $68.3\%, 95\%$ and 99.6% likelihood regions of $\xi(r)$ consistent with a power law (green, blue, and red contours, respectively). Also, as before, we show contours of constant satellite fraction, $f_{\rm sat}$ (solid black curves). The thick horizontal lines at $z = 0$ are meant to emphasize that the parameter space lying below these lines corresponds to *future* epochs.

We have repeated this analysis for higher mass thresholds (values of $M_{\rm min} = 10^{12.0}, 10^{12.5}, 10^{13.0}, 10^{13.5} h^{-1} M_\odot$). However, we do not show those results because we found no parameter combinations within the 99.6% power-law likelihood space. Figure 2.7 showed that the power-law parameter space drifted to higher values of α for lower number density (and hence higher mass) samples in an effort to drive up the two-halo term to meet the enhanced one-halo term. Therefore, it is not surprising that we do not find this space when we restrict the slope to be $\alpha = 1$.

Many interesting results can be drawn from Figure 2.8. Again, we itemize them for the sake of clarity.

1. In order for $\xi(r)$ to have a shape consistent with a power-law assuming $\sim 10\%$ measurement errors, it appears necessary for the "plateau" in the HOD to be sufficiently long. At all masses and redshifts, $M_1/M_{\rm min}$ needs to be at least ~ 20, otherwise the large satellite fraction drives a one-halo term that is too large relative to the two-halo term. Moreover, for past epochs, $z > 0$, the

maximum plateau length is $M_1/M_{\rm min} \lesssim 40$. Higher values of $M_1/M_{\rm min}$ yield a one-halo term that is too weak. In fact, $M_1/M_{\rm min} \sim 30$ seems to be the preferred value to yield a nearly power-law correlation function at all masses so long as $z > 0$. This value is denoted by the vertical dotted lines in all the panels.

2. For $z \geq 0$, a near power-law $\xi(r)$ seems to require a restricted range of $M_{\rm min}/M^*$. Interestingly, the value $M_{\rm min}/M^* \sim 0.05$ can yield a power-law correlation function at all masses for appropriate choices of redshift. This value is denoted by the horizontal dotted lines in all the panels. This restriction on $M_{\rm min}/M^*$ means that higher redshift samples (when M^* is significantly smaller than today) can only exhibit power-law behavior if the relevant host halos are significantly smaller. This possibility becomes irrelevant in a practical sense because star formation is inefficient in small halos ($M \ll 10^{11} h^{-1} M_\odot$, e.g., Conroy & Wechsler, 2009; Behroozi et al., 2010; Guo et al., 2010)), so they cannot host galaxies that are easily observable at high redshift. Figure 2.8 shows that the lowest-mass samples that we consider (top two panels) have a nearly power-law $\xi(r)$ at $1 \lesssim z \lesssim 2$, whereas the highest-mass samples have a nearly power-law $\xi(r)$ only at low redshift.

3. At sufficiently high redshift, near power-law clustering is no longer achievable at any mass threshold corresponding to relatively bright galaxies. Our results generally indicate that power-law clustering at high redshift can only be achieved

if galaxies at high redshift occupy halos in a markedly different and more complicated manner than their low-z counterparts.

4. For future epochs these broad results no longer hold. A broader range of $M_1/M_{\rm min}$ values can be made approximately consistent with a power law at low values of $M_{\rm min}/M^*$, or low/negative redshifts. For the lowest $M_{\rm min}$ samples the power-law likelihood space is clearly bimodal, with possible ways to achieve a power law both at high redshifts and at low/future redshifts.

5. At all masses and redshifts we find that the power-law likelihood parameter space has satellite fractions in the range $f_{\rm sat} \sim 0.1 - 0.25$, with the $f_{\rm sat} = 0.15$ contour slicing through all of the 1σ regions. $f_{\rm sat}$ is naturally strongly dependent on both $M_1/M_{\rm min}$ and $M_{\rm min}/M^*$. Increasing the length of the HOD plateau at fixed $M_{\rm min}$ and redshift makes $f_{\rm sat}$ decrease, as does boosting $M_{\rm min}/M^*$ while keeping $M_{\rm min}$ and the plateau fixed. If we keep both ratios fixed (i.e., both the HOD shape and its position relative to the mass function) then the satellite fraction is also approximately fixed, regardless of $M_{\rm min}$.

2.7 Discussion & Primary Conclusions

It has been recognized for decades that the two-point correlation function has a simple, power-law form with $\xi(r) \sim r^{-2}$. Observational determinations of galaxy two-point clustering spanning more than thirty years all yielded results consistent with a single power law extending from linear and quasi-linear length scales ($r \gtrsim 30\,h^{-1}$Mpc)

to deeply non-linear scales ($r \lesssim 0.1\,h^{-1}$Mpc). In this paper, we cast the problem in the contemporary setting in which galaxies form in halos and subhalos of dark matter and set out to understand the physical processes that drive this surprisingly simple result. Our primary conclusion is that the nearly power-law correlation function of relatively common, L^* and sub-L^* Galaxies at $z \sim 0$ is a coincidence and does not reflect any general principle of structure formation or galaxy evolution. So how did we arrive at this conclusion?

First, the efficiency of galaxy formation is dependent upon halo mass and it has been determined both theoretically and empirically that there is a halo mass scale below which galaxy formation is inefficient, roughly $M_{\rm gal} \sim 10^{10.5}\,h^{-1}M_\odot$ (Conroy & Wechsler, 2009; Behroozi et al., 2010; Guo et al., 2010). A number of things can set this scale including atomic and molecular physics and feedback from supernovae and active galactic nuclei (for a recent review article see **?**). This mass scale is $M_{\rm gal} < M^*$, so L^* and sub-L^* galaxies are common. Had $M_{\rm gal}$ been greater than or similar to M^*, most bright galaxies would lie in comparably rare halos and be rare themselves. In such a case, one-halo clustering would be too strong to be compatible with a power law. M^* is *not* determined by galaxy formation physics but is set by the completely unrelated processes that establish the amplitude of cosmological density fluctuations, presumably primordial inflation.

Second, power-law clustering requires that some of the galaxies formed within relatively large subhalos are destroyed. Destruction is due primarily to mass loss,

and, to a lesser extent, merging with the central galaxy as a result of dynamical friction. Without this destruction, satellite fractions would be too high and small-scale clustering too strong compared with large-scale clustering. In a forthcoming paper, we perform more sophisticated modeling to make the connection between subhalo mass loss and stellar mass loss in order to make predictions for the amount of intracluster light. Large-scale clustering is principally set by large-scale matter density fluctuations and is insensitive to the details of galaxy formation within halos, while the strength of small scale clustering grows in proportion to the fraction of galaxies that are satellites and in inverse proportion to the number density of the galaxies of interest. As it turns out, precisely the right amount of subhalo destruction has occurred by redshift $z \sim 0$ in a concordance cosmology to produce a single, unbroken, power-law $\xi(r)$.

Evolution of the satellite fraction is set by a competition between halo mergers, which increase $f_{\rm sat}$, and destruction by dynamical processes, which occur on a dynamical timescale and reduce $f_{\rm sat}$. At high redshifts, mergers occur more rapidly than destruction for halos with masses $\gtrsim M_{\rm gal}$. The low-redshift merger rate declines in part due to the fact that $M_{\rm gal} < M^*$ at $z \lesssim 1$. Halos with masses below M^* become relatively more likely to merge with a larger object than to acquire new substructure compared to counterparts with masses greater than M^* (see Zentner, 2007). More importantly, the rate of halo mergers is quenched at $z \lesssim 1$ as dark energy begins to suppress further cosmological structure growth. As merger rates decline, satellites are

depleted with time. Therefore, at $z \sim 0$, the correlation function is nearly a power law because the competition between the accretion and destruction rates has struck just the right balance to yield the appropriate value of $f_{\rm sat}$.

The merger and destruction rates will once again become unbalanced in the future as halo merging is stifled by dark energy and existing satellite galaxies are slowly destroyed over many dynamical times through complex interactions in their host environments. We show that this will result in small-scale clustering that will be significantly *too weak* to be consistent with a power law.

Largely as a consequence of the merger/destruction competition, $\xi(r)$ evolves through cosmic time, achieving a power law only near $z \sim 0$ for $L \sim L^*$ and dimmer galaxies. The processes of galaxy formation, the amplitude of cosmological density fluctuations, the abundance of dark matter, and the nature of the dark energy are thought to be completely distinct and determined by *unrelated physics*. So the power-law $\xi(r)$ at $z \sim 0$ is a coincidental conspiracy.

In establishing these broad conclusions, we have performed an exhaustive investigation of the ingredients of the galaxy correlation function, which has revealed many interesting, more detailed conclusions. These can be summarized as follows.

1. We find that satellite halo mass loss is the principle dynamical process responsible for depleting sufficient substructure so as to nearly align the one- and two-halo terms to yield a power-law correlation function at low redshift. Dynamical friction plays a smaller supporting role, accounting for an additional

$\sim 15\%$ of subhalo destruction.

2. The shape of the correlation function is strongly mass dependent. For instance, at low redshift deviations from a power law $\xi(r)$ grow with increasing host halo mass. This drives stronger deviations from a power law for higher luminosity galaxy samples. The best power-law fits derived from our model are for galaxies residing in halos that are common enough to correspond to $\sim L^*$ and dimmer galaxies, in agreement with observations.

3. The correlation function is highly redshift-dependent. The sensitivity of the one-halo term to the HOD, coupled with the relative insensitivity of the two-halo term, implies that achieving a power-law requires fine-tuning the number of satellite galaxies per halo. The satellite galaxy abundance evolves with redshift, driven by the evolving balance between accretion and destruction, with an enhanced amount of substructure at high redshift. Therefore, the correlation function can only achieve a power law during those epochs when substructure has evolved to align the one- and two-halo terms. The correlation function is boosted on small scales at high z, the one- and two-halo terms join at $z = 0$ to form a power-law, then the power law is once again broken in future epochs.

4. For three chosen number densities corresponding to low-redshift, $\sim L^*$ and dimmer galaxies, we probed the most likely power-law space as a function of redshift for a parametrized HOD. We find that there is a relatively narrow

range of satellite fractions for $\xi(r)$ to be consistent with a single power law (assuming $\sim 10\%$ measurement errors) at any given redshift. At all redshifts and masses, power-law correlation functions have satellite fractions in the range $f_{\rm sat} \sim 0.1 - 0.25$. It is difficult to achieve a power-law correlation function at $z \gtrsim 3$ for any number density.

5. We find that to achieve a power law $\xi(r)$ at high mass or redshift, the slope α of the satellite galaxy occupation function must be significantly steeper than unity (for instance, greater than 2 at $z = 3$). This would imply that the mapping of galaxies to halos is much more complicated than we think, since the number of galaxies would have to be very different than the number of subhalos of a particular size. Instead, it appears that the processes that govern galaxy formation do not care about the conditions needed to achieve a power law $\xi(r)$.

6. The ratio $M_1/M_{\rm min}$ (the "plateau" of the HOD) is a key ingredient for predicting the shape of $\xi(r)$. The prominence of the plateau is a measure of substructure abundance. Along with $M_1/M_{\rm min}$, it is also necessary to characterize the ratio $M_{\rm min}/M^*$, which specifies what halo masses galaxies occupy relative to the halo mass function. By maintaining the combination of $M_1/M_{\rm min} \sim 30$ and $M_{\rm min}/M^* \sim 0.05$ we can achieve a near power law for redshifts in the range $0 - 1.5$ and the appropriate mass threshold at each redshift (the mass threshold is $M_{\rm min} \sim M^*/20$, with M^* set by the redshift). At higher redshifts this criterion is met for galaxies that are most likely too dim to be observed. For example,

achieving the requisite $M_{\rm min} \sim M^*/20$ at $z = 2$ corresponds to a halo mass of $M_{\rm min} \sim 10^9\,h^{-1}M_\odot$ in which star formation is inefficient.

This work has allowed us to formulate a general picture of the nature of the galaxy two-point correlation function. Halo abundances and subhalo populations evolve with time. At high redshifts, halos large enough to harbor galaxies are rare and subhalos are abundant within these hosts. With time, host halos that harbor galaxies generally become more common (though the specifics of this evolution can be subtle) and subhalos within these hosts become relatively less abundant. All the while, large-scale matter correlations grow, but the clustering bias of large halos evolves to largely compensate for this large-scale growth of structure. These effects, considered either individually or in tandem, change the HOD and the shape of $\xi(r)$. As a result, the correlation function evolves through an epoch where it is close to a power law and this epoch happens to be near $z \sim 0$. From our broad discussion and detailed conclusions, it is clear that a nearly power-law correlation function requires a conspiracy between otherwise unrelated processes such as the early Universe physics that established the initial conditions for low redshift structure, the detailed physical processes that determine galaxy and star formation efficiency, and the growth rate of cosmic structure set largely by the abundances of dark matter and dark energy. The low-redshift power-law galaxy two-point function is thus a mere cosmic coincidence.

Chapter III

CONSTRAINING SATELLITE GALAXY STELLAR MASS LOSS AND PREDICTING INTRAHALO LIGHT

Abstract

We introduce a new technique that uses *galaxy clustering* to constrain how satellite galaxies lose stellar mass and contribute to the diffuse "intrahalo light" (IHL). We implement two models that relate satellite galaxy stellar mass loss to the detailed knowledge of subhalo dark matter mass loss. Model 1 assumes that the fractional stellar mass loss of a galaxy, from the time of merging into a larger halo until the final redshift, is proportional to the fractional amount of dark matter mass loss of the subhalo it lives in. Model 2 accounts for a delay in the time that stellar mass is lost due to the fact that the galaxy resides deep in the potential well of the subhalo and the subhalo may experience dark matter mass loss for some time before the galaxy is affected. We use these models to predict the stellar masses of a population of galaxies and we use *abundance matching* to predict the clustering of several r-band luminosity threshold samples from the Sloan Digital Sky Survey. Abundance matching assuming no stellar mass loss (akin to abundance matching at the time of subhalo infall) over-estimates the correlation function on small scales ($\lesssim$ 1Mpc), while allowing too much stellar mass loss leads to an under-estimate of small-scale clustering. For each luminosity threshold sample, we are thus able to constrain the amount of stellar mass

loss required to match the observed clustering. We find that satellite galaxy stellar mass loss is strongly luminosity dependent, with less luminous satellite galaxies experiencing substantially more efficient stellar mass loss than luminous satellites. With constrained stellar mass loss models, we can infer the amount of stellar mass that is deposited into the IHL. We find that both of our model predictions for the mean amount of IHL as a function of halo mass are consistent with current observational measurements. However, our two models predict a different amount of scatter in the IHL from halo to halo, with Model 2 being favored by observations. This demonstrates that a comparison to IHL measurements provides independent verification of our stellar mass loss models, as well as additional constraining power.

3.1 Introduction

In Chapter II, we aimed to qualitatively understand the physics governing the power-law shape of the correlation function based on the detailed knowledge of subhalo evolution and dynamics. Here, we extend that theoretical framework to investigate another puzzling aspect of galaxy formation.

To review, in the concordance ΛCDM cosmology, galaxies, galaxy groups, and galaxy clusters form hierarchically. High-density regions condense and virialize, forming bound structures known as halos. Halos grow through the continual accretion of smaller objects. These accreted objects may survive within the virialized region of the primary halo as smaller, self-bound, orbiting dark matter clumps dubbed "subhalos"

or "substructure" (Ghigna et al., 2000; Klypin et al., 1999a; Diemand et al., 2004; Kravtsov et al., 2004a). Halos of sufficient mass are the natural sites of galaxy formation, with baryons cooling and condensing towards potential well minima (White & Rees, 1978; Blumenthal et al., 1986). When a halo is accreted by a larger halo, thus becoming a subhalo, the galaxy within it becomes a "satellite" galaxy within a group or cluster. Understanding the detailed relationship between (satellite) galaxies and (sub) halos is a long-standing focus of galaxy formation theory.

In the hierarchical paradigm, these smaller objects, upon merging, become victims of intense tidal fields and interactions within the larger systems in which they reside. The dark matter mass associated with a subhalo may be rapidly stripped upon infall. This stripping acts on the periphery of the subhalo first, suggesting that the luminous galaxy, residing in the center of the subhalo, may be relatively unharmed. After enough time has elapsed, stripping of stars may begin to occur as well. These liberated stars that are ripped from galaxies are the likely source of "intrahalo light" (IHL: e.g., Gallagher & Ostriker, 1972; Merritt, 1983; Byrd & Valtonen, 1990; Gnedin, 2003; Murante et al., 2004; Lin & Mohr, 2004; Willman et al., 2004; Sommer-Larsen, 2006; Conroy et al., 2007; Purcell et al., 2007, 2008; Rudick et al., 2009, 2011). This has been studied in great detail *at the scale of individual galaxies* (Morrison, 1993; Sackett et al., 1994; Wetterer & McGraw, 1996; Morrison et al., 1997; Weil et al., 1997; Chiba & Beers, 2000; Ivezić et al., 2000; Lequeux et al., 1998; Abe et al., 1999; Morrison et al., 2000; Yanny et al., 2000; Siegel et al., 2002; Irwin et al., 2005; Zibetti

& Ferguson, 2004; Guhathakurta et al., 2005; Chapman et al., 2006; Kalirai et al., 2006; McConnachie et al., 2006; Hood et al., 2007; Bailin et al., 2011), *galaxy groups* (Feldmeier et al., 2001; Castro-Rodríguez et al., 2003; White et al., 2003; Da Rocha & Mendes de Oliveira, 2005; Aguerri et al., 2006; Feldmeier, 2006; Da Rocha et al., 2008), and *galaxy clusters* (where it is known as the intra-cluster light, or ICL, e.g., Gallagher & Ostriker, 1972; Merritt, 1983; Melnick et al., 1977; Thuan & Kormendy, 1977; Byrd & Valtonen, 1990; Uson et al., 1991; Bernstein et al., 1995; Calcáneo-Roldán et al., 2000; Gnedin, 2003; Murante et al., 2004; Lin & Mohr, 2004; Willman et al., 2004; Mihos et al., 2005; Zibetti et al., 2005; Krick et al., 2006; Sommer-Larsen, 2006; Conroy et al., 2007; Seigar et al., 2007; Gonzalez et al., 2007; Pierini et al., 2008; Rudick et al., 2009, 2011; Toledo et al., 2011).

In this paper, we seek to understand the liberation of stars from satellite galaxies by connecting stellar mass loss[1] to subhalo dark matter mass loss using *galaxy clustering* and *intrahalo light* observations. We employ the model for halo substructure introduced in Zentner et al. (2005, hereafter Z05) in order to constrain this relationship. We compare our model predictions to observations of the IHL over a large range of host halo mass scales. The aim of this paper (Paper I) is to introduce our modeling framework and its predictive power. In a forthcoming paper (Paper II) we will extend our analysis to high redshift in order to study the assembly of the IHL across cosmic time.

[1]By "stellar mass loss", we refer to stars being stripped from a galaxy and not gas lost from stars via winds.

The paper is laid out as follows. In § 3.2 we discuss the motivation for this study. In § 3.3 we review the Z05 model for cold dark matter (CDM) substructure. In § 3.4 we describe our models that connect stellar mass loss to dark matter mass loss and in § 3.5 we demonstrate how we constrain these models using galaxy clustering. In § 3.6 we show the luminosity dependence of satellite galaxy stellar mass loss. In § 3.7 we use our models to make IHL predictions, and compare to observations at low redshift. Finally, in § 3.8 we give a summary of our results and discuss directions for future work.

3.2 Motivation

A simple, yet remarkably powerful technique for connecting dark matter halo mass to either stellar mass or luminosity has emerged in recent years. By assuming a monotonic relation between halo mass (or maximum circular velocity $V_{\rm max} = \max[\sqrt{GM(<r)/r}]$) and luminosity L (or stellar mass) one can "abundance match" to make the correspondence between dark matter (sub)halos and an observable galaxy property (e.g., Kravtsov et al., 2004a; Vale & Ostriker, 2004; Tasitsiomi et al., 2004; Vale & Ostriker, 2006; Conroy et al., 2006; Conroy & Wechsler, 2009; Moster et al., 2010; Behroozi et al., 2010; Guo et al., 2010; Simha et al., 2010). For example, this can be done by matching the observed number density of galaxies, n_g, above some

luminosity to the number density of halos and subhalos, n_h, above a certain $V_{\rm max}$,

$$n_g(> L) = n_h(> V_{\rm max}). \tag{3.1}$$

This yields an implicit relationship between L and $V_{\rm max}$ that preserves the observed luminosity function of galaxies.

Conroy et al. (2006) used this method to assign luminosities to halos and subhalos in a cosmological N-body simulation at several redshifts. They predicted the luminosity-dependent clustering of galaxies and found that the two-point correlation function (2PCF) of halos and subhalos matched that of galaxies for a wide range of luminosities and redshifts. The authors made the physically-motivated choice that $V_{\rm max}$ should be the maximum circular velocity of subhalos *at the time of accretion*, $V_{\rm max}^{\rm acc}$, instead of at the time of observation (see also Nagai & Kravtsov, 2005; Vale & Ostriker, 2006; Berrier et al., 2006).

The reasoning behind this choice is as follows. Upon merging into a larger host, the $V_{\rm max}$ of a subhalo will decrease due to mass loss (Hayashi et al., 2003; Kravtsov et al., 2004a). Dark matter on the periphery of the subhalo will be lost first, because it is less bound to the subhalo. On the other hand, the stellar mass of the satellite galaxy is concentrated at the center of the subhalo and thus more tightly bound. Tidal stripping can significantly alter the surrounding subhalo, but possibly leave the galaxy largely unperturbed for some period of time (in numerical tests, Purcell et al. 2011 found that Milky Way satellites lose $\sim 90\%$ of their dark matter before stars are

stripped away). Consequently, while $V_{\rm max}$ of the subhalo decreases, the stellar mass of the galaxy may remain unchanged for long periods of time. It follows that galaxy observables such as luminosity or stellar mass should correlate with $V_{\rm max}^{\rm acc}$ instead of the final $V_{\rm max}$ (Nagai & Kravtsov, 2005). Conroy et al. (2006) lent empirical support to this picture by showing that the choice of $V_{\rm max}^{\rm acc}$ was essential in order to achieve agreement with the observed clustering of galaxies.

It is well known that galaxy groups and clusters are replete with diffuse stellar material. This material is widely thought to be the remains of disrupted satellites (see § 5.1). However, the choice to associate galaxy luminosity with $V_{\rm max}$ at the time of satellite accretion is tantamount to assuming that no stars become unbound from satellite galaxies. In this case, why can using $V_{\rm max}^{\rm acc}$ accurately reproduce the observed clustering?

There is a crucial subtlety to simply using $V_{\rm max}^{\rm acc}$ for abundance matching. When matching galaxy and subhalo number densities with the $L-V_{\rm max}$ relation by choosing $V_{\rm max}^{\rm acc}$, there is an inherent second threshold in the final $V_{\rm max}$ of subhalos. This is a threshold below which objects are "operationally removed from consideration" due to the limited resolution of the simulation that is used to perform the calculation. In the study of Conroy et al. (2006), this threshold was ~ 80km s^{-1} – the completeness limit of halos in their simulation. Therefore, an accreted subhalo will be artificially destroyed if it becomes sufficiently small such that its structure is not well resolved within the simulation. These so-called "orphans" are neglected and they unwittingly

act to model the stripping of stars. The galaxies that would have been associated with these halos, had they not become unresolved, are effectively removed from the final galaxy sample, just as if they were disrupted. This elimination of subhalos directly affects the 2PCF, which is very sensitive to subhalo abundance (see Watson et al., 2011b). Including these *orphans* should result in a boost of the small-scale correlation function, implying that pure abundance matching using $V_{\rm max}^{\rm acc}$ may not accurately reproduce the observed clustering on small scales (see Kitzbichler & White, 2008; Moster et al., 2010; Wetzel & White, 2010). In fact, we have performed a test in which we selected a $V_{\rm max}^{\rm acc} > 210$km s^{-1} (corresponding to $\sim L^*$ galaxies and brighter) threshold with two, secondary final $V_{\rm max}$ thresholds, $V_{\rm max} > 20$km s^{-1} and $V_{\rm max} > 80$km s^{-1}, to mimic this resolution limit effect. Increasing this threshold from 20 to 80km s^{-1} resulted in a $\sim 20\%$ decrease in the 2PCF[2] at scales less than 1Mpc. We speculate that below this resolution limit is where much of the stripped stellar material may originate.

The above discussions bring us to the motivation of this work. Including stellar mass loss in the abundance matching technique is necessary to describe the observed clustering of galaxies in a manner that does not include implicit selections. Observed galaxy clustering therefore has the potential to constrain the typical amount of stellar mass loss from a subhalo. In this work, we develop models that relate satellite galaxy stellar mass loss to subhalo dark matter mass loss. We use these models, together

[2]We explain the tools we use to calculate correlation functions in § 3.5.

with the abundance matching technique, to predict the observed 2PCF (see § 3.4 and § 3.5 for details). Comparing to measurements allows us to constrain our stellar mass loss models. This requires a detailed understanding of the evolution of subhalos within hosts. We use the Z05 analytic model for halo substructure, which is not subject to any intrinsic resolution effects. The model is capable of tracking surviving subhalos down to $V_{\rm max} \ll 80$ km s^{-1}, so predictions are not affected by the "orphan" population of galaxies. Our models yield stellar mass loss histories from satellite galaxies, so we can make predictions for the amount of intrahalo light at varying scales and compare to observations. This provides an independent check of our stellar mass loss constraints. This modeling can also be done at varying redshifts in order to study the evolution of stellar mass loss and the assembly of IHL over time. Ultimately, this investigation could enable a single model to track the stellar-to-halo mass relation as a function of time such that abundance matching at multiple redshifts would be unnecessary.

3.3 The Subhalo Evolution Model

We construct models in which the stellar mass loss of a satellite galaxy is linked to the dark matter mass loss of its subhalo. Consequently, we require a detailed understanding of the evolution of subhalos within hosts. For this we use the Z05 model, which is based on Zentner & Bullock (2003) and is similar to the independent models of Taylor & Babul (2004, 2005a,b) and Peñarrubia & Benson (2005), and shares

many features with other approximate treatments of subhalo populations (Oguri & Lee, 2004; van den Bosch et al., 2005; Faltenbacher & Mathews, 2005; Purcell et al., 2007; Giocoli et al., 2008, 2009; Gan et al., 2010). The Z05 model produces subhalo mass functions, occupation statistics, and radial distributions within hosts that are in good agreement with a number of high-resolution N-body simulations (Z05, and the recent comparison in Koushiappas et al., 2010).

The analytic model proceeds as follows. For a host halo at a given redshift z, and mass M, we generate a halo merger tree using the mass-conserving implementation of the excursion set formalism (Bond et al. 1991; Lacey & Cole 1993, 1994; see Zentner 2007 for a review) developed by Somerville & Kolatt (1999). This provides the entire history of all halos that merged to form the final, host halo. We assign all halos Navarro et al. (1997, hereafter NFW) density profiles with concentrations determined by their merger histories according to Wechsler et al. (2002). When a halo merges into a larger halo, it becomes a subhalo and is assigned initial orbital parameters drawn from distributions measured in N-body simulations (Z05; also see Benson 2005 for similar formalisms). We then integrate each subhalo orbit within the gravitational field of the host, subjecting the subhalos to orbital decay via dynamical friction and mass loss through tides and interactions. We estimate dynamical friction with an updated form of the Chandrasekhar (1943) approximation (Hashimoto et al., 2003; Zentner & Bullock, 2003), and allow for dark matter mass loss beyond the tidal radius on a timescale comparable to the local dynamical time. Finally, we account

for internal heating so that scaling relations describing the internal structures of subhalos are obeyed (Hayashi et al., 2003; Kazantzidis et al., 2004; Kravtsov et al., 2004b). We refer the reader to Z05 for specific details of these ingredients.

The lack of a resolution limit in the Z05 model allows us to track subhalos regardless of how much mass they have lost. Therefore, we do not lose subhalos due to mass loss. However, we do consider a subhalo to be effectively "destroyed" if its orbital apocenter sinks to less than $r_{\rm apo} < 5$ kpc distance from the center of its host halo. This choice is physically motivated because the galaxy within such a subhalo would likely have merged with the central galaxy, or at least be observationally indistinguishable from it. This criterion thus models the cannibalism of satellite galaxies by central galaxies. We show in § 3.7 that inclusion of these cannibalized subhalos in our predictions for intrahalo light is negligible, so this criterion actually has little effect on our modeling results. In practice, subhalos lose the vast majority of their mass prior to achieving such small pericenters, so this cut serves only to terminate the integration of that particular orbit. In the end, we amass catalogs of all surviving subhalos in the final host halo at the time of "observation" and we know exactly how much dark matter has been lost from each subhalo. A halo that merges into a larger host may contain subhalos of its own. These "subs-of-subs" of sufficiently high mass to host an observable galaxy are only abundant inside very large host masses. They are present in our model, but rare.

To properly sample the distribution of halos in the universe, we compute subhalo

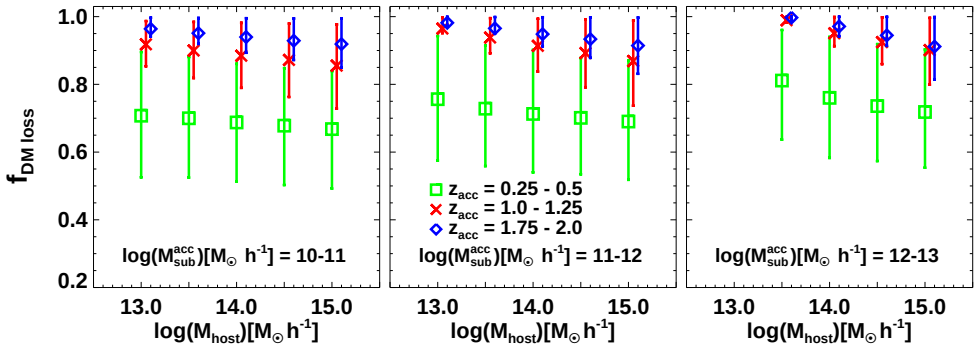

Figure 3.1: The average fraction of dark matter lost from subhalos, $f_{\rm DM\ loss} = (M_{\rm acc}^{\rm dm} - M_{\rm fin}^{\rm dm})/M_{\rm acc}^{\rm dm}$, as a function of host halo mass for three bins of subhalo accretion epoch $z_{\rm acc}$ (shown by the three point types), and three bins of subhalo mass (at accretion; shown by the three panels), according to the Z05 semi-analytic model. Each point represents an average over all subhalos in a given bin of accretion epoch and subhalo mass, from 500 model realizations of a specific host mass, and errorbars show the 1σ scatter. The points representing different accretion epoch bins are slightly staggered for clarity. Accretion time is the dominant factor that determines $f_{\rm DM\ loss}$, with subhalos that have merged earlier having more time to be stripped of their dark matter.

populations for a grid of host halo masses in the range $11 \leq \log(M/h^{-1}M_\odot) \leq 15$ (in steps of 0.1). To account for statistical variation among halos and subhalos, we perform 500 statistical realizations of the subhalo population at each host mass. The result is 500 host halos along with their subhalos at each of 41 distinct masses, giving a total of 20,500 distinct subhalo populations. The model predicts the amount of dark matter lost from each subhalo as it orbits in the tidal field of its host halo. Figure 3.1 shows the fraction of subhalo mass lost as a function of host halo mass, in bins of accretion epoch $z_{\rm acc}$, and subhalo mass (at accretion). This fraction is defined as $f_{\rm DM\ loss} = (M_{\rm acc}^{\rm dm} - M_{\rm fin}^{\rm dm})/M_{\rm acc}^{\rm dm}$, where $M_{\rm acc}^{\rm dm}$ is the subhalo mass at accretion and $M_{\rm fin}^{\rm dm}$ is the final subhalo mass. Each panel of the figure represents a bin of subhalo

mass and the three sets of points in each panel represent bins of accretion epoch: $z_{\rm acc} = 0.25-0.5$ (green circles), $z_{\rm acc} = 1.0-1.25$ (red X symbols), and $z_{\rm acc} = 1.75-2.0$ (blue diamonds). Each point thus represents an average over all subhalos in a bin of accretion epoch and subhalo mass, from the 500 model realizations of a specific host halo mass, and errorbars show the 1σ scatter. It is clear that accretion time is crucial towards determining $f_{\rm DM\ loss}$, with subhalos that have merged earlier having more time to be stripped of their dark matter. Moreover, the scatter in $f_{\rm DM\ loss}$ shrinks for earlier accretion times. At fixed accretion epoch, the average value of $f_{\rm DM\ loss}$ is remarkably constant. However, there is a slight increase as we move to lower host halo mass at fixed subhalo mass, or as we move to higher subhalo mass at fixed host mass. This is a result of dynamical friction playing a stronger role for subhalos that are considerable in size compared to their host halos. The larger a subhalo relative to its host, the more rapidly its orbit will decay and it will sink within the host potential. The tidal field of the host is stronger towards the host center, and this induces more dark matter mass loss.

3.4 Models for Satellite Galaxy Stellar Mass Loss

We now present the models we use to describe satellite galaxy stellar mass loss. The exact way in which stars are stripped from the subhalo they inhabit is likely quite complicated. However, we can make some simple, physically-motivated approximations aimed at capturing the gross, relevant behavior. In this sense, we pursue

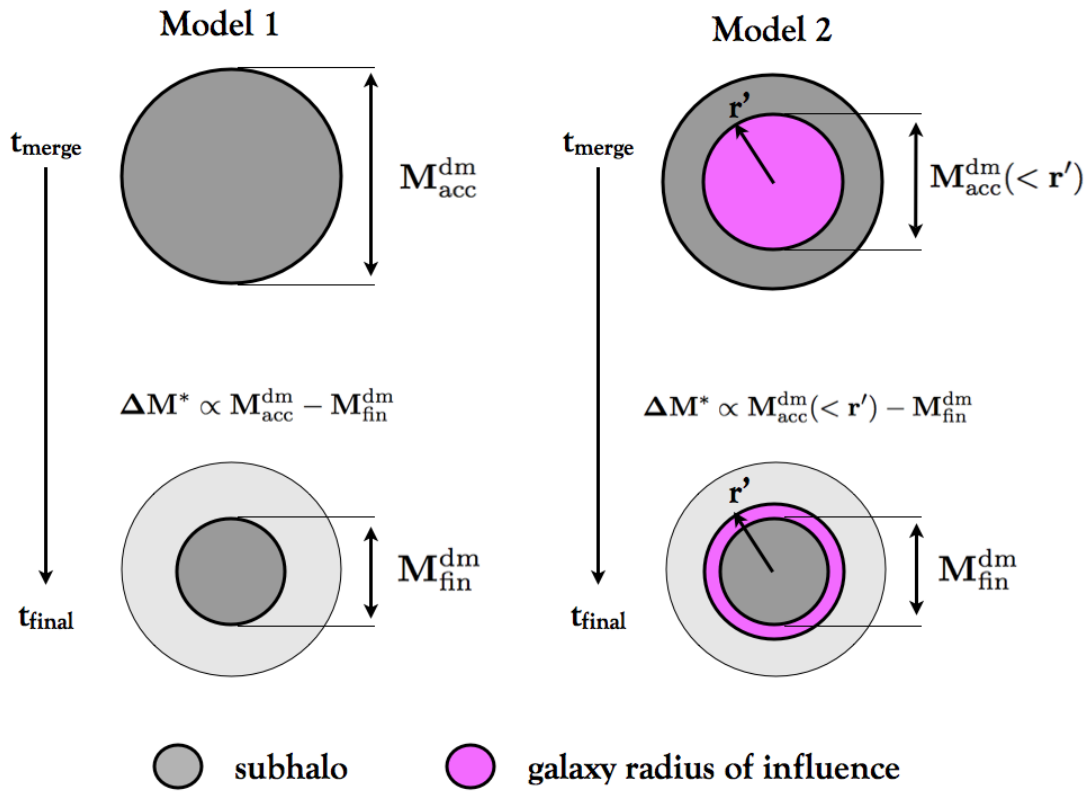

Figure 3.2: Schematic of how satellite galaxy stellar mass loss occurs in Model 1 and Model 2. From the time the subhalo merges into the host halo, $t_{\rm merge}$, until the final redshift under consideration, $t_{\rm final}$, our semi-analytic subhalo model predicts the amount of dark matter mass loss, $\Delta M^{\rm dm} \equiv M_{\rm acc}^{\rm dm} - M_{\rm fin}^{\rm dm}$. Model 1 assumes that the amount of stellar mass lost, ΔM^*, is proportional to $\Delta M^{\rm dm}$. Model 2 defines a radius, r', such that stellar mass is only lost if dark matter is lost within that radius. If this is the case, then ΔM^* is only proportional to the amount of dark matter lost inside of this radius. See § 3.4 for detailed descriptions of the models.

the question of the evolution of stellar mass using a philosophy similar to that which underlies abundance matching. We aim to make a set of minimal, yet effective assumptions that serve to distill the enormous amount of information contained in survey data. Indeed, we aim in part to extend the abundance matching techniques by making the lower threshold for stellar mass explicit, rather than implicit.

We consider two models in which we relate the amount of satellite galaxy stellar mass lost to the corresponding amount of subhalo dark matter lost. Combined with the Z05 model that makes detailed predictions for dark matter mass loss, these models can predict the stellar mass loss for any given halo.

3.4.1 Model 1

Our first model sets the fraction of stellar mass that is lost from a galaxy to a fixed proportion of the fraction of dark matter that is lost from its subhalo. The model works as follows. Any halo of sufficiently large dark matter mass will have some stellar mass associated with the galaxy it contains at the time of accretion, $M^{*}_{\rm acc}$. This stellar mass will be some fraction of the mass in dark matter, $M^{\rm dm}_{\rm acc}$. After the halo merges into a larger halo, becoming a subhalo, it orbits within the host halo potential and loses mass. At the time of observation, the subhalo has a smaller mass, $M^{\rm dm}_{\rm fin}$. We relate the fraction of stellar mass that is lost during this time to the fraction

of dark matter mass that is lost through a single parameter ϵ,

$$\frac{\Delta M^*}{M^*} = \epsilon \, \frac{\Delta M^{\rm dm}}{M^{\rm dm}}, \tag{3.2}$$

$$\frac{M^*_{\rm acc} - M^*_{\rm fin}}{M^*_{\rm acc}} = \epsilon \, \frac{M^{\rm dm}_{\rm acc} - M^{\rm dm}_{\rm fin}}{M^{\rm dm}_{\rm acc}}, \tag{3.3}$$

which can be re-written as,

$$M^*_{\rm fin} = M^*_{\rm acc} \left[1 - \epsilon \times \left(\frac{M^{\rm dm}_{\rm acc} - M^{\rm dm}_{\rm fin}}{M^{\rm dm}_{\rm acc}} \right) \right] \tag{3.4}$$

The left-hand side of Figure 3.2 is a cartoon schematic of how stellar mass loss occurs in Model 1. From the time the subhalo merges into the host halo, $t_{\rm merge}$, until the final redshift under consideration, $t_{\rm final}$, the Z05 model (see § 3.3 for model details) predicts the amount of subhalo dark matter mass loss $\Delta M^{\rm dm}$ with the stellar mass loss ΔM^* being related to the dark matter mass loss via ϵ. Therefore, we are left with a simple parametric equation governed by a single free parameter. For example, if $\epsilon = 0.5$, then a subhalo that loses 50% of its dark matter will lose 25% of its stellar mass. As we mentioned above, stellar mass loss should be less efficient than dark matter mass loss, so we should generally expect $\epsilon < 1$.

In order to compute the final stellar mass of a galaxy via Eqn. 3.4, we need to know the stellar mass of a satellite galaxy as a function of the subhalo mass at the time of accretion. The stellar mass of a galaxy depends on many physical processes, including mergers, gas cooling, star formation, feedback from supernovae, feedback from active

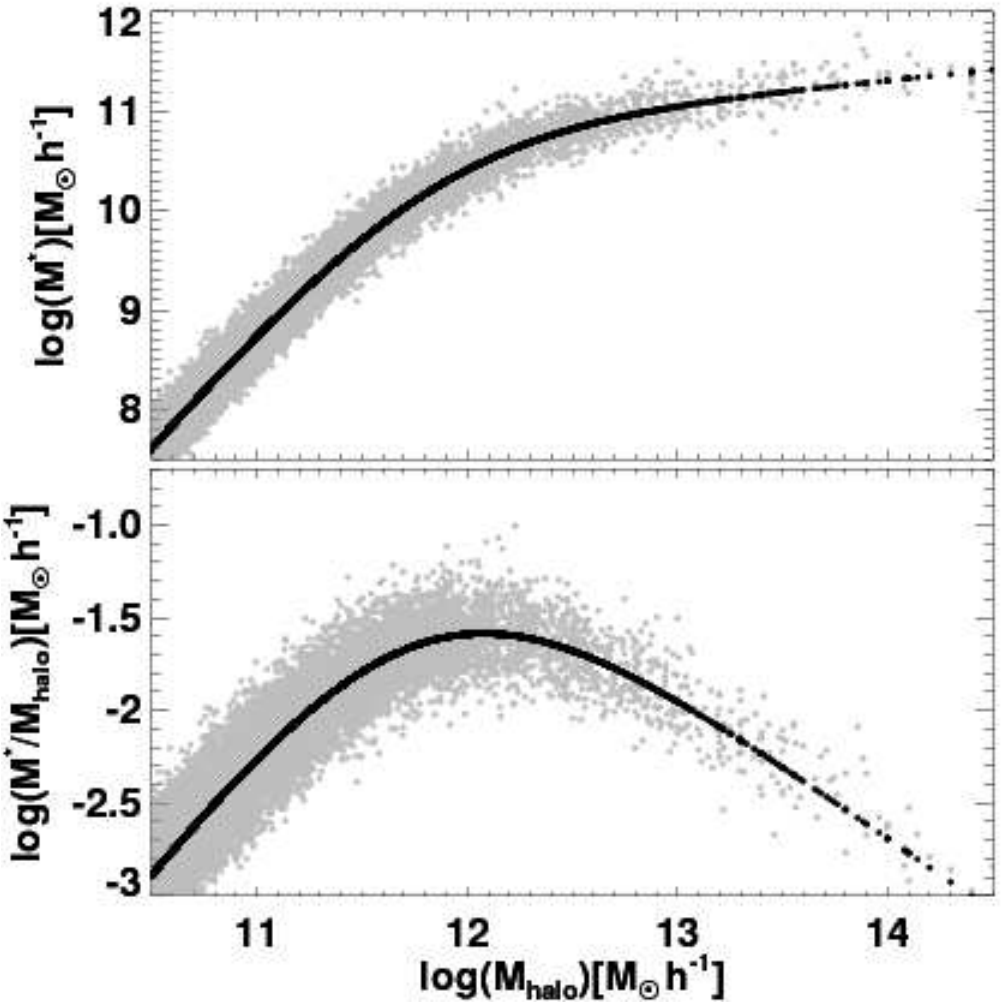

Figure 3.3: The stellar-to-halo mass relation (SHMR) for our host halos and subhalos with the adopted Behroozi et al. (2010) SHMR. The black curve shows the mean of the SHMR and grey points illustrate the assumed 0.15 dex scatter. The bottom panel is the same as the top with the y-axis divided by halo mass to highlight the characteristic mass ($\sim 10^{12} h^{-1} M_{\odot}$) where star formation is most efficient.

galactic nuclei, making *ab initio* predictions highly non-trivial. However, there are several empirical methods for obtaining the stellar-to-halo mass relation (SHMR), which have recently appeared in the literature (e.g., Yang et al., 2003; Wang et al., 2006; Conroy & Wechsler, 2009; Wang & Jing, 2010; Moster et al., 2010; Guo et al., 2010; Behroozi et al., 2010; Neistein et al., 2011). We assign stellar masses to halos with the SHMR of Behroozi et al. (2010, hereafter B10). Specifically, we employ the relation used in Eqn. 21 of B10, with the mean parameter values given by the $\mu = \kappa = 0$ model in their Table 2. Therefore, for every halo and subhalo in our catalog, we can use the halo mass *at the time of accretion* to assign a stellar mass to the galaxy hosted by the halo. The top panel of Figure 3.3 shows how stellar masses are related to our host halos and subhalos with the B10 SHMR. The black curve shows the mean of the SHMR and grey points illustrate the assumed 0.15 dex scatter given in B10. We show one million points randomly drawn from the full distribution of halos and subhalos over the host halo mass range $11 \leq \log(M/h^{-1}M_{\odot}) \leq 15$. Stellar mass rapidly increases as a function of halo mass at low masses before turning over and becoming shallower at higher host masses. The bottom panel is the same as the top with the y-axis divided by halo mass in order to highlight the characteristic mass where this turnover occurs, $M_{\rm halo} \sim 10^{12}h^{-1}M_{\odot}$. This characteristic mass is the halo mass at which star formation is most efficient.

For most applications, SHMRs are developed by linking the halo mass function to the galaxy stellar mass function (SMF) through abundance matching. This is

typically done using the subhalo mass at accretion which, by definition, presumes that no stellar stripping occurs. However, even if stellar stripping occurs (i.e., if ϵ is non-zero) we can still use a SHMR relation that assigns stellar mass at the time the subhalo merges, due to the fact that the SMF is *strongly* dominated by central galaxies. We emphasize that while there are many SHMRs in the literature, we are not very sensitive to the particular choice of SHMR. As we will discuss in § 3.5, we assign stellar masses to halos and subhalos and then rank them in stellar mass in order to find the stellar mass cut-off ($M^*_{\rm fin}$) that matches the observed number density of a given galaxy luminosity threshold sample. Therefore, two SHMRs that yield the same rank order for the halos and subhalos will be indistinguishable from each other, even though the values of $M^*_{\rm fin}$ will be different (as well as the mass-to-light ratios). All published SHMRs are monotonically increasing functions, so this behavior is general. On the other hand, the scatter in the SHMR is important, as this will change the rank order. We use the B10 scatter of 0.15 dex throughout our analysis, though we test the effect of changing the scatter on our results in § 3.5.1. We also note that we do not consider the fact that the stellar mass of a galaxy may actually *increase* for some time after merging and becoming a satellite, as it has been recently shown that star formation in active satellites may continue for several Gyr (see Wetzel et al., 2011). Such detailed modeling is beyond the scope and intention of this work.

In summary, we take the following steps in Model 1 for assigning final stellar masses to an ensemble of halos.

1. We use the Z05 model for subhalo evolution to obtain a list of halos and subhalos for a range of host halo masses, and we determine the fractional amount of dark matter mass lost from each subhalo.

2. We use the B10 stellar-to-halo mass relation to assign stellar masses to host halos and subhalos at the time of accretion.

3. For every subhalo, we compute a final stellar mass by relating the fractional amount of stellar mass lost to the fractional amount of dark matter mass lost through the single free parameter ϵ, as described in Eqn. 3.4.

3.4.2 Model 2

Model 1 operates under the basic assumption that the fractional amount of satellite galaxy stellar mass loss is proportional to subhalo dark matter loss through the free parameter ϵ. This means that even a small amount of dark matter stripping will be accompanied by some stellar stripping. However, as we argued in § 3.2, a subhalo may lose a considerable amount of dark matter before its galaxy is significantly disturbed. For example, subhalos in high-resolution simulations lose a significant fraction of mass at their outskirts rapidly upon merging into a larger system, while their interiors remain unaltered by this mass loss (e.g., Diemand et al., 2007). Accordingly, we consider an alternative model that incorporates a delay between the initial loss of dark matter mass and stellar mass loss.

Our second model states that stellar mass will only be lost if a sufficient amount of

dark matter is lost first. The model works as follows. We first define an approximate *radius of influence* that a galaxy has within its subhalo, corresponding to the region within which the gravity due to the stellar component is comparable to that from dark matter. To estimate this radius, we first assign a stellar mass to each subhalo at the time of accretion, $M^*_{\rm acc}$, using the B10 formalism. Next we assume, for simplicity, that this is a point mass and we do not consider the total amount of "cold baryons" or assume a galaxy profile. To find the radius of influence, $r_{\rm infl}$, of the stellar mass associated with the galaxy, we calculate where the dark matter mass enclosed within the subhalo is equal to $M^*_{\rm acc}$. We thus integrate the NFW mass profile,

$$M^{\rm dm}_{\rm acc}(< r_{\rm infl}) = 4\pi\rho_0 r_s^3 \left[\ln\left(1+\frac{r_{\rm infl}}{r_s}\right) - \frac{r_{\rm infl}/r_s}{1+r_{\rm infl}/r_s}\right], \tag{3.5}$$

where ρ_0 and r_s are the NFW parameters, and solve for $r_{\rm infl}$ by setting $M^{\rm dm}_{\rm acc}(< r_{\rm infl}) = M^*_{\rm acc}$.

The radius $r_{\rm infl}$ gives the rough scale within which mass must be lost before significant *stellar* mass is lost; however, we allow for flexibility in this final prescription for stellar mass loss. We assume that a galaxy will start losing stellar mass once dark matter is stripped from inside a radius that scales linearly with $r_{\rm infl}$. We define a new radius, $r' = \psi \times r_{\rm infl}$, where ψ is a free parameter of order unity. If the subhalo loses so much dark matter that its final mass is less than $M^{\rm dm}_{\rm acc}(< r')$, we allow stellar stripping to occur. Furthermore, we assume that the fraction of stellar mass lost is equal to the fraction of dark matter lost *after the bound mass of the subhalo crosses*

below this threshold. The final stellar mass of the galaxy is thus

$$M^*_{\rm fin} = M^*_{\rm acc}\left[1 - \max\left\{0, \left(\frac{M^{\rm dm}_{\rm acc}(< r') - M^{\rm dm}_{\rm fin}}{M^{\rm dm}_{\rm acc}(< r')}\right)\right\}\right], \tag{3.6}$$

which is analogous to Eqn. 3.4.

The right-hand side of Figure 3.2 illustrates how Model 2 works. After accretion, if the subhalo shrinks enough due to mass loss such that its mass at the final redshift of interest is less than $M^{\rm dm}_{\rm acc}(< r')$, then stellar mass will be lost (ΔM^*) in proportion to the additional amount of dark matter lost. However, if mass loss does not reduce the subhalo mass to less than $M^{\rm dm}_{\rm acc}(< r')$, no stellar mass is lost. Model 2 incorporates a delay between the stripping of the outer layers of dark matter and the stripping of the stellar material residing in the depths of the subhalo potential well. The single free parameter of Model 2, ψ, allows us to vary the amount of lag. As was the case for $\epsilon = 0$ in Model 1, setting $\psi = 0$ in Model 2 leads to zero stellar mass loss in all subhalos.

In summary, we take the following steps in Model 2 for assigning final stellar masses to an ensemble of halos.

1. We obtain a population of halos and assign stellar masses at the time of accretion as described in the first two steps of the Model 1 summary.

2. For each subhalo, we calculate $r_{\rm infl}$ using Eqn. 3.5. We then scale this radius using the free parameter ψ, to get $r' = \psi \times r_{\rm infl}$.

3. We calculate the dark matter mass at accretion that is enclosed by r', $M_{\rm acc}^{\rm dm}(< r')$. If insufficient dark matter loss has occurred, such that the final subhalo mass is greater than this, then we assume that no stellar mass loss has taken place. Otherwise, we estimate a final stellar mass using Eqn. 3.6.

3.5 Constraining Satellite Galaxy Stellar Mass Loss Using Galaxy Clustering

We now turn to constraints on the relationship between stellar mass and halo mass imposed by the clustering of galaxies. Our two stellar mass loss models specify the final stellar mass in any halo or subhalo, given a value for the parameter ϵ (for Model 1) or ψ (for Model 2). With stellar masses assigned to all halos and subhalos, we can predict a *halo occupation distribution* (HOD: e.g., Peacock & Smith, 2000; Scoccimarro et al., 2001; Berlind & Weinberg, 2002; Cooray & Sheth, 2002) for any given stellar mass threshold. In particular, we compute the mean number of galaxies as a function of host halo mass, $\langle N \rangle_{\rm M}$. We calculate the mean over the 500 host halo realizations at each host mass. We use this function to compute the number density of galaxies by weighting the host halo abundances by $\langle N \rangle_{\rm M}$ and integrating over all halo masses,

$$\bar{n}_g = \int_0^\infty dM \frac{dn}{dM} \langle N \rangle_M. \tag{3.7}$$

We adopt the Warren et al. (2006) halo mass function, dn/dM, in this calculation, though our results are not sensitive to the specific choice of mass function. In this way, we find the stellar mass threshold that yields a galaxy number density equal to

that of the observed sample with which we aim to compare.

We compare our model predictions to four of the Sloan Digital Sky Survey (SDSS: York et al., 2000) luminosity threshold galaxy samples measured by Zehavi et al. (2011). Specifically, we consider volume-limited samples with r-band absolute magnitude thresholds of $M_r \leq -18$, -19, -20, and -21 (number densities for these samples are listed in Table 2 of Zehavi et al. 2011). We do not consider the fact that the observed relationship between stellar mass and luminosity is not one-to-one (i.e., galaxies of a fixed luminosity can have different stellar masses which, for instance, is manifested as scatter in the Tully-Fisher relation – Bell & de Jong 2001). However, including this scatter should be similar to increasing the scatter in the B10 relation between dark matter mass and $M^*_{\rm acc}$, which has a very small effect, as we show in § 3.5.1.

Once we have determined the appropriate stellar mass threshold, we use the resulting HOD to calculate the predicted clustering of the model. We place galaxies within the host halos in a N-body simulation to measure the 2PCF. We use a single realization of the "Consuelo" simulation (with a box size of $420h^{-1}$Mpc and 1400^3 particles), which is part of the *LasDamas* suite of simulations (McBride et al., in prep.). The cosmology assumed in our semi-analytic subhalo model is set to match that of the LasDamas simulations[3] and is similar to the recent WMAP7 values (Ko-

[3]Throughout the paper, we work within the standard, vacuum-dominated, cold dark matter (ΛCDM) cosmological model with $\Omega_{\rm m} = 0.25$, $\Omega_\Lambda = 0.75$, $\Omega_{\rm b} = 0.04$, $h_0 = 0.7$, $\sigma_8 = 0.8$, and $n_{\rm s} = 1.0$.

matsu et al., 2011). We use the spherical over-density (SO) halo finder "Rockstar" (Behroozi et al., 2011) to identify halos. We use an SO halo finder because the SO algorithm mimics the assumptions made in our semi-analytic model. Both the Z05 model and the halo finder define virial masses based on the virial threshold definition of Bryan & Norman (1998). We note, however, that our results are not sensitive to the choice of halo finder. We have repeated our analysis using a Friends-of-Friends halo finder and derived similar results. We populate host halos with galaxies according to our $\langle N \rangle_M$ model predictions.

In order to compare to data, we convert our real-space correlation functions, $\xi(r)$, to *projected* correlation functions, $w_p(r_p)$, by integrating along lines of sight (Davis & Peebles, 1983; Zehavi et al., 2004):

$$w_{\rm p}(r_{\rm p}) = 2 \int_0^{y_{\rm max}} \xi\Big(\sqrt{r_{\rm p}^2 + y^2}\Big) dy. \tag{3.8}$$

For each luminosity threshold, we integrate out to the same $y_{\rm max}$ as Zehavi et al. (2011, listed as $\pi_{\rm max}$ in their Table 2). We predict $w_p(r_p)$ for the four luminosity samples, given any value of ϵ from Model 1 or ψ from Model 2. In order to constrain our stellar mass loss models, we run a grid of ϵ and ψ values in steps of $\Delta\epsilon = 0.1$ and $\Delta\psi = 0.05$. For each parameter value and each luminosity threshold, we compute χ^2 by comparing our model prediction to the Zehavi et al. (2011) measurement of $w_p(r_p)$, using only diagonal errors (not the full covariance matrices).

Figure 3.4 shows clustering results for Model 1 compared to measurements from

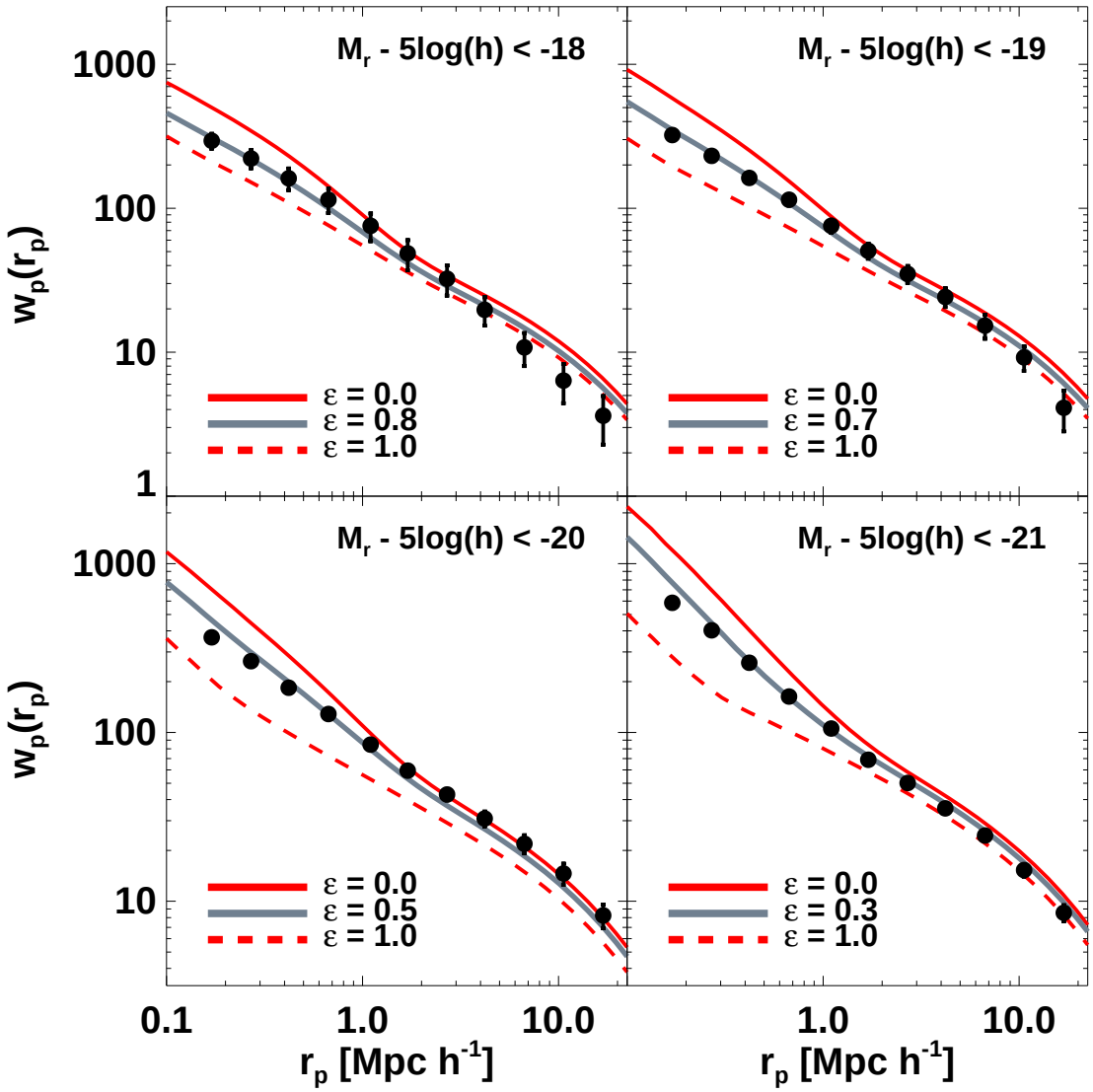

Figure 3.4: Clustering predictions for Model 1. Model 1 sets the fractional amount of satellite galaxy stellar mass loss to be proportional to the fractional amount of subhalo dark matter mass loss through the free parameter ϵ (see §3.4.1 for model details and Fig. 3.2 for an illustration). Solid red curves show model predictions for $\epsilon = 0$, equivalent to no stellar mass loss. Dashed red curves show the $\epsilon = 1$ case, where the stellar mass loss occurs at the same rate as subhalo dark matter mass loss. Grey curves show the ϵ values that match the observed SDSS clustering measurements of Zehavi et al. (2011) at each luminosity threshold (black points).

Zehavi et al. (2011) for our four SDSS luminosity threshold samples: $M_r < -18, -19, -20$ and -21. To reiterate, Model 1 assumes that the fractional amount of satellite galaxy stellar mass loss is proportional to the fractional amount of subhalo dark matter mass loss with proportionality constant ϵ. Adopting $\epsilon = 0$ specifies no stellar mass loss and is equivalent to using $V_{\rm max}$ at the epoch of accretion for abundance matching. On the other hand, adopting $\epsilon = 1$ means that stellar mass is lost at the same rate as dark matter. For each luminosity sample, we show the $\epsilon = 0$ and 1 cases as red solid and dashed lines, respectively.

At each luminosity, $\epsilon = 0$ predicts small-scale clustering that is stronger than the data indicate and this gets to the essence of using clustering to constrain stellar mass loss. This over-prediction can be attributed to the fact that no stellar mass loss has occurred for satellite galaxies, resulting in too many satellites with high stellar masses. This leads to enhanced clustering on small scales (e.g. Watson et al., 2011b). To be consistent with the data, some stellar mass loss needs to occur. However, the $\epsilon = 1$ result demonstrates that too much stellar mass loss leads to weaker clustering than the data require. The grey curves in Figure 3.4 correspond to intermediate amounts of stellar mass loss and represent the ϵ with the lowest χ^2 values.[4] Despite the fact that Model 1 paints a simplified picture of how stars are stripped from the galaxies they reside in, we show that it is very effective at matching the observed clustering.

[4]We note that none of our model predictions match the large-scale clustering for the $M_r < -18$ sample. This may be attributed to the finite volume of the sample, as discussed in § 3.2 of Zehavi et al. (2011).

Moreover, it is striking that ϵ decreases with increasing luminosity. We will discuss this luminosity dependence in detail in § 3.6.

Figure 3.5 shows similar results for Model 2. This model was designed to allow dark matter on the periphery of a subhalo to be lost due to the strong tidal field of the host, without significantly altering the luminous galaxy residing deep in the core of the subhalo. Model 2 mimics this "lag" by defining a critical radius within each subhalo and only allowing for stellar mass loss if the subhalo loses mass from within that radius. This radius can be varied through the parameter ψ. The limit $\psi = 0$ corresponds to no stellar mass loss and is equivalent to abundance matching using $V_{\rm max}$ at accretion. In Model 1, $\epsilon = 1$ is analogous to using the subhalo mass at the final redshift output for abundance matching. In Model 2, this happens when the critical radius is larger than the size of the subhalo at accretion. This occurs at a different value of ψ for each subhalo. Thus, we choose an arbitrary value $\psi = 2$ to again illustrate how too much stellar mass loss will under-predict clustering.

As was the case for Model 1, we are able to match the observed clustering and we see a strong evolution in ψ as a function of luminosity. This emphasizes what was found for Model 1, that low-luminosity galaxies experience more efficient stellar stripping throughout their evolution in a host halo than luminous galaxies.

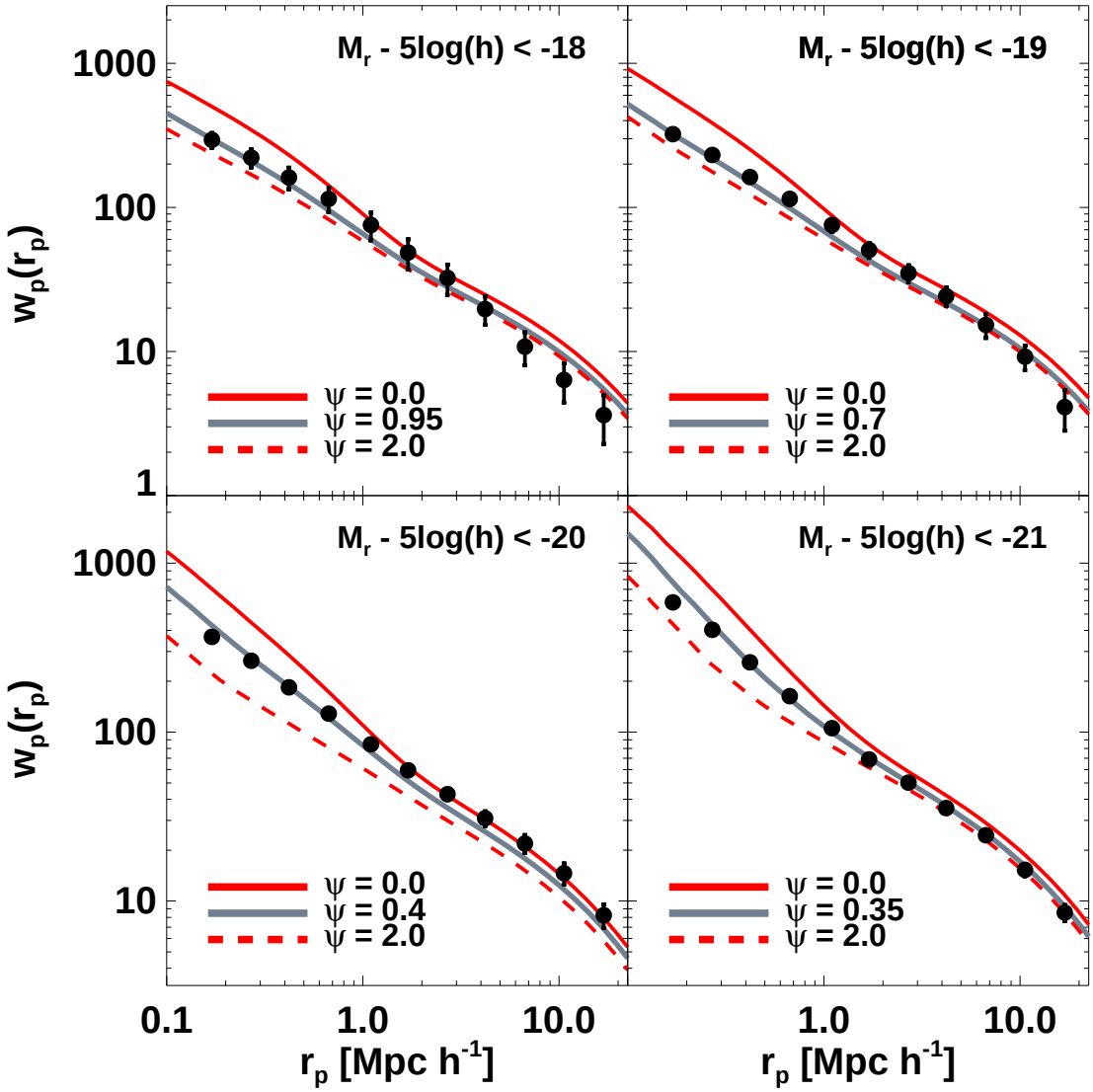

Figure 3.5: Clustering results for Model 2. Model 2 defines a radius of influence, $r_{\rm infl}$, for a galaxy within a subhalo. If a subhalo loses sufficient dark matter mass such that it starts to lose mass inside of $r_{\rm infl}$, then stellar mass is lost at a rate proportional to the subsequent subhalo mass loss. The free parameter ψ allows $r_{\rm infl}$ to grow or shrink, thus a larger value of ψ means that more stellar mass loss will occur on average for satellite galaxies. Solid red curves show model predictions for $\psi = 0$, equivalent to no stellar mass loss, thus the same as $\epsilon = 0$ for Model 1. Dashed red curves show the predictions for $\psi = 2$, an arbitrary value chosen to represent how too much stellar mass loss will under-predict $w_p(r_p)$. Grey curves show the ψ values that match the observed clustering for the same luminosity threshold samples as in Fig. 3.4.

3.5.1 The Effect of Scatter in the Stellar-to-Halo Mass Relation

Observations indicate that halos of a given mass can host galaxies with a range of luminosities and stellar masses (e.g., van den Bosch et al., 2007; Zheng et al., 2007; Yang et al., 2008; More et al., 2009). For this reason, it is overly restrictive to assume a one-to-one relation between halo mass and stellar mass, whereas a relationship with some intrinsic scatter is more appropriate. This is especially true for abundance matching because the presence of scatter changes the rank order of galaxies. We rank our halos and subhalos by stellar mass, so the rank order will be affected by the assumed amount of scatter. Scatter is typically accounted for by assuming a distribution of stellar mass at fixed halo mass, with the mean value of stellar mass given by a particular SHMR. For example, the B10 scatter that we adopt in this paper is a log-normal distribution with a dispersion $\sigma = 0.15$. We implement this scatter by randomly drawing from this distribution when we assign stellar masses to halos and subhalos at the time of accretion. The results shown in Figures 3.4 and 3.5 include this scatter.

We repeat our analysis with different dispersions in order to test the sensitivity of our results to uncertainty of the scatter in the SHMR. Figure 3.6 Shows the effect of changing the SHMR dispersion for one of the models that matches the clustering of $M_r < -21$ galaxies: Model 1 with $\epsilon = 0.3$. This sample is the most sensitive to scatter because the slope of the SHMR is shallowest for luminous galaxies and thus a given amount of scatter in stellar mass at fixed halo mass translates into a large

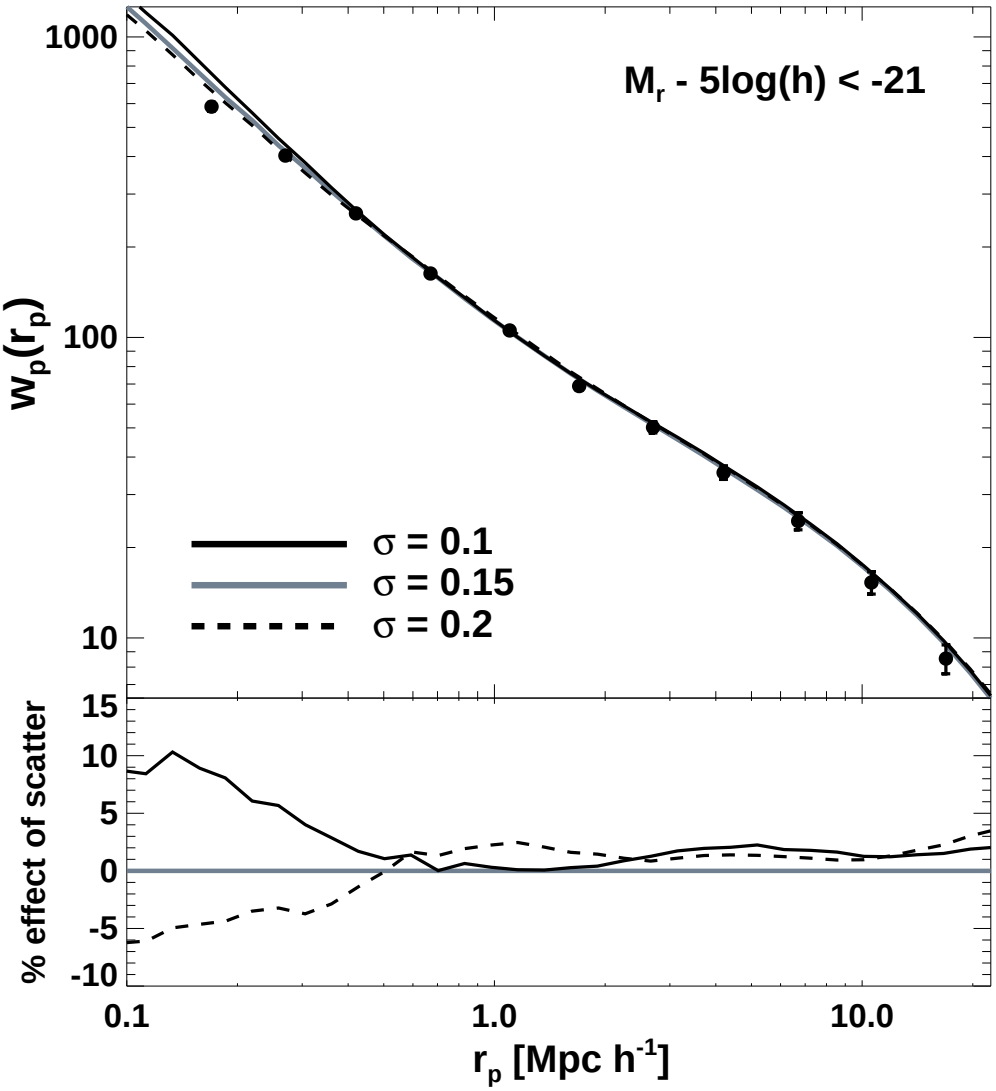

Figure 3.6: The effect of the scatter in the stellar mass – halo mass relation, on the clustering of a stellar mass threshold galaxy sample. *Top panel*: The grey curve shows the predicted correlation function from Model 1 with $\epsilon = 0.3$ and our assumed scatter of $\sigma = 0.15$ dex, given by Behroozi et al. (2010). Solid and dashed black curves show results for changing the scatter to $\sigma = 0.1$ dex and 0.2 dex, respectively. Each curve is averaged over three realizations of that amount of scatter. *Bottom panel*: The percent deviations in the correlation function from the fiducial scatter of $\sigma = 0.15$. At the scale of the innermost data point of Zehavi et al. (2011) that we compare our model results to ($\sim 0.17h^{-1}$Mpc), lowering the scatter to $\sigma = 0.1$ increases $w_p(r_p)$ by $\sim 8\%$ and increasing the scatter to $\sigma = 0.2$ lowers $w_p(r_p)$ by $\sim 5\%$. On larger scales the effect is much smaller.

scatter in halo mass at a fixed stellar mass threshold (see Fig. 3.3). The top panel of Figure 3.6 shows the correlation function for three SHMR dispersions: $\sigma = 0.1$, 0.15, and 0.2. The bottom panel depicts percent deviations from the fiducial scatter of $\sigma = 0.15$. This range is conservative, as it is larger than the errors in scatter quoted in B10 (especially at the low end). The figure demonstrates that changing the scatter has a small effect on $w_p(r_p)$, in the sense that more scatter generally leads to a lower amplitude of clustering on small scales. Over the range of data points from the Zehavi et al. (2011) data that we model, there is a maximum $\sim 8\%$ and $\sim 5\%$ shift in $w_p(r_p)$ for the $\sigma = 0.1$ and $\sigma = 0.2$ cases, respectively. This is not a large effect and does not result in a significant change to the best-fit values of ϵ or ψ. Uncertainties in the scatter of the SHMR do not significantly alter our results or our primary conclusions.

3.6 Luminosity Dependence of Satellite Galaxy Stellar Mass Loss

Figures 3.4 & 3.5 indicate that the best-fit values of both ϵ and ψ vary with luminosity. We highlight these trends in Figure 3.7. The left-hand panel summarizes results from Model 1, and demonstrates that the best-fit value of ϵ drops from $\epsilon = 0.8$ for $M_r < -18$ galaxies to $\epsilon = 0.3$ for $M_r < -21$ galaxies. There is a strong luminosity dependence associated with satellite galaxy stellar mass loss, such that relatively low-luminosity satellite galaxies lose more stellar material per unit of dark matter than more luminous satellite galaxies. The right-hand panel of Figure 3.7 summarizes results from Model 2, which show a consistent trend. The best-fit value of ψ drops

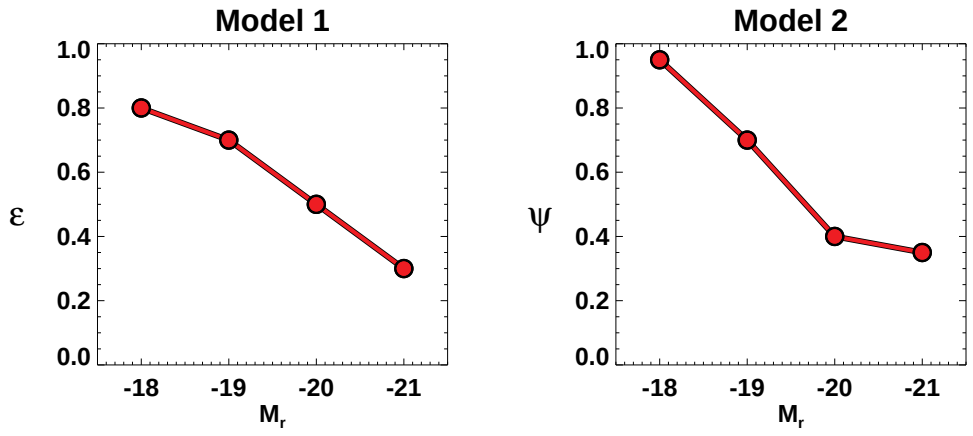

Figure 3.7: The luminosity dependence of satellite galaxy stellar mass loss. *Left panel*: The best-fit Model 1 parameter ϵ as a function of absolute r-band magnitude. The decreasing trend of ϵ with increasing luminosity means that low-luminosity satellite galaxies experience greater stellar mass loss relative to subhalo dark matter mass loss than luminous galaxies. *Right panel*: The best-fit Model 2 parameter ψ as a function of absolute r-band magnitude. The decreasing trend of ψ with increasing luminosity means that low-luminosity satellite galaxies have a greater radius of influence (causing more stellar mass loss) than luminous galaxies. In other words, the same qualitative luminosity trend is seen in both models.

from $\psi = 0.95$ for $M_r < -18$ galaxies to $\psi = 0.35$ for $M_r < -21$ galaxies. Lower values of ψ indicate less stellar mass loss for a given amount of dark matter mass loss. The two models we explore absorb a significant number of subtle effects into simple assumptions. Model 1 and Model 2 differ substantially in detail, yet both analyses indicate that the luminosity dependence of galaxy clustering can be explained if low-luminosity satellite galaxies lose stars more efficiently than luminous galaxies.

What does this result mean? Presumably it means that the stars within luminous galaxies are more tightly bound – relative to their surrounding dark matter – than the stars in less luminous galaxies. This could be due to luminous galaxies having more compact stellar density profiles. In fact, it may be that this result can be ex-

plained by the well-known correlation between galaxy luminosity and morphology, whereby luminous galaxies are more likely to be ellipticals than low-luminosity galaxies. For example, Blanton et al. (2003) showed that the mean Sércic index of galaxies roughly doubles from $M_r = -18$ to $M_r = -21$ (looking at their Fig. 9 and converting i-band to r-band magnitudes). We must, of course, keep in mind that these morphology-luminosity correlations apply to all galaxies, of which satellites are only a small portion. It may be that these correlations would vanish in samples containing only satellite galaxies.

An ancillary consideration is the relative size of galaxies compared to the typical (sub)halos they occupy. For instance, using a sample of 140,000 SDSS galaxies, Shen et al. (2003) showed the size distribution (half-light radii) of early- and late-type galaxies as a function of r-band luminosity and stellar mass. Examining their Figs. 2 & 3, the half-light radius $\overline{R}$ increases roughly by a factor of ~ 3 from $M_r < -19.25$ to -22.25 for late-type galaxies, and by a factor of ~ 5 for early types. However, if we consider the typical halo masses that host these galaxies (see $M_{\rm min}$ values for $M_r < -19$ and -22 from Table 3 of Zehavi et al. 2011), they correspond to virial radii of $\sim 125h^{-1}$kpc and $\sim 750h^{-1}$kpc, respectively, a factor of 6. In other words, at a very approximate level, larger (more luminous) galaxies are slightly deeper within their host halo potential wells than smaller (less luminous) galaxies, and are relatively less susceptible to stellar stripping.

The luminosity trend that we have found demonstrates the power of our modeling

approach. We use one observational measurement, galaxy clustering, to shed light on an important physical process that is essentially unobservable: stellar mass loss from satellite galaxies relative to dark matter mass loss. In the next section we show how our models can be used to predict a different observable, the IHL. The IHL is a remnant of stellar mass loss, so it may be used to probe the liberated stellar debris, and thus provide an important cross-check on our results.

3.7 Predictions for Intrahalo Light at Varying Scales

If stars are freed from their host galaxies they will presumably become part of the IHL. Some of the IHL is a diffuse background, while some may be composed of coherent streams, a prominent example of which is the Sagittarius Stream in our own galaxy (e.g., Ibata et al., 2001; Dohm-Palmer et al., 2001; Newberg et al., 2002), if the stars were stripped from a subhalo in the past few dynamical times. Observations of the IHL are notoriously difficult, and Gonzalez et al. (2007) argue that the proper quantity to measure is the sum of the light from the host central galaxy (the "brightest halo galaxy" or BHG) and the diffuse intrahalo light component, because it is non-trivial to disentangle the two. Our models assign stellar masses to all halos (both hosts and subhalos), so we can compute the contribution of the BHG to the total stellar mass of the system. This combination is also less subject to theoretical uncertainty because collisions between the BHG and an infalling satellite can disperse stellar mass into the IHL. While parsing of the stellar mass of the BHG and IHL individually is

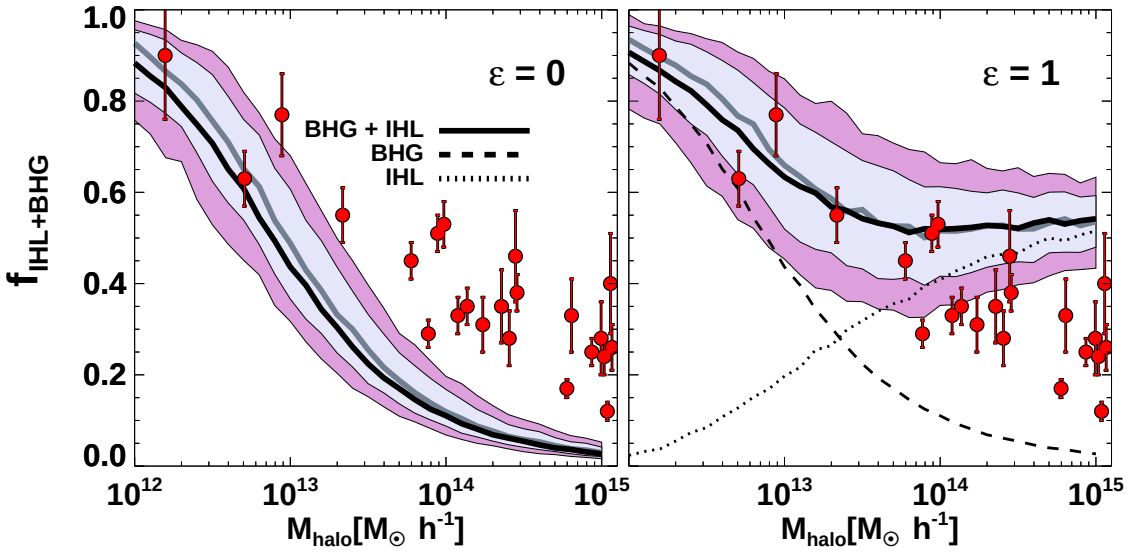

Figure 3.8: $f_{\rm IHL+BHG}$ predictions for the two extreme cases of Model 1: $\epsilon = 0$ and 1. $f_{\rm IHL+BHG}$ is the combined amount of stellar mass from the brightest halo galaxy (BHG) and the intrahalo light (IHL) divided by the total stellar mass of a system (the BHG, IHL, and the stellar mass still associated with surviving subhalos). Thick solid black curves show the mean $f_{\rm IHL+BHG}$ as a function of host halo mass and are computed from 500 model realizations of each host mass, while grey curves represent the median. Light and dark purple shaded regions represent the 68% and 95% range of the model distributions. BHG and IHL contributions are shown individually as dashed and dotted curves, respectively. Red points show the Gonzalez et al. (2007) data measurements for comparison. *Left panel*: $\epsilon = 0$ means that no stellar mass loss occurs, resulting in no IHL. As a result, $f_{\rm IHL+BHG}$ is strongly under-predicted at cluster scales ($M_{\rm halo} \sim 14 - 15h^{-1}M_\odot$) relative to the data. *Right panel*: $\epsilon = 1$ means that stellar mass loss occurs at the same rate as subhalo dark matter mass loss. This results in an over-prediction of the IHL. Note: theory curves are shifted by $\sim 40\%$ in order to convert our virial masses (using the definition $\Delta_{\rm vir} = 377$) to the M_{500} ($\Delta_{\rm crit} = 500$) masses given in Gonzalez et al. (2007).

sensitive to the fraction of stellar mass ejected in such collisions, the sum is robust to uncertainties in this process.

We start by investigating the predictions for the $\epsilon = 0$ and $\epsilon = 1$ cases from Model 1. These extremes were shown in § 3.5 to over- and under-predict the observed clustering, respectively, for each luminosity threshold. In Figure 3.8, we show the fraction of the total stellar mass of a system (including stellar mass in satellite galaxies), that is contained within both the IHL and the BHG, $f_{\rm IHL+BHG}$, as a function of host halo mass, $M_{\rm halo}$. The thick solid black curves in Figure 3.8 show the mean value of $f_{\rm IHL+BHG}$ obtained from our 500 realizations of host halos, and grey curves represent the median. The inner and outer shaded regions represent the 68% and 95% ranges of the model distributions. The mean individual BHG and IHL contributions are shown distinctly as dashed and dotted curves, respectively. The $f_{\rm IHL+BHG}$ data from Gonzalez et al. (2007) are shown as red circles with errorbars, and are the same in both panels.

For $\epsilon = 0$ there is no stellar mass loss, and thus no contribution to the total stellar mass of the system from the IHL. The stellar mass of the BHG alone provides a decent description of the data for halo masses below group mass scales, $M_{\rm halo} \lesssim 10^{13}\,h^{-1}M_{\odot}$. While less massive systems have been observed to have some detectable IHL (see § 5.1), it is mainly large group- and cluster-size objects that are known to have significant IHL components. It is therefore not surprising that the $\epsilon = 0$ model underestimates $f_{\rm IHL+BHG}$ on these scales.

At the other extreme, the $\epsilon = 1$ model assumes that stellar mass is lost with the same efficiency as dark matter. We argued in § 3.4 that this over-estimates stellar mass loss, so it is not surprising that choosing $\epsilon = 1$ leads to an overestimate of $f_{\rm IHL+BHG}$ for systems greater than large groups ($M_{\rm halo} \gtrsim 10^{13.5}\,h^{-1}M_{\odot}$). At lower masses, typical infalling satellites have halo masses below $M_{\rm acc}^{\rm dm} \lesssim 10^{11}\,h^{-1}M_{\odot}$ and bring with them only a small amount of stellar mass (B10). This is the regime of the SHMR where stellar mass rapidly decreases with decreasing halo mass (see Fig. 3.3). Data are not yet precise enough to be sensitive to the stellar mass carried into the systems by such small, infalling subhalos. Consequently, $f_{\rm IHL+BHG} \approx f_{\rm BHG}$ and can be adequately described in low-mass systems at both the $\epsilon = 1$ and $\epsilon = 0$ extremes.

We note that in our model predictions for the IHL, we only consider the stellar mass stripped from satellite galaxies that have stellar masses equivalent to $M_r < -18$ galaxies and brighter. We ignore stellar mass loss from less luminous (less massive) satellites in the $f_{\rm IHL+BHG}$ calculation. However, the stellar mass locked up in these lower mass "uncounted" subhalos only amounts to $\sim 3\%$ of the total stellar mass within a given host halo, so neglecting them has a negligible effect on our $f_{\rm IHL+BHG}$ model predictions. We also note that in Figure 3.8 we have shifted the data points to higher masses by $\sim 40\%$ in order to convert the M_{500} ($\Delta_{\rm crit} = 500$) masses given in Gonzalez et al. (2007) to our virial masses (using the definition $\Delta_{\rm vir} = 377$). We assumed an NFW profile to perform this conversion.

Having shown that these two extreme cases are not able to describe the data

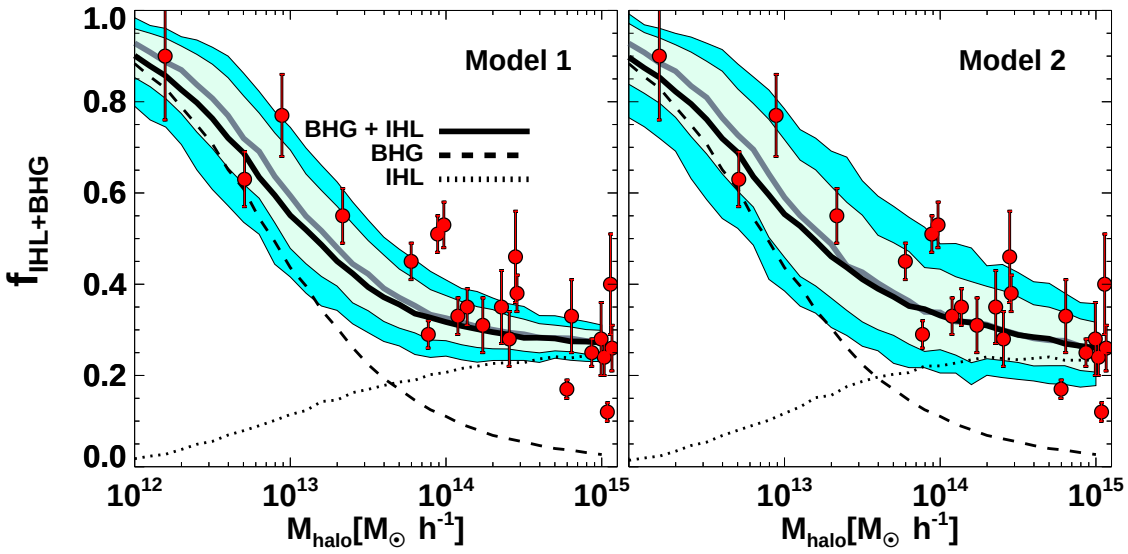

Figure 3.9: $f_{\rm IHL+BHG}$ predictions for our best-fit Model 1 (left panel) and Model 2 (right panel). We compute each subhalo's contribution to the IHL according to its initial stellar mass by using the appropriate best-fit values of ϵ or ψ. For example, a subhalo with a stellar mass that corresponds to a galaxy of absolute r-band magnitude equal to -18.5 loses stellar mass according to $\epsilon = 0.8$ (in Model 1), whereas a subhalo with a stellar mass corresponding to $M_r = -20.5$ loses stellar mass according to $\epsilon = 0.5$. Shaded regions, curves, and points are as in Fig. 3.8. Our stellar mass loss models predict that the mean IHL fraction in halos increases from a few percent at the scale of individual galaxies ($M_{\rm halo} \sim 10^{12} h^{-1} M_\odot$) to $\sim 20 - 25\%$ at cluster scales ($M_{\rm halo} \sim 10^{14} - 10^{15} h^{-1} M_\odot$). Both models succeed in matching the mean trend observed by Gonzalez et al. (2007). However, Model 1 seems to under-predict the scatter in $f_{\rm IHL+BHG}$, whereas Model 2 predicts a scatter that is more consistent with the data measurements. We thus find that this more physically-motivated model for satellite galaxy stellar mass loss is favored over Model 1.

accurately, we turn to the predictions of our models. To make $f_{\rm IHL+BHG}$ predictions at a given host halo mass scale we need to assign each (sub)halo an ϵ value for Model 1 and a ψ value for Model 2. Let us examine just the Model 1 case for simplicity. When we found the best-fit value of ϵ for each luminosity threshold sample in § 3.5, we also determined a final stellar mass threshold for the sample through abundance matching. For example, the $M_r < -20$ sample was found to correspond to halos and subhalos with final stellar masses greater than some value $M^*_{\rm fin,20}$, where final stellar masses are predicted using $\epsilon = 0.5$. The $M_r < -21$ sample corresponds to stellar masses greater than $M^*_{\rm fin,21}$, where final stellar masses are predicted using $\epsilon = 0.3$, and so on. We assign each subhalo a value of ϵ using these stellar mass thresholds. For example, if a subhalo has a stellar mass at accretion that falls between $M^*_{\rm fin,20}$ and $M^*_{\rm fin,21}$, we assign it $\epsilon = 0.5$. If, instead, it has a mass between $M^*_{\rm fin,19}$ and $M^*_{\rm fin,20}$, we assign it $\epsilon = 0.7$. It is awkward to use the stellar mass at accretion to assign subhalos to ranges in $M^*_{\rm fin}$, but we cannot estimate final stellar masses without having a value of ϵ in the first place, so we are stuck with this approximate method. We follow the same process for Model 2 by choosing the appropriate ψ values. We emphasize that these ϵ and ψ values are not "tuned" to agree with the $f_{\rm IHL+BHG}$ observations, rather are genuine predictions that result from parameter values found from matching to clustering data.

Figure 3.9 shows the Model 1 (left panel) and Model 2 (right panel) $f_{\rm IHL+BHG}$ predictions, as well as the individual IHL and BHG contributions. While $f_{\rm IHL+BHG}$

rapidly decreases with increasing host halo mass, the contribution to $f_{\rm IHL+BHG}$ from the IHL increases. This supports a picture in which galaxy-mass halos have very few luminous satellite galaxies and little IHL, so the stellar masses of these systems are dominated by the BHGs. Galaxy size halos accrete the majority of their mass from small subhalos that have very high mass-to-light ratios (Purcell et al., 2007). Therefore, shredded satellites deposit very little stellar mass into the IHL. The number of large satellites increases with host halo mass. The larger and more common subhalos within larger host halos may form stars more efficiently (have lower mass-to-light ratios) and provide a source for developing significant IHL. Both models find that host masses of $M_{\rm host}/h^{-1}M_{\odot} = 10^{12}, 10^{13}, 10^{14}$, and 10^{15}, contain mean IHL fractions of $f_{\rm IHL} \sim 2\%, 10\%, 20\%$, and 25%, respectively. This is in good agreement with several previous studies, as we discuss in § 3.8. The IHL thus provides an independent check of our stellar mass loss results.

Figure 3.9 contains a comparison between our model predictions and the Gonzalez et al. (2007) data. Both models predict mean $f_{\rm IHL+BHG}$ fractions that are consistent with the observations.[5] Interestingly, we find that the scatter predicted by Model 1 is substantially smaller than it is for Model 2 and it appears to be inconsistent with the scatter found by Gonzalez et al. (2007). On the other hand, Model 2 is more successful in reproducing the observed scatter in $f_{\rm IHL+BHG}$. To quantify this, we

[5]We note that this discussion assumes that the Gonzalez et al. (2007) data are accurate, whereas they may be systematically overestimated due to an assumed constant mass-to-light ratio (Leauthaud et al., 2011).

calculate the probability that the scatter in the Gonzalez et al. (2007) data points could result from the model distributions. We do this as follows. First, we restrict the comparison to the high mass regime (the last 8 data points) because we wish to investigate the scatter at fixed mass (if we include lower mass points, the measured scatter will be affected by the mean trend of $f_{\rm IHL+BHG}$ vs. mass). We next create a model data set by choosing a single model realization of a host halo (out of the 500) for each Gonzalez et al. (2007) data point, at the appropriate halo masses. This leads to 8 model values of $f_{\rm IHL+BHG}$. We then add a Gaussian random error to these values, using the corresponding Gonzalez et al. (2007) errorbars. To fully sample the distribution of data sets that could arise from our models, we repeat this process 10,000 times. Finally, we measure the weighted standard deviation of $f_{\rm IHL+BHG}$ values for the observed data, as well as each of the 10,000 model data sets. We find that in Model 1, only 0.8% of the model data sets have a scatter that exceeds that of the Gonzalez et al. (2007) data, whereas in Model 2, 25% of the model data sets have a larger scatter.

This statistical test indicates that Model 1 should be rejected (at the 2.7σ level) in favor of Model 2, an indication that is not entirely surprising given that Model 2 accounts for delayed stellar mass loss that is to be expected on physical grounds. Model 1 assumes that stellar mass loss is simply proportional to subhalo mass loss, so the scatter predicted by this model must be primarily caused by the scatter in the total amount of dark matter mass loss, with a secondary amount of scatter coming

from the stellar to halo mass relation. On the other hand, Model 2 allows for greater variation in the amount of stellar mass loss. For example, let us suppose two subhalos start with the same mass at accretion and lose the same amount of dark matter. Now let us suppose one contains 10% more stellar mass at accretion due to the scatter in the SHMR. According to Model 1, both galaxies will lose the same fraction of their stellar mass and so the one galaxy will inject 10% more stars into the IHL. According to Model 2, however, the actual fraction of stars lost depends on stellar mass through the galaxy's radius of influence. The more massive galaxy will lose a higher fraction of its stellar mass, thus causing a larger than 10% discrepancy in the total stellar mass lost between the two galaxies.

3.8 Summary & Discussion

While galaxy formation is complex, we have shown in this paper that an understanding of the fates of satellite galaxies provides key insight into the galaxy formation puzzle. Satellite galaxies live extremely tumultuous lives. Their spatial clustering can shed light on how they lose stellar mass and contribute to building the IHL over a large range of host halo mass scales. Part of our motivation for using galaxy clustering to constrain stellar mass loss stems from possible shortcomings in the commonly-employed abundance matching technique (e.g., Wetzel & White, 2010; Yang et al., 2011, Reddick et al., in prep.), which suggest natural generalizations with the gross form of the particular models we study. The standard method of abundance

matching involves mapping galaxies to halos by assuming a relationship between halo (and subhalo) mass (or circular velocity) and a galaxy property (luminosity or stellar mass) at a particular time. A galaxy luminosity assignment according to halo mass *at the time the halo was first accreted onto a larger system* provides a very useful description of known galaxy clustering properties (e.g., Conroy et al., 2006). However, this type of assignment implies that *no stellar mass loss will occur*. This is contrary to many aspects of galaxy, group, and cluster evolution, including the prevailing paradigm in which the IHL is produced by stellar mass liberated from infalling galaxies by interactions in the group environment (e.g., Conroy et al., 2007; Purcell et al., 2007). Abundance matching is also sensitive to the resolution of the cosmological simulation on which it is implemented. Subhalos are artificially destroyed by falling below the numerical resolution limit and immediately removed from the galaxy population irrespective of their circular velocities at their accretion times. This can lead to differing predictions for the small-scale clustering of galaxies of a particular luminosity among simulations with a fixed mapping of halo size onto luminosity.

These considerations persuaded us to explore simple models that associate stellar masses to subhalo masses and constrain satellite galaxy *stellar mass loss* by matching to clustering data. We implemented two distinct models. Model 1 related the fractional amount of stellar mass loss to that of the subhalo dark matter mass loss from the time of accretion until the final redshift through a single free parameter ϵ. Model 2 was introduced to mimic a "lag" in stellar mass loss wherein the satellite

galaxy at the core of the subhalo experiences no stellar mass loss until the subhalo has been stripped of sufficient dark matter on its periphery. Stellar mass loss in this model only occurs once dark matter has been lost interior to a radius of influence of the satellite galaxy. We introduced the free parameter ψ that dictated how the radius of influence could expand or shrink allowing for more or less stellar mass loss. We calculated the values of ϵ and ψ that matched the observed clustering of SDSS galaxies over a large range of luminosity threshold samples. Matching to the observed clustering at each luminosity threshold directly informs us of the amount of stellar mass lost from satellite galaxies and, thus, will comprise the IHL.

This procedure enables predictions for the amount of IHL or IHL+BHG compared to the total stellar mass of a host system of a given mass ($f_{\rm IHL}$ and $f_{\rm IHL+BHG}$, respectively). Observationally, it has been established that the amount of diffuse material is nearly negligible at the scale of individual galaxies (e.g., Sackett et al., 1994; Morrison et al., 1997; Weil et al., 1997; Lequeux et al., 1998; Abe et al., 1999; Zibetti & Ferguson, 2004; Bailin et al., 2011). For example, M33, which is $\sim 10^{11}\ M_{\odot}$, has been estimated to have an $f_{\rm IHL} \leq 1\%$ (McConnachie et al., 2006; Hood et al., 2007). Our own Milky Way is thought to have an $f_{\rm IHL} \sim 1\%$ (e.g., Morrison, 1993; Wetterer & McGraw, 1996; Chiba & Beers, 2000; Ivezić et al., 2000; Morrison et al., 2000; Yanny et al., 2000; Siegel et al., 2002) or $\sim 2\%$ when including the stars from the Sagittarius stream (Law et al., 2005). Our analog M31 has an $f_{\rm IHL} \sim 2-5\%$ (Irwin et al., 2005; Guhathakurta et al., 2005; Chapman et al., 2006; Kalirai et al., 2006). Recently, Bailin

et al. (2011) showed that NGC 235, which is of comparable luminosity to the Milky Way and M31, has $f_{\rm IHL} \sim 6\%$. On group scales, $\sim 10^{13} - 10^{14}$ $M_{\odot}$, measured $f_{\rm IHL}$ percentages tend to be higher than on galaxy scales, though there can be considerable variation from group to group (e.g., $f_{\rm IHL}$ on the order of a few percent: Feldmeier et al. 2001; Castro-Rodríguez et al. 2003; Feldmeier 2006, $f_{\rm IHL} \sim 5 - 30\%$: Da Rocha & Mendes de Oliveira 2005; Aguerri et al. 2006; Da Rocha et al. 2008, and as high as $f_{\rm IHL} \sim 45\%$: White et al. 2003; McGee & Balogh 2010). For clusters scales, IHL fractions are typically much higher. There is still substantial scatter, but $f_{\rm IHL}$ values range from $\sim 10 - 40\%$ (Melnick et al., 1977; Thuan & Kormendy, 1977; Uson et al., 1991; Bernstein et al., 1995; Calcáneo-Roldán et al., 2000; Lin & Mohr, 2004; Mihos et al., 2005; Zibetti et al., 2005; Krick et al., 2006; Seigar et al., 2007). As discussed in §3.7, Gonzalez et al. (2007) posit that the relevant quantity is $f_{\rm IHL+BHG}$, because it can be difficult to disentangle the stellar mass associated with central galaxy from the diffuse IHL component. It has been found that $f_{\rm IHL+BHG} \sim 30\%$ on average on cluster scales (Zibetti et al., 2005; Gonzalez et al., 2007; Pierini et al., 2008; Toledo et al., 2011).

Our modeling of satellite galaxy stellar mass loss has yielded the following principal results and conclusions.

- Abundance matching with $\epsilon = 0$ and $\psi = 0$ ("traditional" abundance matching, akin to using the subhalo mass at the time of infall) over-predicts the correlation function on small scales ($\lesssim$ 1Mpc) for each luminosity threshold sample.

- For each luminosity threshold, we found both the ϵ and ψ value that predicted a correlation function that matched the data. We found that ϵ and ψ were decreasing functions of luminosity. This means that low-luminosity satellite galaxies are more efficiently stripped of stellar material than luminous satellites.

- Our predictions for $f_{\rm IHL}$ from both Model 1 and Model 2 are in good agreement with observational studies over an enormous range of host halo mass scales. For host masses of 10^{12} (individual galaxy scale), $10^{13} - 10^{14}$ (group to small cluster scales), and $10^{14} - 10^{15}$ (cluster scales), we find mean IHL fractions of a few percent, $10 - 20\%$, and $20 - 25\%$, respectively. These are in accord with previous observational studies, though there is substantial scatter in the $f_{\rm IHL}$ measurements in the literature.

- The more physically-motivated Model 2 is consistent with the $f_{\rm IHL+BHG}$ measurements of Gonzalez et al. (2007) from small group scales all the way through cluster mass systems. The scatter in the Model 2 results is comparable to the scatter observed in the data. On the contrary, the scatter among $f_{\rm IHL+BHG}$ values predicted by Model 1 is insufficient to describe the scatter among the observed systems. This suggests that Model 1, in which stellar mass loss occurs in proportion to dark matter mass loss, can be rejected by current data.

We have shown that *galaxy clustering* can be used as a powerful tool to understand how satellite galaxies lose stellar mass. We have found the interesting result that low-luminosity galaxies lose more stellar mass relative to subhalo dark matter mass loss

than luminous galaxies. Moreover, we were able to predict current IHL observations and thus further constrain our stellar mass loss models. These results show that our modeling framework can mitigate potential problems associated with the conventional abundance matching approach. Also, our approach is generalizable. It allows for the flexibility to make more detailed predictions within this framework (for instance, examining the photometric properties of the IHL as compared to galaxies).

In Paper II, we will take advantage of clustering measurements at high redshifts, allowing us to study the evolution of satellite galaxy stellar mass loss as a function of *time*. This will enable us to make predictions for the build-up of the IHL over cosmic time. A possible extension of this program is to also explore stellar mass-selected threshold samples directly rather than the luminosity threshold samples we have used in this paper. This is a natural choice for refining this class of studies because dynamical models most directly treat stellar mass loss. A further useful avenue to pursue as a result of this work will be to connect detailed theoretical models of stellar mass loss in individual galaxies more directly to the statistical models of stellar mass loss that can be explored with large-scale survey data, such as we have done. Models of stellar mass loss that are consistent with survey data must also be representative of detailed dynamical models of stellar mass loss. It will be very interesting to develop a set of simple, yet powerful models for the build-up and dispersal of the stellar mass in satellite galaxies that simultaneously describe the evolution of galaxy clustering and intrahalo light over cosmic time.

Chapter IV

MODELING THE VERY SMALL-SCALE CLUSTERING OF LUMINOUS RED GALAXIES

Abstract

We model the small-scale clustering of luminous red galaxies (LRGs; Masjedi et al. 2006) in the Sloan Digital Sky Survey (SDSS). Specifically, we use the halo occupation distribution (HOD) formalism to model the projected two-point correlation function of LRGs on scales well within the sizes of their host halos ($0.016h^{-1}$Mpc $\leq r \leq$ $0.42h^{-1}$Mpc). We start by varying $P(N|M)$, the probability distribution that a dark matter halo of mass M contains N LRGs, and assuming that the radial distribution of satellite LRGs within halos traces the NFW dark matter density profile. We find that varying $P(N|M)$ alone is not sufficient to match the small-scale data. We next allow the concentration of satellite LRG galaxies to differ from that of dark matter and find that this is also not sufficient. Finally, we relax the assumption of an NFW profile and allow the inner slope of the density profile to vary. We find that this model provides a good fit to the data and the resulting value of the slope is -2.17 ± 0.12. The radial density profile of satellite LRGs within halos is thus not compatible with that of the underlying dark matter, but rather is closer to an isothermal distribution.

4.1 Introduction

In Chapter II, we studied the physical processes responsible for the $\sim r^{-2}$ power-law nature of the galaxy correlation function. In Chapter III, we constrained satellite galaxy stellar mass loss and made predictions for both galaxy clustering and intra-halo light observations. Both of these investigations considered were constrained by clustering measurements from small to intermediate scales ($\sim$ 100kpc to $\sim$ 20Mpc). But what about on scales much deeper within individual halos, $r <$ 100kpc, where chaotic, non-linear processes are presumably strongest? These processes most certainly have an effect on the way galaxies cluster, and will give rise to features in the correlation function $\xi(r)$ on very small scales.

The Sloan Digital Sky Survey (York et al., 2000) has produced the largest ever spectroscopic sample of luminous red galaxies (LRGs). The clustering of these galaxies has been considered in great detail on both intermediate (Zehavi et al., 2005a) and very large scales (Eisenstein et al., 2005). However, it is especially difficult to measure the correlation function on small scales due to "fiber collision" incompleteness, and deblending issues. Masjedi et al. (2006, hereinafter M06) were able to overcome these observational impasses. They corrected for fiber collisions by cross-correlating the spectroscopic sample with the imaging sample and testing the results against mock data sets. They addressed deblending errors by introducing artificial galaxies of known magnitudes into the data and studying how they are recovered by the SDSS software. These adjustments allowed them to properly measure $\xi(r)$ down to a sep-

aration of $r \sim 15h^{-1}$kpc. The clustering on these scales has also been measured for lower luminosity galaxies (Wang et al., 2006; Li & White, 2009), though these studies did not include deblending corrections, which M06 showed can be significant.

In this paper, we model this recently measured very small-scale LRG clustering. On intermediate scales ($0.3-40h^{-1}$Mpc), Zehavi et al. (2005a) measured the two-point correlation function for 35,000 LRGs. Zheng et al. (2009) modeled this data using the halo occupation distribution (HOD; see, e.g., Peacock & Smith 2000; Scoccimarro et al. 2001; Berlind & Weinberg 2002; Cooray & Sheth 2002) framework and found a nice fit. However, the extrapolation of their best-fit model to smaller separations does not agree with the M06 small-scale data: it predicts a correlation function that is too low (see M06, Fig. 4). Our motivation is to model these innermost data points ($0.016 - 0.42h^{-1}$ Mpc) to see if we can find a model that works. The paper is laid out as follows. In § 5.2, we review the M06 measurement. In § 5.3, we discuss our method for modeling the small-scale correlation function. In § 5.4, we discuss our results in a sequential format: in § 4.4.1, we use four free parameters from the probability distribution, $P(N|M)$; in § 4.4.2, we introduce the concentration of satellite LRGs as a new free parameter; in § 4.4.3, we allow the inner slope of the density profile of satellite LRGs to vary. Finally, in § 5.5, we discuss the implications of our results.

4.2 Data

M06 measured the small-scale ($0.016 - 8h^{-1}$Mpc) projected two-point correlation function for a volume-limited sample of 24,520 luminous red galaxies in the SDSS. The luminosity range of LRGs in the sample was $-23.2 < M_g < -21.2$ and the redshift range was $0.16 < z < 0.36$. Measuring the correlation function on such small scales is non-trivial, and requires overcoming two main observational hurdles: fiber collisions and deblending.

The SDSS spectroscopic sample is incomplete due to the physical size of the fiber-optic cables used to take spectra of targeted galaxies. If two galaxies are closer than 55 arcsec on the sky, they cannot both get measured spectra. These "fiber collisions" thus result in a minimum possible pair separation of 55 arcsec. Fiber collision incompleteness is reduced by the SDSS tiling method, which overlaps the spectroscopic plates to achieve continuous sky coverage. However, this still results in $\sim 7\%$ of targeted galaxies without measured redshifts. Naturally, this incompleteness affects galaxy clustering measurements most severely at very small scales. To get around this problem, M06 cross-correlated the spectroscopic LRG sample with the entire sample of LRG targets in the SDSS imaging. For every LRG from the spectroscopic sample, nearby LRG targets (whether or not they have an observed spectrum) were considered to be at the same redshift as the spectroscopically observed LRG. This allowed M06 to assign absolute magnitudes to the LRG targets and thus decide if they made it into the volume-limited sample. M06 then statistically removed the contribution

of galaxies that were not at the same redshift, but were considered to be by the algorithm, by constructing random samples with the same redshift distribution as the spectroscopic sample, and cross-correlating them with the LRG imaging sample. M06 tested this procedure on mock galaxy catalogs and found that it successfully recovers the LRG auto-correlation function.

The SDSS photometry of LRG galaxies is biased in cases where pairs of LRGs are separated by tens of kpc or less. These galaxies have a region of overlap, and the light contained in this region needs to be properly distributed between the LRG pair. This process is called deblending. Since the LRG sample is defined by luminosity cuts ($-23.2 < M_g < -21.2$), any systematic errors in deblending will lead to incorrect measurements of the correlation function. M06 tested the deblending method by introducing artificial, overlapping galaxies of assigned magnitudes into the SDSS imaging. They then deblended the images using the SDSS imaging pipeline *PHOTO* (Lupton et al., 2001), and discovered that too much light was being systematically allocated to the fainter galaxy of the pair. In many cases, this pushed the fainter galaxy above the luminosity cut and into the LRG sample, whereas it should have stayed out. This photometric bias thus led to a boost in the correlation function on small scales. M06 corrected their correlation function for deblending errors using the results of their tests with artificial data.

After applying these corrections and deprojecting $w_{\rm p}(r_{\rm p})$, M06 found that the LRG correlation function on small scales is a continuation of the $\xi(r) \propto r^{-2}$ power

law found previously for larger scales (Zehavi et al., 2005a). Only their smallest scale data point ($\sim 10h^{-1}$kpc) shows a downturn, which presumably occurs because at such a small scale, it is no longer possible to distinguish two merging LRGs from each other. In this paper, we use M06's measurements of the projected correlation function $w_{\rm p}(r_{\rm p})$ from 16 to $420h^{-1}$kpc, which consist of eight data points. Restricting ourselves to this range guarantees that we are safely within the 1-halo regime (i.e., all LRG pairs are coming from within the same halos). We use the full covariance matrix for this data, which M06 estimated using jackknife resampling.

We incorporate the measured number density of galaxies as an additional constraint in our modeling. The number density of LRGs with $M_g < -21.2$ is $\bar{n}_{\rm g} = 9.73 \times 10^{-5} h^3 {\rm Mpc}^{-3}$ (Zheng et al., 2009) and this provides us with a ninth data point. We estimate an error for this number density using 50 jackknife samples on the sky and obtain $\sigma_{\bar{n}_{\rm g}} = 1.46 \times 10^{-6} h^3 {\rm Mpc}^{-3}$.

4.3 Method

4.3.1 The Halo Occupation Distribution

The HOD framework characterizes the bias between galaxies (of any class) and mass and is completely defined by (1) the probability distribution $P(N|M)$ that a virialized dark matter halo of mass M will host N galaxies, (2) the relative spatial distribution of the galaxies and dark matter within their host halo, and (3) the relative velocity distribution between the galaxies and dark matter within the halo (**?**). We

may neglect (3) in this study due to the fact that $w_{\rm p}(r_{\rm p})$ is velocity independent.

The first moment of $P(N|M)$ is the mean number of galaxies as a function of halo mass $\langle N\rangle_M$, and we parametrize it as a sum of a central and a satellite component (Kravtsov et al., 2004b; Tinker, 2007; Zheng et al., 2009). We assume that there is a minimum halo mass cut-off (hereinafter referred to as $M_{\rm min}$) below which a halo will always be empty and above which a halo will always contain at least a single central galaxy. We next assume that the mean number of satellite galaxies is a power-law function of mass with a low-mass exponential cutoff at M_0. The power-law slope is α and the normalization is M_1, which represents the mass where halos contain, on average, a single satellite galaxy. Specifically, the average number of galaxies as a function of mass is $\langle N\rangle_M = 1 + \langle N_{\rm sat}\rangle_M$, where

$$\langle N_{\rm sat}\rangle_M = \exp[-M_0/(M_{\rm halo} - M_{\rm min})] \times (M_{\rm halo}/M_1)^{\alpha}. \tag{4.1}$$

The correlation function $\xi(r)$ depends on the second moment of $P(N|M)$ and so specifying $\langle N\rangle_M$ is not sufficient. We assume that the actual number of satellite galaxies in a halo of mass M follows a Poisson distribution of mean $\langle N_{\rm sat}\rangle$. Therefore, the second moment is $\langle N_{\rm sat}(N_{\rm sat}-1)\rangle_M = \langle N_{\rm sat}\rangle_M^2$. Our choice of a Poisson distribution is motivated by theoretical results (Kravtsov et al., 2004b; Zheng et al., 2005). We note, however, that our results will not be very sensitive to the specific form of the satellite galaxy distribution because of the high mass regime that we are considering in this study. LRGs live in halos of mass greater than the non-linear mass M^* (Zheng

et al., 2009), which means that they are on the exponentially declining part of the halo mass function. As a result, most of our LRG pairs will be central-satellite pairs in halos of mass $\sim M_1$, rather than satellite-satellite pairs in higher mass halos.

In addition to $P(N|M)$, we must also characterize the spatial distribution of galaxies within halos. We naturally assume that the central galaxy sits at the center of its halo. As for satellite galaxies, we assume at first that they trace the density distribution of dark matter within their halo, but we eventually relax that assumption, as we describe in § 5.4. We assume that halos have dark matter density profiles that are described by the NFW relation $\rho(\mathbf{r}) \propto (r/r_s)^{-1}(1 + r/r_s)^{-2}$ (Navarro et al., 1997). The NFW scale radius r_s controls where the profile transitions from r^{-1} in the inner parts to r^{-3} in the outer parts, but we parametrize it instead through the concentration parameter, which is defined as the ratio of a halo's virial radius to its scale radius ($c \equiv R_{\rm vir}/r_s$). Finally, we adopt the concentration - mass relation given by Zheng et al. (2007) for the modification of Bullock et al. (2001): $c = \frac{c_0}{(1+z)} \times (\frac{M_{\rm halo}}{M_*})^{-\beta}$, where $c_0 = 11$, M_* is the non-linear mass at the median redshift ($M^* = 1.2 \times 10^{12} h^{-1} M_\odot, z = 0.286$) of the sample for our choice of cosmology, and $\beta = .13$.

4.3.2 The Galaxy Number Density

We can calculate the galaxy number density for a given HOD by integrating over halo mass and weighting the abundance of halos by the mean occupation of galaxies

$\langle N \rangle_M$:

$$\bar{n}_{\rm g} = \int_{M_{\rm min}}^{\infty} dM \frac{dn}{dM} \langle N \rangle_M, \tag{4.2}$$

where dn/dM is the differential halo mass function. We adopt the Warren et al. (2006) halo mass function with the following cosmological model: $\Omega_m = 0.25, \Omega_\Lambda = 0.75, \Omega_b = 0.04, h_0 = 0.7, \sigma_8 = 0.8, n_s = 1.0$.

4.3.3 The Galaxy 2-point Correlation Function

In the halo model, the galaxy two-point correlation function is given as the sum of the "1-halo" and "2-halo" terms (Zheng, 2004),

$$\xi_{\rm gg}(r) = \xi_{\rm gg}^{\rm 1halo} + \xi_{\rm gg}^{\rm 2halo} + 1. \tag{4.3}$$

The 2-halo term is the contribution of galaxy pairs found in separate dark matter halos. Therefore, at scales smaller than the virial diameter of the smallest halos considered, the 1-halo term completely dominates the correlation function. Zheng et al. (2009) found that the minimum halo mass for LRGs is $M_{\rm min} \cong 10^{13.7} M_\odot$, which corresponds to virial radii of $0.8 - 0.9 h^{-1}$Mpc. Therefore, it is sufficient to only consider the 1-halo term when modeling $\xi(r)$ for our small-scale data.

The 1-halo term of the two-point correlation function can be written as an integral over halo mass, where at each mass we add the contribution of central-satellite and

satellite-satellite pairs:

$$1 + \xi_{\rm gg}^{\rm 1halo}(r) = \frac{1}{2\pi r^2 \bar{n}_{\rm g}^2} \int_{M_{\rm min}}^{\infty} dM \frac{dn}{dM} \times \Big[\langle N_{\rm sat} \rangle_M F_{\rm cs}(r) + \frac{\langle N_{\rm sat}(N_{\rm sat}-1) \rangle_M}{2} F_{\rm ss}(r) \Big], \tag{4.4}$$

where $F_{\rm cs}(r)$ and $F_{\rm ss}(r)$ are the pair separation distributions of central-satellite and satellite-satellite pairs, respectively. The pair distribution for central-satellite pairs is essentially the same as the density profile of satellite galaxies, whereas the satellite-satellite pair distribution is equivalent to a convolution of the density profile with itself. We use the Sheth et al. (2001) calculation for the convolution of a truncated NFW profile with itself. As we discussed in § 4.3.1, central-satellite pairs will dominate the LRG correlation function due to the large halo masses involved. Therefore, the shape of the small-scale LRG correlation function should be very close to the shape of the satellite galaxy density profile.

M06 measured the projected correlation function, so we must transform our theoretical $\xi(r)$ into $w_{\rm p}(r_{\rm p})$ by integrating along the line of sight (Davis & Peebles, 1983; Zehavi et al., 2004):

$$w_{\rm p}(r_{\rm p}) = 2 \int_0^{\infty} \xi\Big(\sqrt{r_{\rm p}^2 + y^2}\Big) dy. \tag{4.5}$$

Since we need to integrate $\xi(r)$ to large radii in order to get $w_{\rm p}(r_{\rm p})$, we cannot completely ignore the 2-halo term. However, $\xi(r)$ is a rapidly declining function of r and so $w_{\rm p}(r_{\rm p})$ at the small scales we are considering is not sensitive to variations in

the 2-halo term. For this reason, we use the best-fit 2-halo term from Zheng et al. (2009) instead of calculating it explicitly each time we vary our HOD parameters. We tested this by shifting the amplitude of the 2-halo term by 20% in each direction and we found that $w_{\rm p}(r_{\rm p})$ is not appreciably affected.

4.3.4 Probing the Parameter Space

Now that we have measurements of $\bar{n}_{\rm g}$ and $w_{\rm p}(r_{\rm p})$, as well as a mechanism to predict these quantities from a given set of HOD parameters (e.g., $M_{\rm min}$, M_0, M_1, α), we can probe the parameter space and find the region that gives a good fit to the data. We use a Markov Chain Monte Carlo (MCMC) method for this purpose. Specifically, we adopt the Metropolis-Hastings algorithm, which works as follows. The free parameters are given initial values and χ^2 is computed for this starting point in parameter space. Steps are then chosen for the parameters and χ^2 is computed for this new location. The new location is added to the chain if $\chi^2_{new} < \chi^2_{old}$ or $n < \exp[-(\chi^2_{new} - \chi^2_{old})/2]$, where n is a random number between 0 and 1. If these conditions are not met, then the old location is repeated in the chain. This process then repeats until the chain has converged. We test for convergence by starting three chains with different initial parameter values and checking whether their final parameter distribution functions are in agreement. We assume uniform priors for all parameters and do not impose restrictions on their ranges.

Once a given chain has converged, we can plot the histogram of parameter values

in the chain. The most likely value for each parameter is given by the mean of its distribution, and the associated errors are given by the extrema of the middle 68.3% of the distribution. The best-fit parameters correspond to the combination of parameter values for which χ^2 is a minimum. For more details on MCMC techniques, see Dunkley et al. (2005).

4.4 Results

4.4.1 Varying $P(N|M)$

As discussed in § 5.1, the Zheng et al. (2009) fit to the intermediate-scale LRG correlation function does not match the M06 data points when extrapolated inwards. We first investigate whether we can achieve a good fit to these new M06 small-scale data points while only varying the $P(N|M)$ part of the HOD. We vary the following parameters (also defined in § 4.3.1):

1. $M_{\rm min}$ - the minimum halo mass to contain a central galaxy.
2. M_0 - the minimum halo mass to contain satellite galaxies.
3. M_1 - the halo mass to contain, on average, one satellite galaxy.
4. α - the slope of the power-law relation between the mean number of satellite galaxies and halo mass.

We refer to this model as PNM. Our MCMC rapidly converges and we find a best-fit model with a reduced χ^2 of 6.06 (χ^2 of 30.3 with 5 degrees of freedom). The dotted

green curves in Figure 4.1 show this best fit. It is clear that the model provides a poor fit to the data, as it deviates downward from a power law on small scales. We therefore find that by varying the $P(N|M)$ free parameters alone we are unable to reproduce the innermost M06 data points. We have essentially reproduced the discrepancy between the very small-scale M06 data and the Zheng et al. (2009) modeling, and thus shown that including the small-scale points in the fit does not repair the discrepancy.

4.4.2 Varying the Concentration of Satellite Galaxies

Since we cannot reproduce the small-scale LRG clustering by varying the $P(N|M)$ distribution, we naturally set our sights next on the radial distribution of LRG satellites within their dark matter halos. As described in § 4.3.1, we have assumed that these galaxies trace the dark matter halo density distribution, which is in turn described by an NFW density profile. The simplest change we can make is to allow galaxies to have a different NFW concentration than the halos they occupy. We thus introduce a new free parameter $f_{\rm gal}$ that relates the satellite galaxy concentration $c_{\rm gal}$ to that of the dark matter halo c:

$$c_{\rm gal} = f_{\rm gal} \times c. \tag{4.6}$$

In the previous 4 parameter PNM model we found that M_0 was very poorly constrained. In order to keep the same number of free parameters, we fix M_0 to $M_{\rm min}$, setting the exponential cut-off for satellite galaxies to occur at $M_{\rm min}$. Therefore, we

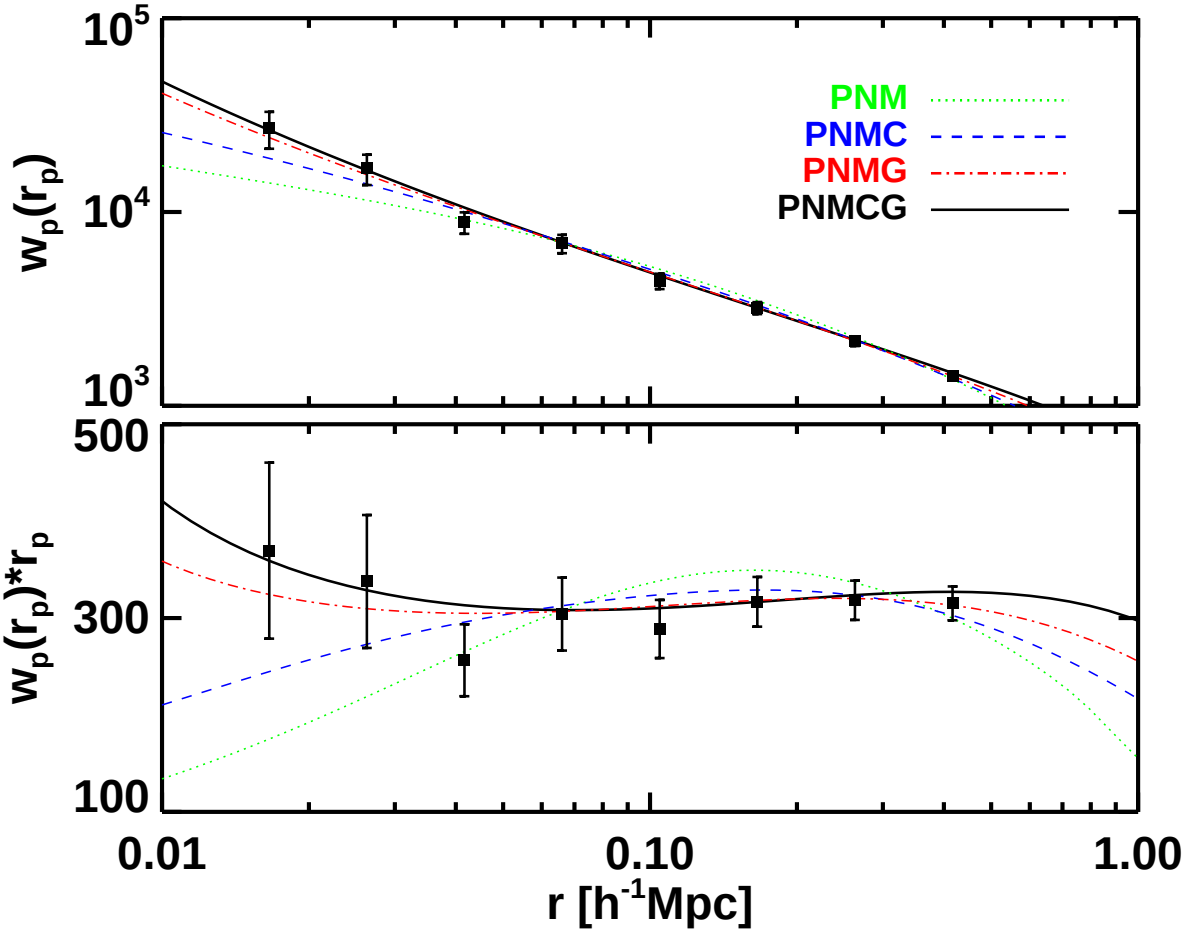

Figure 4.1: Model fits to the projected correlation function of LRGs. Points show the Masjedi et al. (2006) $w_{\rm p}(r_{\rm p})$ measurements along with their jackknife errors. The four curves show the best-fit models for four sets of free parameters. The PNM model (*dotted green curve*) uses 4 free parameters that describe the probability distribution $P(N|M)$ - $M_{\rm min}$, M_0, M_1, and α. The PNMC model (*dashed blue curve*) replaces M_0 with $f_{\rm gal}$, which is the concentration of the density profile of LRG satellites relative to dark matter. The PNMG model (*dashed-dotted red curve*) replaces this with the inner slope of the density profile γ. The PNMCG model (*solid black curve*) is the same as the PNMG model with the concentration of satellite LRGs $f_{\rm gal}$ added as a fifth free parameter. The *top panel* shows $w_{\rm p}(r_{\rm p})$, and the *bottom panel* shows the residuals from an $r_{\rm p}^{-1}$ power law.

now vary the following 4 free parameters: $M_{\rm min}$, M_1, α, and $f_{\rm gal}$. We refer to this model as PNMC.

We find a best-fit model with a reduced χ^2 of 2.52 (χ^2 of 12.6 with 5 degrees of freedom). The dashed blue curves in Figure 4.1 show this best fit. The PNMC model clearly does better than the PNM model in explaining the small-scale LRG clustering; however, it still provides a poor fit. We find that $f_{\rm gal}$ values of $\sim 5-10$ are preferred, showing that LRGs are more concentrated than the dark matter for this PNMC model. This makes sense because increasing $c_{\rm gal}$ means that we are adding more satellite galaxies towards the center of halos. This forces the scale radius inwards and boosts the amplitude of the inner part of $\xi(r)$. However, while simply moving more galaxies towards the center may aid in fitting the very inner most 2-3 data points, this can result in a poorer fit to the outermost data points. In other words, varying $c_{\rm gal}$ can shift $w_{\rm p}(r_{\rm p})$ in the $r_{\rm p}$ direction, but it cannot alter its *shape*, which is fundamentally not a power law in the case of an NFW satellite profile (see dashed blue curve in bottom panel of Fig. 4.1).

4.4.3 Varying the Density Profile

Adopting an NFW form for the density profile of satellite LRGs is not capable of reproducing the small-scale correlation function, no matter what concentration we use. We therefore relax the NFW assumption by allowing the inner slope of the profile to vary. Recall that the NFW profile has a logarithmic slope $d\ln\rho/d\ln r$ of

-1 at scales much less than the scale radius r_s, and -3 at scales much larger than r_s. We assume a new density profile for satellite LRG galaxies that is similar to NFW, except that the inner slope is no longer fixed to -1, but is a new free parameter $-\gamma$:

$$\rho(r) = \frac{\rho_s}{\left(\frac{r}{r_s}\right)^{\gamma}\left(1+\frac{r}{r_s}\right)^{3-\gamma}}. \tag{4.7}$$

This reduces to NFW for $\gamma = 1$. A model of this form has been used by papers that study the inner slope of the dark matter density profile (e.g., Fukushige et al. 2004; Reed et al. 2005).

In order to use this new profile in our modeling, we need to compute the pair distributions $F_{\rm cs}(r)$ and $F_{\rm ss}(r)$, as described in § 4.3.3. While $F_{\rm cs}(r)$ is the profile itself, $F_{\rm ss}(r)$ is the convolution of the profile with itself and quite non-trivial to calculate analytically for arbitrary values of γ and concentration. We therefore calculate $F_{\rm ss}(r)$ in a numerical fashion. We make a dense grid of γ and concentration values, and at each grid point we create an artificial spherical halo by putting down 30k particles that satisfy the radial profile for that grid point. We then measure the pair distribution by counting all the particle pairs in our constructed halo. Once we have a table of $F_{\rm ss}(r)$ functions on our grid, we can estimate $F_{\rm ss}(r)$ for any values of γ and concentration by interpolating in the grid.

As before, we wish to keep the same number of free parameters in order to more fairly compare different models. We thus keep M_0 fixed to $M_{\rm min}$ and we keep $f_{\rm gal}$ fixed to unity. Therefore, we now vary the following 4 free parameters: $M_{\rm min}$, M_1, α,

and γ, and we refer to this model as PNMG. We find a best-fit model with a reduced χ^2 of 0.82 (χ^2 of 4.11 with 5 degrees of freedom). The dashed-dotted red curves in Figure 4.1 show this best fit. The PNMG model is clearly successful in fitting the M06 small-scale data. Allowing the inner slope of the satellite LRG density profile to become steeper than r^{-1} is exactly what was needed to match the data. The value of γ is well constrained and our MCMC yields $\gamma = 2.06 \pm 0.21$. It is certainly not surprising that the inner slope of the satellite density profile is similar to the slope of $\xi(r)$ at small scales because, as we argued in § 4.3.3, most LRG pairs should be central-satellite pairs whose pair distribution $F_{\rm cs}(r)$ is essentially the density profile itself.

We have established that neither $P(N|M)$, nor the concentration of satellite LRGs, are sufficient to explain the M06 small-scale data, and that a profile other than NFW is needed. We thus now allow our model to have more than 4 free parameters and we vary both γ and $f_{\rm gal}$. Since our density profile is no longer NFW, there is no reason to keep the concentration fixed to what was found for NFW dark matter halos. In our final model, we thus vary 5 parameters: $M_{\rm min}$, M_1, α, $f_{\rm gal}$, and γ, and we refer to this model as PNMCG. Our goal for investigating this model is to determine exactly what constraints the M06 data place on the density profile of satellite LRGs.

We find a best-fit model with a reduced χ^2 of 0.71 (χ^2 of 2.82 with 4 degrees of freedom). Figure 4.2 shows our 1-,2- and 3-σ contours for γ and $f_{\rm gal}$. As before, we find that the satellite LRG profile is much steeper than NFW (for NFW, $\gamma = 1$ and

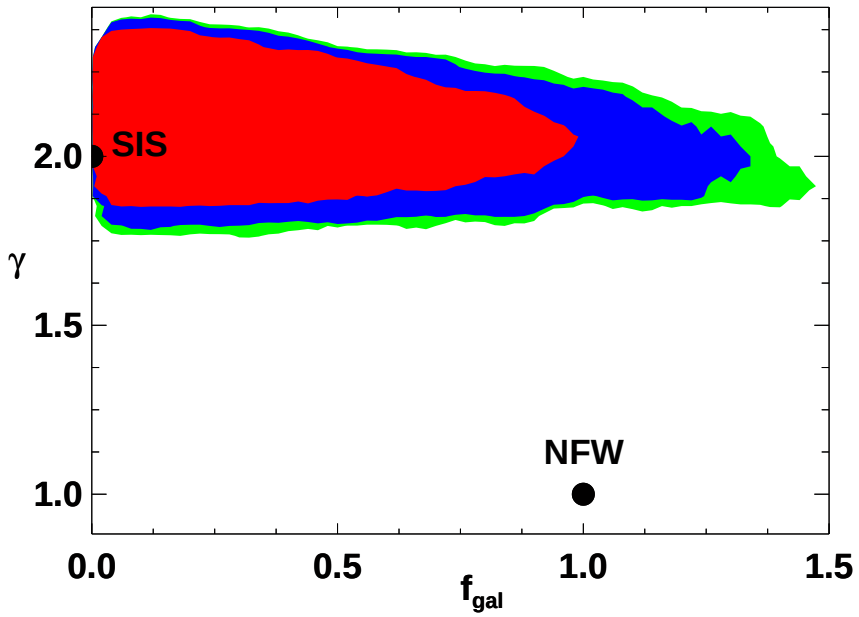

Figure 4.2: Allowed density profiles for LRG satellite galaxies within their dark matter halos. Shaded regions show the 1-σ (*red*), 2-σ (*blue*) and 3-σ (*green*) allowed regions for γ and $f_{\rm gal}$ for the PNMCG model. Filled circles mark the locations of the NFW profile ($\gamma = 1$, $f_{\rm gal} = 1$) and the Singular Isothermal Sphere (SIS) profile ($\gamma = 2$, $f_{\rm gal} \to 0$).

$f_{\rm gal} = 1$), with $\gamma = -2.17 \pm 0.12$. As we argued in § 4.3.1, most of the LRG satellites reside in halos of mass close to M_1. At our best-fit value for M_1 ($10^{14.62} h^{-1} M_\odot$), the dark matter concentration fitting formula from § 4.3.1 gives a halo concentration of $c = 4.25$. Applying our 1-σ range for $f_{\rm gal}$ implies that $c_{\rm gal} \sim 0.1 - 4.1$. Concentration values of unity or less mean that the scale radius r_s is larger than the virial radius, which essentially means that the density profile retains its inner slope most of the way out. In other words, our fit shows that the density profile for LRG satellites is consistent with a simple isothermal profile.

4.5 Discussion

Our results show that the distribution of satellite LRGs within dark matter halos requires a steeper inner density profile than NFW, which suggests that these galaxies are poor tracers of the dark matter distribution at these scales. The density profile of dark matter halos in the ΛCDM model has been measured extensively using high resolution N-body simulations, and recent inner profile measurements seem to confirm the NFW $\sim r^{-1}$ predictions (Navarro et al., 2010) – with some slight deviations found in separate work (Diemand et al., 2004; Fukushige et al., 2004; Reed et al., 2005; Del Popolo & Kroupa, 2009). However, NFW does not consider baryons, which can affect the dark matter density profile at small scales. The interaction between baryons and dark matter is addressed by the adiabatic contraction model that describes the gravitational effect of baryons on dark matter as the gas condenses and sinks to the center of the dark matter potential well. The gravitational influence of the baryons draws the dark matter in, and this can steepen the density profile (Gnedin et al., 2004; Romano-Díaz et al., 2008; Weinberg et al., 2008; Sommer-Larsen & Limousin, 2009). Although it has been shown that the inner profile can significantly steepen (Gustafsson et al., 2006), the majority of results show only a moderate steepening. This has also been observationally confirmed using galaxy-galaxy lensing by Mandelbaum et al. (2006) who find that the mass density profile of LRG clusters is consistent with NFW. LRG satellites therefore have a steeper density profile than dark matter even with the effects of baryons taken into consideration.

It is not necessarily surprising that LRGs are poor tracers of the dark matter density distribution within halos. LRGs presumably live in subhalos, which can certainly have a different distribution than their host halos. Nagai & Kravtsov (2005) found that subhalos actually have a shallower profile than dark matter at larger scales, but this has not been studied for the massive halos and small scales we consider here. It is difficult to model this regime because simulations must have, both a very large volume that contains many cluster-sized halos, and high mass and spatial resolution to resolve scales of $\sim 10h^{-1}$kpc. In fact, on these very small scales, it is likely that dark matter subhalos have already been disrupted by tidal forces, while the LRGs, being smaller and denser, have survived. So pure dark matter simulations may be insufficient to predict these LRG results. However, semi-analytic models that include galaxies and can have arbitrarily high resolution should be able to make these predictions (see Kitzbichler & White 2008 for semi-analytic modeling of the very-small scale clustering of lower luminosity galaxies).

In any case, our results have implications for the modeling of LRG clustering because a standard NFW profile cannot describe the spatial distribution of LRGs on scales $\lesssim 0.03h^{-1}$Mpc. It would be interesting to see if lower luminosity galaxies exhibit the same behavior or if this is simply a feature for LRGs. It would also be interesting to see if LRGs maintain their steep density profile at high redshift.

Chapter V

THE EXTREME SMALL SCALES: DO SATELLITE GALAXIES TRACE DARK MATTER?

Abstract

We investigate the radial distribution of galaxies within their host dark matter halos as measured in the Sloan Digital Sky Survey by modeling their small-scale clustering. Specifically, we model the Jiang et al. (2011) measurements of the galaxy two-point correlation function down to very small projected separations ($10 \leq r \leq 400h^{-1}$kpc), in a wide range of luminosity threshold samples (absolute r-band magnitudes of -18 up to -23). We use a halo occupation distribution (HOD) framework with free parameters that specify both the number and spatial distribution of galaxies within their host dark matter halos. We assume one galaxy resides in the halo center and additional galaxies are considered satellites that follow a radial density profile similar to the dark matter Navarro-Frenk-White (NFW) profile, except that the concentration and inner slope are allowed to vary. We find that in low luminosity samples ($M_r < -19.5$ and lower), satellite galaxies have radial profiles that are consistent with NFW. $M_r < -20$ and brighter satellite galaxies have radial profiles with significantly steeper inner slopes than NFW (we find inner logarithmic slopes ranging from -1.6 to -2.1, as opposed to -1 for NFW). We define a useful metric of concentration, $M_{1/10}$, which is the fraction of satellite galaxies (or mass)

that are enclosed within one tenth of the virial radius of a halo. We find that $M_{1/10}$ for low luminosity satellite galaxies agrees with NFW, whereas for luminous galaxies it is $2.5 - 4$ times higher, demonstrating that these galaxies are substantially more centrally concentrated within their dark matter halos than the dark matter itself. Our results therefore suggest that the processes that govern the spatial distribution of galaxies, once they have merged into larger halos, must be luminosity dependent, such that luminous galaxies become poor tracers of the underlying dark matter.

5.1 Introduction

Determining the relationship between the spatial distributions of galaxies and dark matter remains one of the central problems of theoretical and observational cosmology. We saw in Chapter IV that the radial distribution of galaxies within their host dark matter halos dictates the correlation function on scales smaller than the virial radii of the largest dark matter halos ($\lesssim 1h^{-1}$Mpc). Therefore, the measured galaxy correlation function itself is a powerful tool for shedding light on how galaxies trace the underlying dark matter within halos.

The halo occupation distribution (HOD) framework has been established as a robust method for modeling galaxy clustering by simply characterizing the biased relationship between galaxies and mass (see, e.g., Peacock & Smith 2000; Scoccimarro et al. 2001; Berlind & Weinberg 2002; Cooray & Sheth 2002; Zheng et al. 2005). The HOD describes this relation by specifying the probability distribution $P(N|M)$

that a halo of mass M contains N galaxies, along with a prescription for the spatial distribution of galaxies within halos. For this latter component, it is typically assumed that a single 'central' galaxy lives at the center of each halo, with additional 'satellite' galaxies tracing the dominant dark matter component. This assumption has been used successfully to model galaxy clustering on scales larger than $r \sim 100h^{-1}$kpc (e.g., Zehavi et al., 2004, 2005b, 2011; Zheng et al., 2007, 2009). However, Watson et al. (2010) showed that this assumption does not work to explain the smaller-scale clustering of luminous red galaxies (LRGs) in the Sloan Digital Sky Survey (SDSS; York et al. 2000). In order to achieve a good fit to the clustering of LRGs on scales smaller than $\sim 100h^{-1}$kpc (measured by Masjedi et al., 2006), they found that the radial profile of satellite LRGs must have a much steeper inner slope compared to the Navarro-Frenk-White (NFW; Navarro et al. 1997) dark matter profile. Watson et al. (2010) concluded that the distribution of satellite LRGs within halos is better described by an isothermal distribution (see Chapter IV for details).

Recently, Jiang et al. (2011) measured the projected two-point correlation function $w_p(r_p)$ for several luminosity samples from the SDSS, extending the measurements done by Zehavi et al. (2011) on intermediate scales ($\sim 0.1 - 40h^{-1}$Mpc) down to extremely small galaxy-galaxy separations ($0.01 - 7h^{-1}$Mpc). Our motivation for this paper is to model the innermost data points ($0.01 - 0.4h^{-1}$Mpc) in the same vein as Watson et al. (2010, hereafter W10) to see if there is a luminosity dependence of the

radial profile of satellite galaxies [1].

The paper is laid out as follows. In §5.2, we review the Jiang et al. (2011, hereafter J11) measurements. In §5.3, we discuss our modeling method in the following manner: in §5.3.1 we provide an overview of the general technique used to model the small-scale correlation function; in §5.3.2 we revisit the W10 four-parameter PNM model that allows the the probability distribution $P(N|M)$ to vary, and the five-parameter PNMCG model that also allows the radial distribution of galaxies within halos to vary. We present our results in §5.4. Finally, we summarize and discuss the implications of our results in §5.5. Throughout the paper, we assume a ΛCDM cosmology with $\Omega_m = 0.25, \Omega_\Lambda = 0.75, \Omega_b = 0.04, h_0 = 0.7, \sigma_8 = 0.8, n_s = 1.0$.

5.2 Data

J11 measured the projected two-point correlation function down to very small scales ($0.01 < r < 7h^{-1}$Mpc) for a large range of volume-limited galaxy luminosity threshold samples. Galaxy number densities and median redshifts for each sample can be found in Table V.1. These samples are constructed from the NYU VAGC (Blanton et al., 2005) V7.2 data (Abazajian et al., 2009) which contains 8.6×10^5 SDSS Main Sample galaxies (Strauss et al., 2002). Spectra for each luminosity threshold sample are cross-correlated with the full imaging sample to compute $w_p(r_p)$ (details of the method can be seen below). The full imaging sample consists of $\sim 10^8$ galaxies drawn

[1] Chapter IV is based on W10, thus any reference to W10 in this chapter can be found in Chapter IV

from the SDSS imaging catalog.

Measuring $w_p(r_p)$ on very small scales is a non-trivial task. The SDSS spectroscopic sample suffers from incompleteness due to the physical size of the fiber-optic cables, which impede the ability to take spectra of two galaxies closer than $55''$ on the sky. These "fiber collisions" thus result in a minimum pair separation of $55''$. This effect is partially mitigated by the tiling method (Blanton et al., 2003), which overlaps spectroscopic plates in order to yield full sky coverage. In plate overlap regions, galaxy pairs closer than $55''$ can be recovered. However, this still leaves $\sim 9\%$ of galaxies without measured redshifts (J11) and this can strongly affect clustering measurements on very small scales. Following the approach described in Masjedi et al. (2006, 2008), J11 used a cross-correlation technique between the imaging and spectroscopic samples to correct for fiber collisions and obtain unbiased $w_p(r_p)$ measurements down to the $10h^{-1}$kpc scale. Details of the method can be found in §5.3 of J11.

A second potential problem that affects very small scales is that galaxies may be overlapping and the light within this region needs to be properly distributed between the two galaxies. This is known as "deblending". M06 found a systematic error in the SDSS pipeline wherein too much light was allocated to the dimmer of the two galaxies. As a result, a galaxy that may have been too dim to make the LRG brightness cut could now be included in the sample. This increased the number of small-scale pairs and boosted the correlation function on very small scales. M06 quantified this effect

and corrected their measurements accordingly. Since the physical sizes of galaxies decrease rapidly with decreasing luminosity, this photometric deblending error diminishes in lower luminosity samples. For this reason, J11 ignored this effect in the luminosity samples they considered ($M_r < -18$ through -21). Nevertheless, we estimate the maximum effect of deblending by applying the M06 LRG correction to the $M_r < -21$ sample and repeating our analysis. We find that our results do not change qualitatively.

We restrict ourselves to modeling the J11 data points from $\sim 10 - 400h^{-1}$kpc. These can be seen in Figure 5.1, which shows $w_p(r_p)$ scaled by an r_p^{-1} power law, with each panel corresponding to a distinct luminosity threshold. The bottom right panel of Figure 5.1 shows the LRG data points measured by M06 and modeled by W10. Along with these 9 data points used in our modeling, we also incorporate the measured number density for each luminosity sample (see Table V.1), providing a tenth data point. We use the full covariance matrices from the 9 J11 $w_p(r_p)$ data points for each sample, which were estimated using jackknife resampling of 50 regions on the sky. The same jackknife samples were used to estimate the error on each calculated number density.

5.3 Review of the Method

5.3.1 The HOD and the Galaxy 2PCF

Here we briefly review the method used in W10, which is based on the halo occupation distribution (HOD) formalism. The HOD fully characterizes the number, velocity and spatial distribution of galaxies within dark matter halos. The probability distribution that a virialized dark matter halo of mass M will host N galaxies is designated as $P(N|M)$. $\langle N \rangle_M$ is the first moment of $P(N|M)$, and is the mean number of galaxies as a function of halo mass. Motivated by theory (e.g., Berlind et al., 2003; Kravtsov et al., 2004a; Zheng et al., 2005), we consider central galaxies that live at the center of their host halo and satellite galaxies that orbit within the host potential as separate terms. We thus write the first moment of the HOD as $\langle N \rangle_M = 1 + \langle N_{\rm sat} \rangle_M$. Furthermore, we assume that there is some minimum halo mass, $M_{\rm min}$, below which a halo will contain no galaxies and above which there will always be at least one central galaxy. For the satellite component, we adopt the parametric form, $\langle N_{\rm sat} \rangle_M = \exp[-M_0/(M_{\rm halo} - M_{\rm min})] \times (M_{\rm halo}/M_1)^{\alpha}$, where the satellite galaxies obey a power-law function of slope α with an exponential cut-off at the low mass end at M_0. M_1 is the characteristic mass scale where a halo will contain, on average, one central and one satellite galaxy.

To calculate the mean number of satellite galaxy pairs $\langle N_{\rm sat}(N_{\rm sat} - 1) \rangle$,the second moment of the satellite $P(N|M)$, we assume that the number of satellite galaxies in a halo of mass M follows a Poisson distribution of mean $\langle N_{\rm sat} \rangle_M$. This sort of

HOD parameterization is widely used to model galaxy clustering data (Zehavi et al., 2005a,b, 2011; Tinker et al., 2005; Conroy et al., 2006; Zheng et al., 2007, 2009; Watson et al., 2011b).

Our fiducial model for characterizing the spatial distribution of galaxies within their host halos places one galaxy at the center and assuming that the satellites trace the underlying dark matter density distribution. The dark matter density profiles are described by the NFW relation $\rho(r) \propto (c\frac{r}{R_{vir}})^{-1}(1 + c\frac{r}{R_{vir}})^{-2}$ (Navarro et al., 1997), where c is the concentration parameter, $c \equiv R_{\rm vir}/r_s$, and r_s is the characteristic scale radius. We use the virial definition of a halo to calculate the virial radius of host halos, such that $R_{\rm vir} = ((3M)/(4\pi\Delta_{\rm vir}\bar{\rho}))^{1/3}$, where $\Delta_{\rm vir}$ is the mean halo overdensity ($\Delta_{\rm vir} = 200$), and $\bar{\rho}$ is the mean density of the universe. The concentration - mass relation is given by Zheng et al. (2007) for the modification of Bullock et al. (2001): $c = \frac{c_0}{(1+z)} \times (\frac{M_{\rm halo}}{M_*})^{-\beta}$, where $c_0 = 11$, M_* is the non-linear collapse mass at the median redshift of the sample for our choice of cosmology (M^* is redshift dependent and is thus uniquely defined for each luminosity sample and is given in Table V.1) and $\beta = 0.13$.

The mean number density of galaxies can be calculated for a given HOD by weighting the abundance of halos by $\langle N\rangle_M$ and integrating over all halo mass (see Eq.[2] of W10). We adopt the Warren et al. (2006) halo mass function, dn/dM, in all of our calculations, but our results are not sensitive to the specific choice of mass function.

Table V.1.

M_r[a]	$\bar{n}_g$[b]	z_{med}[c]	$\log(M^*)$[d]
−18.0	3.209 (0.169)	0.032	12.4228
−18.5	2.405 (0.131)	0.039	12.4147
−19.0	1.689 (0.092)	0.046	12.4057
−19.5	1.326 (0.058)	0.059	12.3887
−20.0	0.749 (0.018)	0.078	12.3647
−20.5	0.377 (0.009)	0.097	12.3397
−21.0	0.123 (0.002)	0.116	12.3057
LRGs	0.009 (0.001)	0.286	12.0791

[a]LRGs correspond to −21.2 in the g band.

[b]$\bar{n}_g$ is measured in units of $10^{-2}h^3\mathrm{Mpc}^{-3}$ and the associated error from 50 jackknife samples on the sky is shown in parentheses.

[c]z_{med} is the median redshift as measured in J11.

[d]M^* is the non-linear collapse mass and is in units of $h^{-1}M_\odot$.

To model the galaxy two-point correlation function (2PCF), $\xi_{\rm gg}$, we use the halo model. $\xi_{\rm gg}$ can be decomposed into contributions due to galaxies residing in the same halo (the "one-halo" term) as well as galaxies living in separate, distinct halos (the "two-halo" term). Therefore, $\xi_{\rm gg}$ can be written as the sum of the one-halo and two-halo terms (e.g., Cooray & Sheth 2002; for this particular form of the equation see Zheng 2004): $\xi_{\rm gg}(r) = \xi_{\rm gg}^{\rm 1halo} + \xi_{\rm gg}^{\rm 2halo} + 1$. Since we are probing such small scales we need only consider the one-halo term for modeling ξ. However, it is possible that omitting the two-halo term entirely could cause a bias in the best-fit parameters for the one-halo term. This bias would be largest for the dimmest galaxy sample, because these galaxies live in the smallest halos, and the two-halo term will become important

at small scales. However, even for these galaxies the effect is limited. For instance, while it is true that isolated -18 galaxies will reside in halos with radii much smaller than $0.4h^{-1}$Mpc, the relevant halo size is set by M_1. Furthermore, this is a threshold sample, so although the -18 sample will be dominated by galaxies of that brightness, there will still be much brighter galaxies that live in larger halos that influence M_1. As seen in the upper-left panel of Fig. 5.3, $\langle M_1 \rangle$ for the -18 sample is $10^{12.77}$. This corresponds to a virial radius of order $0.4h^{-1}$Mpc. To carefully test the influence of the two-halo term, we have have measured where the 1- and 2-halo terms cross for the -18 sample. This occurs at roughly $1h^{-1}$Mpc, so the influence of the 2-halo term at $0.4h^{-1}$Mpc has a small effect on $w_p(r_p)$. We find that the amplitude of the 2-halo term is $\sim 7\%$ of the one-halo term at $0.4h^{-1}$Mpc for the -18 sample. Nevertheless, we do approximately account for the effect of the 2-halo term on our modeling, and we discuss these assumptions in detail below.

The one-halo term depends on the second moment of $P(N|M)$, as well as the pair separation distributions of central-satellite and satellite-satellite pairs (see Eq.[4] of W10 for the particular form). The pair separation distribution for central-satellite pairs is essentially the same as the density profile of satellite galaxies. The satellite-satellite pair distribution is the convolution of the density profile with itself and, as in W10, we use the Sheth et al. (2001) calculation for the convolution of a truncated NFW profile with itself. Therefore, we can start to see the link between the shape of $\xi(r)$ and the shape of the satellite profile on small scales. This is discussed in detail

in §5.4.

For each luminosity threshold, J11 measured the *projected* correlation function, so we convert our theoretical real-space correlation function $\xi(r)$ to $w_p(r_p)$ (Eq.[5] of W10). At each luminosity threshold, we integrate up to the $\pi_{\rm max}$ value given in Zehavi et al. (2011), which ranges from $40-60h^{-1}$Mpc. The method of J11 results in a $\pi_{\rm max}$ that is effectively larger than our choice. However, the difference is insignificant at the small scales we model. Integrating out to large scales means that the two-halo term cannot be entirely ignored. Since calculating the two-halo term correctly is fairly complex and its contribution to $w_p(r_p)$ is minimal at the scales of the data points that we model, we use a simple approximation instead. We use a two-halo term whose shape is the same as Zehavi et al. (2011), but whose amplitude can change with HOD parameters. Thus, for a given set of HOD parameters, we first calculate the large-scale bias of galaxies, b_g,

$$b_g = \bar{n}_g^{-1} \int_{M_{\rm min}}^{\infty} dM \frac{dn}{dM} b_h(M) \langle N \rangle_M, \tag{5.1}$$

where $b_h(M)$ is the large-scale bias of halos from Tinker et al. (2008). The two-halo term has a simple relation to the matter-matter correlation function on large scales: $\xi_{\rm gg}^{\rm 2halo} = b_g^2 \xi_{mm}$. Thus, the relative two-halo terms of two different galaxy samples really only depends on the ratio of the bias of each sample. We consider the best-fit two-halo term from Zehavi et al. (2011) for each luminosity and append a newly

defined two-halo term to our model one-halo term,

$$\xi_{\rm gg}^{\rm 2halo} = \left(\frac{b_g}{b_g{}'}\right)^2 \xi_{\rm gg}^{\rm 2halo\ \prime}, \tag{5.2}$$

where primes designate the Zehavi et al. (2011) values. In effect, we allow the amplitude of the 2-halo term to vary with HOD parameters, but we keep its shape fixed. The error introduced by this approximation is completely negligible as we have checked that even a shift as large as 20% in the amplitude of the two-halo term has no appreciable effect on $w_p(r_p)$ at the maximum pair separation that we consider ($0.4h^{-1}$Mpc) for any of the luminosity threshold samples. This test also emphasizes our insensitivity to the difference between our choice of integrating out to the $\pi_{\rm max}$ given by Zehavi et al. (2011) and the technique used by J11.

5.3.2 The PNM and PNMCG Models

W10 considered 4 distinct models for modeling the small-scale $w_p(r_p)$ of LRGs. In this paper we need only consider two of the models, defined as:

- ***PNM*** - in this model the only free parameters are those associated with the $P(N|M)$ distribution as described in §5.3.1 - $M_{\rm min}, M_0, M_1,$ and α. While these parameters are free to take on any value, the spatial distribution of satellite galaxies within halos is fixed to an NFW dark matter density profile. Since there are 10 data points (9 from the J11 $w_p(r_p)$ measurements along with the

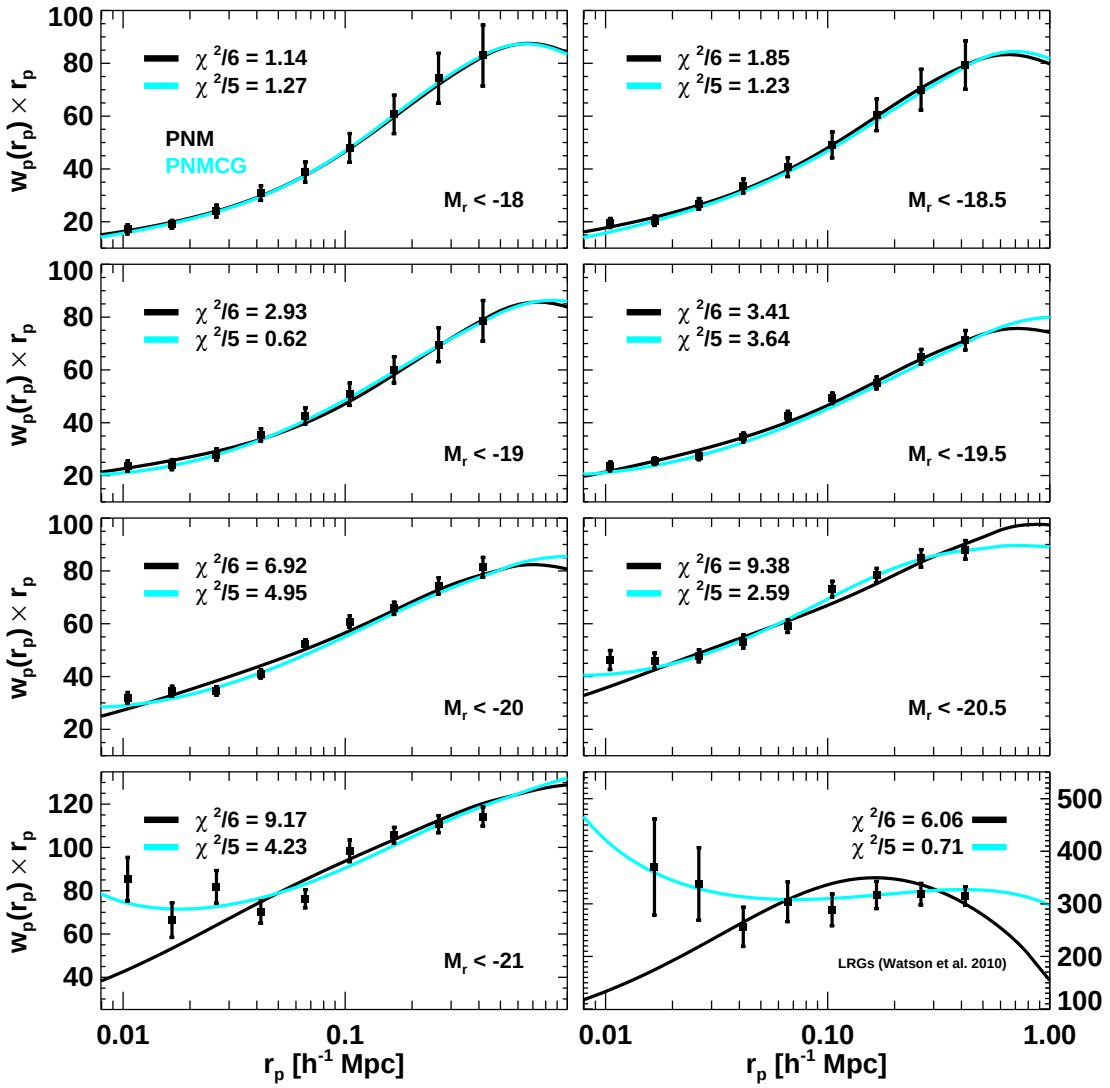

Figure 5.1: Model fits to the projected correlation function for luminosity thresholds spanning $M_r < -18$ to LRGs. The points in the $M_r < -18$ through $M_r < -21$ panels show the Jiang et al. (2011) $w_p(r_p)$ measurements (multiplied by r_p) and their associated jackknife errors. The bottom right panel shows results for LRGs from Watson et al. (2010). The black curves show the best-fit PNM models, which use four-free parameters describing the probability distribution $P(N|M)$ ($M_{\rm min}, M_1, M_0$,and α). The PNMCG model, shown in cyan, considers two additional free parameters (but M_0 is fixed to $M_{\rm min}$): (1) $f_{\rm gal}$, which relates the concentration of the density profile of satellite galaxies relative to dark matter ($f_{\rm gal} = c_{\rm gal}/c$), and (2) γ, which allows for the inner slope of the density profile to differ from the dark matter distribution. The reduced χ^2 values for each best-fit model are listed in each panel.

measured number density for each luminosity sample) and 4 free parameters, the PNM model has 6 degrees of freedom.

- ***PNMCG*** - this model allows for the same free parameters as the PNM model, with the exception of M_0. M_0 was unconstrained in our initial MCMC runs (this was also the case in W10), thus we fixed M_0 to $M_{\rm min}$ throughout our analysis. The PNMCG model also considers a parametrized density profile for satellite galaxies. As in W10, we allow both the concentration and the inner slope of the density profile to be free. The satellite galaxy concentration can differ from the dark matter concentration (defined in §5.3.1) through the free parameter $f_{\rm gal}$,

$$c_{\rm gal} = f_{\rm gal} \times c. \tag{5.3}$$

The inner slope of the density profile is no longer fixed to -1, as is the case for an NFW profile, but rather is specified by the free parameter γ. As in W10, we adopt the following density profile for satellite galaxies

$$\rho(r) = \frac{\rho_s}{(c_{\rm gal}\frac{r}{R_{vir}})^{\gamma}(1 + c_{\rm gal}\frac{r}{R_{vir}})^{3-\gamma}}. \tag{5.4}$$

For an NFW profile $\gamma = 1$, however, the PNMCG model allows γ to take on any value from $0 - 4$. This model considers the same number of data points as the PNM model, but now there are 5 free parameters ($M_{\rm min}, M_1, \alpha, f_{\rm gal}$ and γ) resulting in 5 degrees of freedom.

As detailed in §3.4 of W10, we use a Markov Chain Monte Carlo (MCMC) method to probe the parameter space for a given set of parameters (see Dunkley et al. 2005 for details on MCMC techniques). When a chain has converged, we can find the most likely value for each parameter by calculating the mean of its distribution. Errors for each parameter are given by the extrema of the middle 68.3% of the distribution. Best-fit parameters are found by the combination of parameter values for which χ^2 is a minimum.

5.4 Results

J11 measured $w_p(r_p)$ to very small scales over a large range in luminosity thresholds. Their measurements nicely overlap those of Zehavi et al. (2011) on intermediate scales ($\sim 0.2-7h^{-1}$Mpc, see Fig. 14 in J11), and extend down to very small scales with the innermost data point for each sample at $\sim 10h^{-1}$kpc. As discussed in §5.3.2, for each luminosity threshold sample, we model $w_p(r_p)$ with, (1) the PNM model, which only varies parameters that determine the number of galaxies in a given halo, but forces the satellite galaxies to have an NFW spatial distribution within their halo, and (2) the PNMCG model, which also allows the spatial distribution of satellite galaxies to vary within halos.

Figure 1 shows our modeling results for each luminosity sample. $w_p(r_p)$ has been scaled by an r_p^{-1} power law to more clearly highlight any discrepancies between the PNM and PNMCG models. Each panel shows the SDSS data points as well as the

best-fit model for the PNM (black curve) and PNMCG (cyan curve) cases. It is clear from the figure that as we go to higher luminosities, the PNMCG model provides a significantly better fit to the data. We find that the $P(N|M)$ parameter distributions are nearly the same for the two models, differing by, at most, $\sim 3\sigma$. Therefore, the improved fits for the PNMCG model principally arise from the freedom to vary the density profile of satellite galaxies. Varying the density profile is thus necessary to find a better fit to the data as we go to higher luminosities.

We note that the reduced χ^2 values (listed in each panel) are in many cases quite high, even in the PNMCG case. This could mean that the PNMCG model contains incorrect assumptions or does not have enough freedom. On the other hand, it could mean that the J11 jackknife errors are underestimated. To check the impact of the error estimates on our modeling, we re-estimated errors for the $M_r < -20$ sample using mock galaxy catalogs from the LasDamas project (McBride et al. in prep.). We used 160 catalogs [1] and measured the dispersion of $w_p(r_p)$ between the catalogs, using the same binning method as J11. We then applied the fractional error (with respect to the mean of all mock measurements) to the data (non-mock) measurement to estimate the absolute errors and full covariance. Finally, using our new mock based error estimates, we re-ran the MCMC chains for the PNMCG model. We then compared the best-fit parameter values for the two fits and found that the parameters did not change significantly. By this, we mean the difference in χ^2 between the two

[1] North-only SDSS footprint from the LasDamas "gamma" data release.

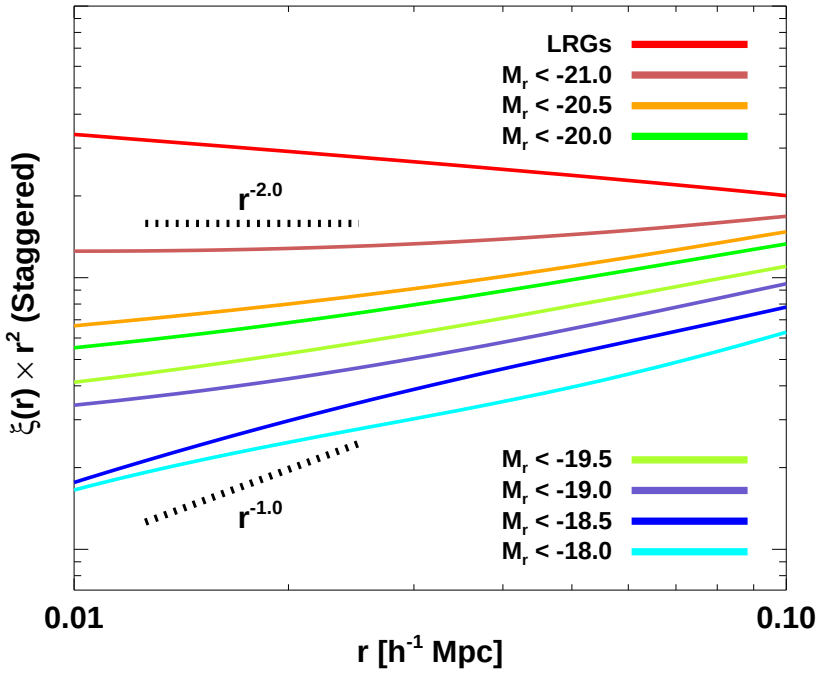

Figure 5.2: The real-space correlation function $\xi(r)$ residuals from an r^{-2} power law from the PNMCG best-fit models before converting to the projected correlation functions of Fig. 5.1. Amplitudes have been arbitrarily shifted for clarity. The slope of $\xi(r)$ on small scales is a reflection of the central-satellite pair distribution, which is essentially just the density profile itself. There is a strong luminosity dependence of the slope of $\xi(r)$ on small scales, becoming steeper and steeper for the brighter galaxy samples and this carries directly over to the luminosity dependence of the radial profile of satellite galaxies. The dotted lines show r^{-1} and r^{-2} power-law slopes.

best-fit points were within 1σ when evaluated with either of the likelihood surfaces (from each of the two MCMC runs with different errors). We conclude two things from this test: (1) our somewhat high χ^2 values are not overly concerning, and are likely due to a slight underestimate of the errors from jackknife re-sampling on the data, and (2) this issue does not seem to affect any of our conclusions.

We now investigate the luminosity dependence of the radial distribution of satellite galaxies and the degree to which it differs from an NFW distribution. As discussed

in §5.3.1, when constructing the real-space correlation function in the halo model, the one-halo term considers contributions from central-satellite and satellite-satellite pairs. The central-satellite contribution, which is essentially just the density profile itself (see Eq. 4 of W10), is steeper than the satellite-satellite pair contribution and thus dominates the correlation function on the very small scales that we are considering (e.g., Figure 4. of Zheng et al., 2009). Therefore, the luminosity dependence of the *slope of* $\xi(r)$ *on small scales* can give a direct indication of the luminosity dependence of the *radial profile of satellite galaxies* (though the slope of $\xi(r)$ will be less steep than the slope of the radial density profile due to the dampening effect of the satellite-satellite term). Figure 5.2 shows the residuals from an r^{-2} power law from the PNMCG best-fit models before converting to the projected correlation functions shown in Figure 5.1. The amplitudes of the curves have been arbitrarily staggered simply to make the plot more clear. The dotted lines highlight the cases of r^{-1} and r^{-2} power laws. The slope of $\xi(r)$ is clearly a strong function of luminosity, being close to -1 for low luminosity galaxies and going more and more towards -2 for the $M_r < -21$ sample and even steeper for LRGs. The W10 result for the steepness of the slope of $\xi(r)$ for LRGs on small scales was also found by Almeida et al. (2008). Using the Bower et al. (2006) semi-analytic model applied to the Millenium simulation (Springel et al., 2005), they found that the LRG real-space correlation function follows an $\sim r^{-2.07}$ power law shape down to the $\sim 10h^{-1}$kpc scale.

We next wish to directly investigate the radial profiles of satellite galaxies that

are required by the data and compare them to the NFW profile. For each luminosity sample, we choose a halo mass equal to the mean value of M_1 in the PNMCG MCMC chain for that sample. We choose M_1 because it represents the typical size halo that contributes central-satellite pairs to $\xi(r)$ (smaller halos have no satellites and larger halos are rare). Specifying the halo mass sets the amplitude, virial radius, and dark matter concentration in Equation 5.4. The radial profile then only depends on the parameters $f_{\rm gal}$ and γ. We then take the full MCMC chain for the PNMCG model and sort it by χ^2 from lowest to highest. We then randomly draw 50 links from the top 95% of the chain. Each of these links has distinct values of $f_{\rm gal}$ and γ, which we insert into Equation 5.4 in order to construct individual radial profiles. The light grey curves in each panel of Figure 5.3 show these 50 profiles (multiplied by $4\pi r^2 dr$ to convert them from density into mass profiles). These curves thus span the 95% confidence region allowed by the data. The green curve in each panel shows the radial profile corresponding to the best-fit PNMCG model. To compare with the NFW profile for dark matter, we also plot the case $f_{\rm gal} = 1$, $\gamma = 1$, shown by the yellow bands. We assume that the dark matter profile of halos has a 20% uncertainty, which we represent as the thickness of the bands (see §5.5 for discussion of the uncertainties in the dark matter distribution in halos). For reference, the scale radius for any particular sample occurs where the dark matter radial profile "turns over". Figure 5.3 shows, once again, that galaxies of increasing luminosity deviate more from an NFW profile. In fact, the figure seems to suggest that there is a

transition point, somewhere between an absolute r-band magnitude of -19.5 and -20, where the radial profile of satellite galaxies goes from being consistent with NFW to completely inconsistent. For the highest luminosity samples, the profiles approach a power-law shape.

Figure 5.4 shows the luminosity dependence of the inner slope and concentration of satellite galaxies as found by the PNMCG model. The dark blue and light blue bands in each panel represent the middle 95% and 68.3% of the MCMC chains after first sorting in γ (top panel) and sorting in $f_{\rm gal}$ (bottom panel). The filled red squares show the mean of the respective parameters in the MCMC chain for each luminosity sample and filled green squares show the best-fit values. The solid black line highlights the NFW dark matter inner slope of the density profile which corresponds to $\gamma = f_{\rm gal} = 1$ and the dotted lines represent the possible 20% ambiguity of an assumed NFW inner slope and concentration. The $M_r < -18, -18.5, -19$ and -19.5 samples have large spreads in γ and $f_{\rm gal}$ values, as there are many parameter combinations that can yield a similar goodness-of-fit to the data. For $M_r < -20$ and brighter galaxies, both γ and $f_{\rm gal}$ have tighter distributions and deviate from NFW. Figure 5.4 shows that there is a strong luminosity dependence of the satellite galaxy profile, i.e. *γ is an increasing function of luminosity, and $f_{\rm gal}$ is a decreasing one.* However, notice the unique coupling of $f_{\rm gal}$ and γ for the -20.5 case, where $f_{\rm gal}$ seems to deviate from the aforementioned trend. γ for -20.5 satellite galaxies also strays from the trend, but it is still significantly larger than NFW, and still lies within 1σ of the $M_r < -20$ and

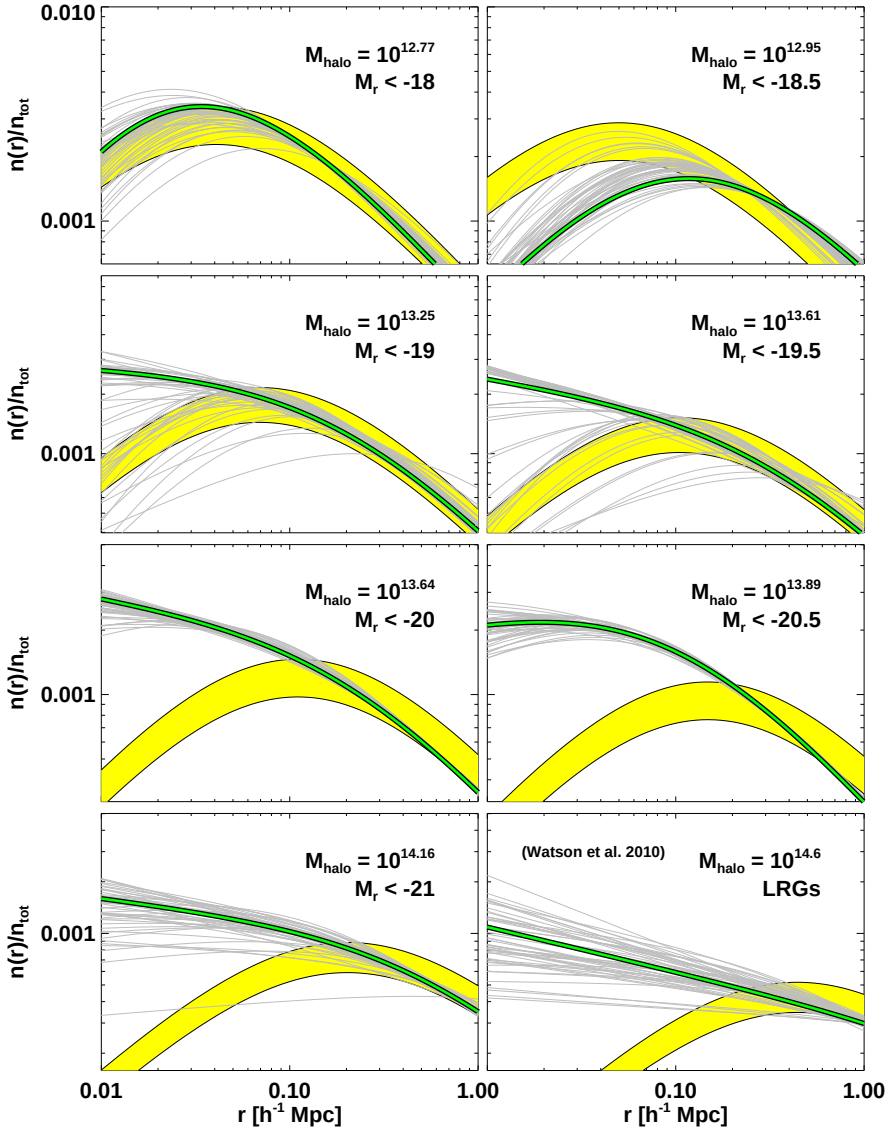

Figure 5.3: The radial profile of satellite galaxies as a function of luminosity. Each panel shows results for a specific luminosity sample, and for a halo mass that is chosen to be the mean value of M_1 from the PNMCG MCMC chain (listed in the top right of the panel). The solid, yellow bands show the NFW profile, with a 20% uncertainty to account for the possible ambiguity in the dark matter distribution. Green curves show the profile corresponding to the best-fit PNMCG model. Each panel also contains 50 grey curves representing 50 randomly drawn links from the top 95% of the PNMCG MCMC chain, after sorting in χ^2 from lowest to highest values. These 50 curves thus span the 95% confidence region allowed by the data. As we probe higher luminosities, the radial profile of satellite galaxies strongly deviates from an NFW distribution on small scales, showing that luminous galaxies are poor tracers of the underlying dark matter.

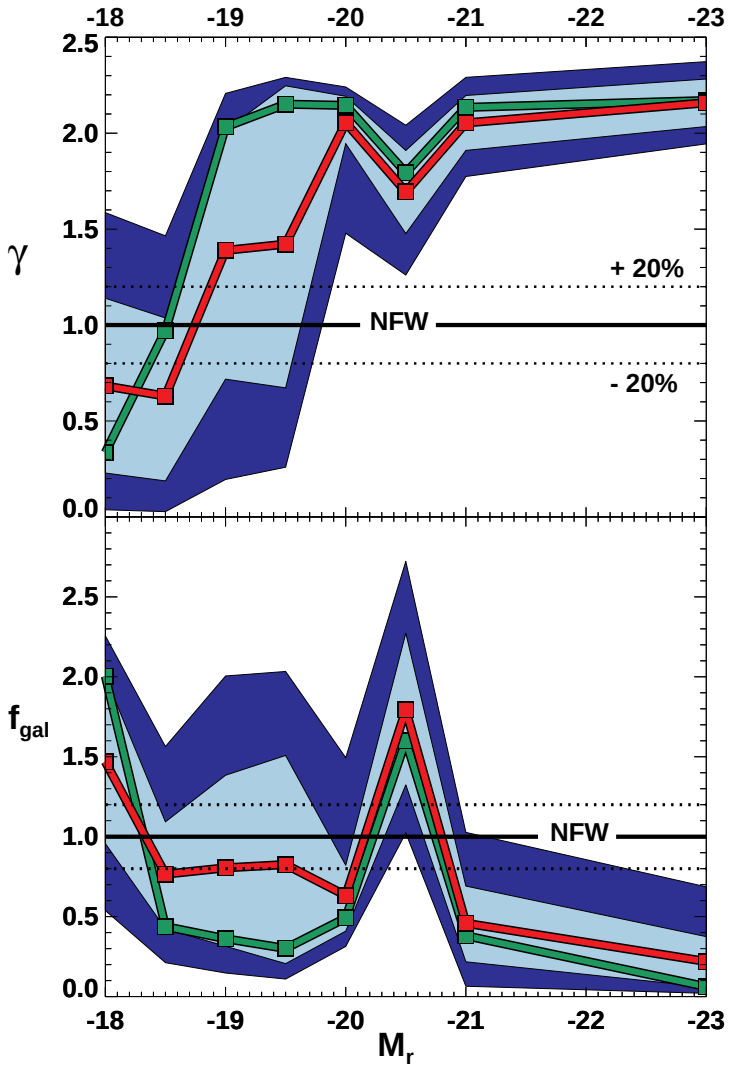

Figure 5.4: *Top Panel*: The slope of the inner density profile of satellite galaxies as a function of galaxy luminosity. The filled red squares (and connecting lines) show the mean value of γ from the MCMC chain of the PNMCG model for each luminosity sample and the green squares represent the best fit. The light blue and dark blue bands are the associated errors from the extrema of the middle 68.3% and 95% of the distribution, respectively. $\gamma = 1$ corresponds to an inner slope for an NFW dark matter profile, and is shown as a solid black line. The dotted black lines highlight an assumed 20% inaccuracy in the dark matter profile. *Bottom Panel*: The same procedure as the top panel, but for the parameter $f_{\rm gal}$ which relates the galaxy and dark matter concentrations ($f_{\rm gal} = c_{\rm gal}/c$). $f_{\rm gal}$ and γ are intrinsically linked and there is a strong trend towards inner slopes becoming steeper than NFW as we go to higher luminosities, with corresponding decreasing values of $f_{\rm gal}$.

$M_r < -21$ values ($f_{\rm gal}$ is within 2σ). However, the reason for this outlier is unclear, though it may be due to the fact that $w_p(r_p)$ has a strong feature at roughly the scale radius of the typical host halo (see the $M_r < -20.5$ panel of Fig. 5.1). This may cause a unique interplay between $f_{\rm gal}$ and γ, resulting in a mild departure from the trends. For $M_r < -20$ and brighter galaxies, the mean value of γ ranges between 1.6 - 2.1, significantly steeper than NFW. This range of γ values persists all the way down to $M_r < -19$ when considering the best-fit values. As mentioned in §5.2, M06 found a systematic error in the manner that light in the overlapping region of LRG pairs was being allocated in the SDSS pipeline. This caused a slight boost in the small-scale correlation function and was corrected for by M06. This effect is expected to rapidly diminish for lower luminosity samples, because the intrinsic sizes of galaxies will be smaller. However, we apply the same LRG correction to the J11 $M_r < -21$ sample to model the maximum effect that this could have. While we expect $\langle\gamma\rangle$ to decrease as a result of the innermost data points being scaled to lower $w_p(r_p)$ values, we still find that $\langle\gamma\rangle \sim 1.6$. Thus, even after assuming a *drastic* over-correction, γ is still strongly discrepant from NFW.

Figure 5.4 showed the luminosity trends for γ and $f_{\rm gal}$ by sorting the MCMC chains separately for each parameter. However, γ and $f_{\rm gal}$ are intrinsically coupled to one another so it is important to investigate the joint $\gamma - f_{\rm gal}$ parameter space. Figure 5.5 Shows the $\gamma - f_{\rm gal}$ parameter space at each luminosity, with the dark blue and light blue regions defined as the top 95% and 68.3% of the MCMC chain,

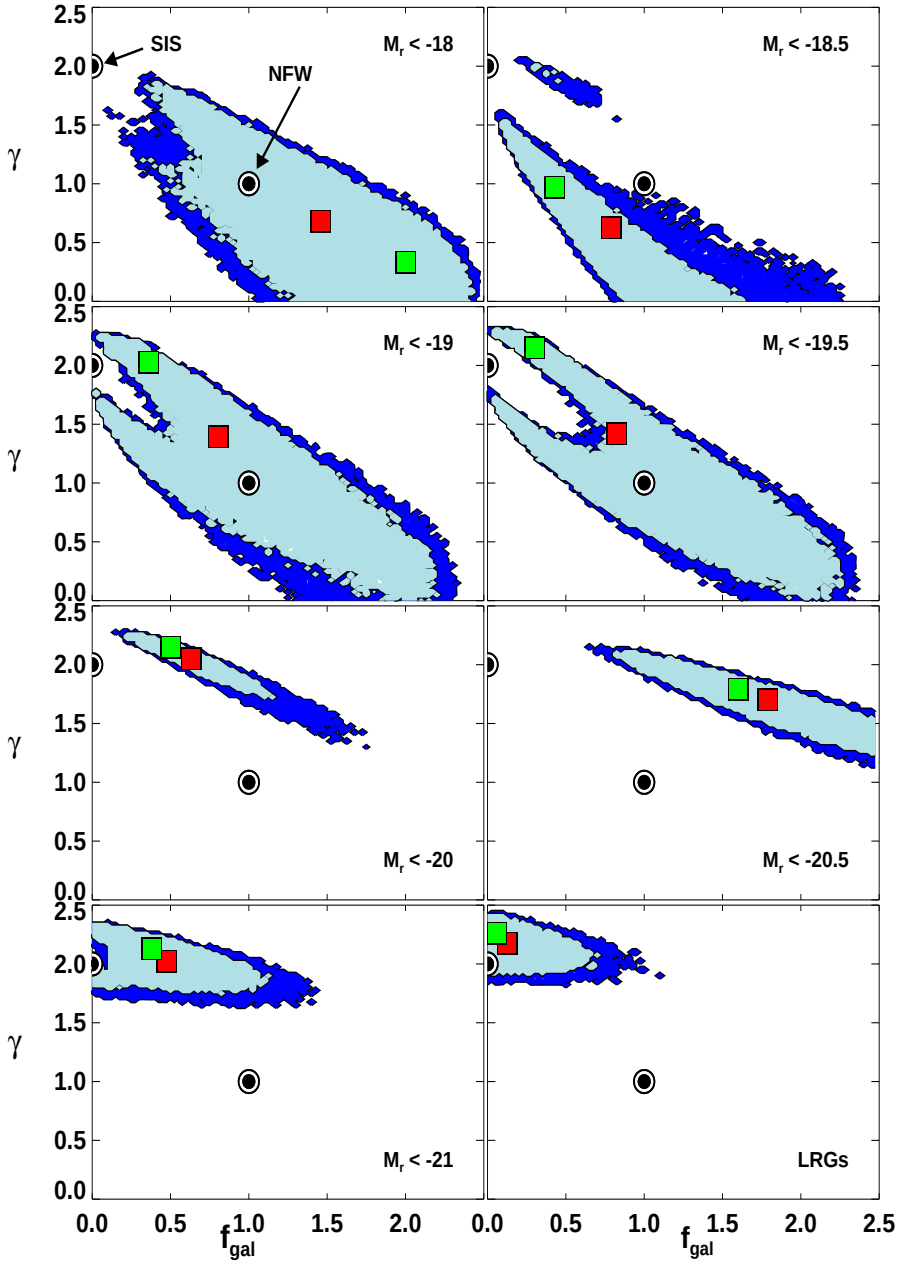

Figure 5.5: The $\gamma - f_{\rm gal}$ parameter space as a function of luminosity, highlighting the relationship between the inner slope and concentration of the density profile of satellite galaxies relative to dark matter. For each panel, the dark blue and light blue regions are defined as the top 95% and 68.3% of the MCMC chain for a given luminosity sample after sorting in χ^2. There are two points of reference designated as filled circles - the $\gamma = 1, f_{\rm gal} = 1$ combination that represents an NFW distribution, and the $\gamma = 2, f_{\rm gal} \to 0$ combination that represents a singular isothermal sphere distribution (SIS). Red squares show the mean values of γ and $f_{\rm gal}$ from our MCMC runs and green squares show the values for the best-fit model. The data for $M_r < -20$ and brighter galaxies strongly rule out the NFW model and are in good agreement with an SIS distribution for $M_r < -21$ and LRGs.

after sorting in χ^2. There are two points of reference designated as filled circles: the $\gamma = 1, f_{\rm gal} = 1$ combination for an NFW distribution and a $\gamma = 2, f_{\rm gal} \to 0$ combination representing a singular isothermal sphere (SIS) distribution. Red squares represent the mean values of γ and $f_{\rm gal}$ from our MCMC runs and green squares show the best-fit combination. As expected, the $M_r < -18$ through -19.5 exhibit a broad range in $\gamma - f_{\rm gal}$ combinations, with the NFW combination lying within the top 68.3% region (with the exception of the -18.5 sample). The $\gamma - f_{\rm gal}$ regions clearly drift away from NFW for $M_r < -20$ and greater luminosities and are well described by an SIS distribution for both the -21 and LRG samples. Figure 5.5 shows that the inner slope and concentration parameters are strongly degenerate with each other, particularly at low luminosities. This can be caused by having the scale radius (the radius within the halo where the slope transitions from $-\gamma$ to -3) too close to the innermost data point. When this happens, the data cannot accurately constrain the inner slope, and only constrains γ and $f_{\rm gal}$ through their degenerate contribution to the amplitude of the density profile. A simple calculation of the scale radius using the virial definition of a halo (see §5.3.1) gives $r_s \sim 10h^{-1}$kpc for the $M_r < -18$ sample (adopting a halo mass equal to the mean value of M_1), which is precisely at the scale of the innermost data point of $w_p(r_p)$. This leads to the large spread in $\gamma - f_{\rm gal}$ combinations. Of course, as we go to brighter samples, the scale radii increase, and the parameters are better constrained.

For each luminosity, as the inner profile steepens, $f_{\rm gal}$ decreases (with the slight

deviation for the $M_r < -20.5$ case). The decrease in concentration does not necessarily imply that the concentration of satellites is low in the traditional sense - i.e., that there are fewer galaxies at small radii - but rather that the radial profiles simply evolve toward a more power-law form. For example, as $f_{\rm gal} \to 0$ in the case of LRGs, this does not mean that the LRG satellites are less concentrated than the underlying dark matter. As $f_{\rm gal} \to 0$, the scale radius is pushed far outside the virial radius, resulting in a pure power-law distribution of slope $-\gamma$. Since the value of $f_{\rm gal}$ can be misleading when thinking about the concentration of satellite galaxies, we consider an alternative definition of "concentration" that is more physically useful: the fraction of satellite galaxies (or mass) that are enclosed within a tenth of the virial radius $R_{\rm vir}$. We call this quantity $M_{1/10}$ and compute it by integrating any radial profile out to one-tenth the virial radius of the host halo and dividing by the total mass out to $R_{\rm vir}$

$$M_{1/10} = \frac{M(r < 0.1R_{\rm vir})}{M(r < R_{\rm vir})}. \tag{5.5}$$

Figure 5.6 (top panel) shows $M_{1/10}$ as a function of luminosity. For each luminosity sample, we assume a halo mass equal to the mean value of M_1 from the MCMC chain, and we calculate $M_{1/10}$ for every link in the chain using each link's values for γ and $f_{\rm gal}$. We then find the mean of the distribution of $M_{1/10}$ values (denoted by the red squares and connecting lines). Errors for $M_{1/10}$ are given by the extrema of the middle 68.3% of the distribution after sorting by $M_{1/10}$. The black filled circles show $M_{1/10}$ for a dark matter NFW profile. The dark matter concentration drops with luminosity because

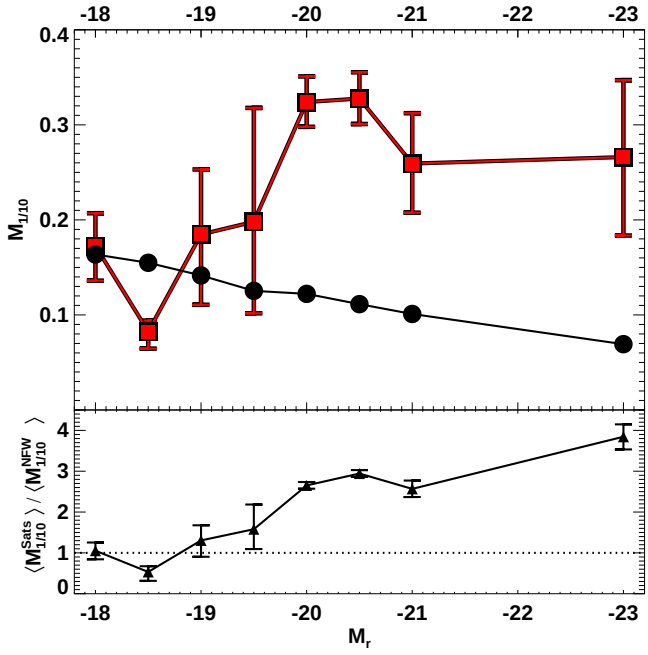

Figure 5.6: A more physically useful definition of concentration: $M_{1/10}$, defined as the fraction of satellite galaxies (or mass) that are enclosed within one tenth of the virial radius of a halo (see Eq. 5.5). *Top Panel*: For each luminosity sample, we choose a mass equal to the mean value of M_1 from the PNMCG MCMC chain, and we compute $M_{1/10}$ for each link in the chain. Red squares (and connecting lines) show the mean of the $M_{1/10}$ distribution for a given luminosity, and errorbars for $M_{1/10}$ show the extrema of the middle 68.3% of the distribution. Black points show $M_{1/10}$ for an NFW distribution. *Bottom Panel*: Ratio of $M_{1/10}$ for satellites with respect to dark matter. The dotted line highlights a ratio of unity. Satellite galaxies clearly become much more centrally concentrated than dark matter with increasing luminosity.

the mean value of M_1 increases with luminosity and concentration is a decreasing function of halo mass (Bullock et al., 2001). The bottom panel of Figure 5.6 shows the ratio of $M_{1/10}$ for satellites with respect to dark matter. The figure clearly shows that low luminosity satellite galaxies ($M_r > -19.5$) have spatial concentrations similar to dark matter, whereas the profiles of luminous satellite galaxies ($M_r < -20$ and brighter) are $\sim 2.5 - 4$ times more concentrated than NFW.

5.5 Summary & Discussion

Do satellite galaxies trace the underlying dark matter distribution? Our modeling of the small-scale $w_p(r_p)$ over an enormous range in galaxy luminosity thresholds, from SDSS Main galaxies to LRGs ($M_r < -18$ through $\lesssim -23$), has revealed a strong luminosity dependence of the radial distribution of satellite galaxies. We have found that for the low luminosity samples (lower than $M_r < -20$), there is a wide range of satellite galaxy concentrations (equal to $f_{\rm gal}$ times the NFW dark matter concentration) and inner density profile slopes, $-\gamma$, that are consistent with the data. This lack of constraining power is due to a strong degeneracy between $f_{\rm gal}$ and γ, which, in turn, is possibly due to the fact that the smallest scale data point in $w_p(r_p)$ is roughly around the scale radius for halos hosting galaxies of this size. Nevertheless, low luminosity satellite galaxies have radial distributions that are generally consistent with the NFW dark matter distribution. When we move to higher luminosity galaxies ($M_r < -20$ and brighter samples) however, satellite profiles change dramatically, with the most striking feature being that γ jumps to much higher values. Our results show that for $M_r < -20$ and brighter galaxies, γ ranges from $\sim 1.6 - 2.1$, highly discrepant from NFW, even after assuming a 20% inaccuracy in the dark matter profile. Luminous satellite galaxies are thus poor tracers of the underlying dark matter within halos on the small scales that we probe. Since the effects of $f_{\rm gal}$ and γ on the radial profile are intertwined, we have calculated a more physically useful quantity $M_{1/10}$, which gives the fractional amount of mass enclosed within one-tenth

of the virial radius. We find that $M_{1/10}$ is a strong function of luminosity, being consistent with NFW for low luminosity galaxies and being $\sim 2.5 - 4$ times more concentrated than NFW for galaxies brighter than $M_r < -20$.

Several other studies have also investigated the radial distribution of galaxies within halos. When considering faint satellites around $\sim L^*$ galaxies, no consensus emerges. Chen (2009) found the satellite distribution to be consistent with NFW. More et al. (2009) found a cored satellite profile best described by a $\gamma = 0, f_{\rm gal} = 0.5$ combination, inconsistent with NFW. Carlberg et al. (2009) found that the radial profiles of dwarf satellites around nearby galaxies are much *more* concentrated than NFW, rendering all of these studies in disaccord. Furthermore, the discrepancies persist when considering a broader range of galaxy systems. Nierenberg et al. (2011) recently studied the radial profile of satellites around massive, early-type galaxies at intermediate redshifts. Assuming a power-law profile model, they find that the satellites have an isothermal distribution of slope -1. Guo et al. (2012) considered SDSS satellite galaxies around host central galaxies of a wide luminosity range and, in general, satellite number density profiles were shown to be consistent with NFW. The NFW dark matter concentration was found to decrease with increasing satellite galaxy luminosity, independent of the host galaxy luminosity (except for the brightest centrals). They also detected a slightly *steeper* profile for *fainter* satellites. These varying results imply that uncovering the spatial distribution of satellite galaxies is a difficult problem. In the end, we have found that there is a strong luminosity

dependence of the radial distribution of satellite galaxies, wherein $\sim L^*$ and brighter satellites within group and cluster sized halos have a *substantially steeper* radial profile than dark matter on scales smaller than $\sim 100h^{-1}$kpc. We emphasize that while the scales involved in all of these studies are similar to ours, galaxy sample selection is different in each case, making it difficult to directly compare their results with ours.

Our results have shown that luminous galaxies are poor tracers of NFW. We now address the possibility that NFW is a poor model for the underlying dark matter distribution. In the established ΛCDM concordance cosmology, recent studies invoking high resolution N-body simulations have shown that the mass profiles of ΛCDM halos slightly, but systematically, deviate from NFW, becoming shallower at smaller radii (Stadel et al., 2009; Del Popolo, 2010). In fact, they may be better described by Einasto profiles, which include a parameter α that controls how the logarithmic slope will vary with radius to accurately account for the fact that halo profiles seem to not be self-similar (Gao et al., 2008; Navarro et al., 2010; Ludlow et al., 2010). These studies find, on average, $\gamma < 1$ (Graham et al., 2006; Navarro et al., 2010). However, on average, the simpler, two-parameter NFW model, which has a characteristic r^{-1} inner slope, is accurate to within $10 - 20\%$ (Benson, 2010). Moreover, Mandelbaum et al. (2008) fit galaxy cluster weak lensing profiles on small scales and found that NFW and Einasto profiles gave the same result to within several percent. Therefore, for simplicity, and to be consistent with previous modeling of LRGs by Watson et al. (2010), we assumed an NFW distribution throughout our modeling analysis. We con-

clude from the aforementioned studies that NFW is not a poor model for the dark matter distribution in collisionless simulations and, to the extent that it is, the true profile is even more discrepant from our results for luminous satellite galaxies.

Of course, by assuming a pure dark matter profile established from high resolution N-body simulations, the effects that baryons can have on dark matter are not considered. *Adiabatic Contraction* (AC) (Blumenthal et al., 1986; Ryden & Gunn, 1987; Gnedin et al., 2004) may cause a steepening of the inner slope of the dark matter density profile as the gas condenses and sinks to to the center of the dark matter potential well (Diemand et al., 2004; Fukushige et al., 2004; Reed et al., 2005; Del Popolo & Kroupa, 2009). However, the majority of results indicate that the steepening is insubstantial or can vary widely from halo to halo (e.g., Tissera et al., 2010). In fact, while AC may cause a steepening of the inner profile, over time, major and minor mergers can cause the dark matter profile to become shallower. (El-Zant et al., 2001; Romano-Díaz et al., 2008, 2009; Johansson et al., 2009). Observational confirmations of AC are notoriously difficult. In the case of galaxy clusters, X-ray analysis by Zappacosta et al. (2006) showed that processes during halo formation (e.g. gravitational heating from merger events) counteract AC and the mass profiles were still well described by NFW. Mandelbaum et al. (2006) used galaxy-galaxy lensing to show that the mass density profile of LRG clusters is consistent with NFW. Recently, Schulz et al. (2010) studied the profiles of a large sample of SDSS ellipticals and found that their dynamical mass measurements suggest that the measured excess mass on

small scales *may* be consistent with the AC hypothesis. However, for bright galaxies, our results are still not reconcilable with current AC models.We thus conclude that luminous satellite galaxies are indeed poor tracers of the underlying dark matter distribution, even accounting for the effects of baryons on the dark matter.

It is perhaps not surprising that galaxies do not behave like test particles as they orbit within a dark matter potential well. Being massive and extended, they are subject to dynamical mechanisms that would not affect test particles, namely dynamical friction and mass loss due to the tidal field of their host halo. In fact, these mechanisms should affect large and massive objects more than small ones, which could explain the luminosity trend that we observe. Satellite galaxies are thought to reside within subhalos, so it makes more sense to compare the radial distribution of galaxies to that of subhalos, rather than just dark matter. While subhalos tend to have a less concentrated radial distribution than dark matter (**?**Ghigna et al., 2000; Gao et al., 2004; De Lucia et al., 2004; Nagai & Kravtsov, 2005), the subhalo distribution has yet to be extended down to the extreme small scales that we have probed. High resolution N-body simulations are just now becoming available that allow for subhalos to be distinguished at the $10h^{-1}$kpc separation level (e.g., Klypin et al., 2011) for all of the luminosity samples that we have studied. Of course, subhalos may not be perfect tracers of galaxies, but it will be interesting to see whether the distribution of subhalos as a function of mass follows the same trend that we have uncovered for satellite galaxies as a function of luminosity. If the primary cause of this trend is

dynamical in nature (e.g., dynamical friction), it should also show up with subhalos. Either way, such a comparison will yield insight into the relation between subhalos and galaxies on very small scales, as well as the complicated non-linear processes occurring towards the centers of host halos, crucial for galaxy formation theory.

Chapter VI

CONCLUSIONS

The last decade has transformed the field of cosmology into a precision science. We now know to great accuracy that the matter content of the Universe consists of approximately 85% in the form of the mysterious dark matter and the remaining 15% in the form of ordinary, baryonic matter. Much of this baryonic matter is locked up in galaxies, and understanding the spatial distribution, or "clustering", of galaxies as they relate to the more ubiquitous dark matter is one of the principal goals of galaxy formation theory. With the large influx of high quality data, there is now an established concordance cosmological model known as ΛCDM. This model has successfully passed a gauntlet of tests on large scales, but studying the small scales ($\lesssim$ 1Mpc) is non-trivial and has received much attention. The physics on these scales is complicated, since many different processes are at work (e.g., gas physics, stellar astrophysics, orbital dynamics). While galaxy formation is complex, an understanding of the fate of satellite galaxies (galaxies that orbit around a brighter galaxy) can provide key pieces to the galaxy formation puzzle. This thesis has been primarily focused on studying the tumultuous lives of satellite galaxies. Specifically, I used their spatial clustering on small scales to reveal important insights into galaxy formation theory.

In Chapter II I explored the power-law nature of the galaxy correlation function. The galaxy correlation function was measured four decades ago and found to be consistent with an r^{-2} power law (Totsuji & Kihara, 1969). I revisited this long-standing problem and addressed the nature of the observed, low-redshift, power-law galaxy correlation function. I modeled the evolution of galaxy clustering through cosmic time to investigate the nature of the power-law shape of the galaxy correlation function, $\xi(r)$. $\xi(r)$ on large scales is set by primordial fluctuations, but departures from a power law are governed by galaxy pair counts on small scales, which are subject to non-linear dynamics. Galaxies reside within their own *host* dark matter halo, like the Milky Way, and satellite galaxies live in microcosms of host halos known as *subhalos*. Therefore, the shape of the correlation function on small scales depends on the amount of surviving subhalos. I used the semi-analytic model of Zentner et al. (2005) to study subhalo populations within host halos. I demonstrated that non-linear processes resulting in the depletion of subhalos (and hence, galaxies) are essential for achieving a power-law $\xi(r)$. I also investigated how the shape of $\xi(r)$ depends on subhalo mass (or luminosity) and redshift. $\xi(r)$ breaks from a power law at high masses, implying that only galaxies of luminosities of L^* (roughly Milky Way luminosity) and dimmer should exhibit power-law clustering. Moreover, I demonstrated that $\xi(r)$ evolves from being far from a power law at high redshift, toward a near power-law shape at $z = 0$. I then argued that $\xi(r)$ will once again evolve away from a power law in the future, in large part caused by the evolving competition between the accretion and destruction

rates of subhalos over time. These rates happen to strike just the right balance at $z \approx 0$. In the end, I demonstrated that the physics responsible for setting the galaxy content of halos do not care about the conditions needed to achieve a power law $\xi(r)$ and these conditions are met only in a narrow mass and redshift range. I concluded that the power-law nature of $\xi(r)$ for L^* and fainter galaxy samples at low redshift is a cosmic coincidence.

The spatial clustering of galaxies also provides insight into how satellite galaxies lose stellar mass. Since satellite galaxies reside within subhalos, it begs the question, *Is there a relationship between the mass loss of the stellar material of satellite galaxies and the dark matter mass loss of subhalos*? A detailed understanding of this relation can lead to predictions for the amount of diffuse "intrahalo light" (IHL, light from stars associated with the halo, but not with any particular galaxy of the system) at the scale of an individual galaxy, galaxy group, and galaxy cluster systems.

In Chapter III, I introduced physically-motivated models to understand how the stellar mass loss of satellite galaxies was related to the dark matter mass loss of subhalos. In Chapter II showed how dark matter mass loss will directly affect the survival of subhalos, and hence, the shape of the correlation function. Therefore, by exploring models that relate stellar mass loss to subhalo dark matter mass loss, we can uncover how much stellar mass loss is required such that our model correlation function prediction matches observations of galaxy clustering. I compared our model predictions to the *projected* correlation function, $w_p(r_p)$, as a function of luminosity

as measured by Zehavi et al. (2011). Through this technique I was able to quantify the rate of stellar mass loss for a large range of luminosity threshold samples. I found the interesting result that this rate is a decreasing function of increasing luminosity. Thus, smaller satellite galaxies experience more stellar mass loss relative to subhalo dark matter mass loss than bright satellites.

Since our model directly predicts the amount of satellite galaxy stellar mass loss, this allowed us to make predictions for the amount of IHL for a large range of host halo mass systems. Our model demonstrated that the IHL contribution to galaxy group-sized system is very small ($\sim$ few percent of the total stellar mass of the system), and becomes the dominant component of the total stellar mass for cluster-sized systems.

Baryonic matter is sub-dominant to dark matter, so is it the case that satellite galaxies trace the spatial distribution of dark matter on small scales? In Chapter IV and Chapter V I demonstrated how galaxy clustering can be utilized to investigate whether or not this is the case.

Modeling the spatial distribution of satellite galaxies requires probing down to scales well within the radii of typical host dark matter halos. This necessitates precision measurements of the correlation function at very small galaxy pair separations. This was recently done using data from the Sloan Digital Sky Survey (York et al., 2000) by our collaborators Jiang et al. (2011) for dim to moderately bright galaxy samples, and in earlier work by Masjedi et al. (2006) for very bright galaxies. I modeled the correlation function for the bright galaxies in Chapter IV and for the dim to

intermediate luminosity samples in Chapter V. Typically, modeling galaxy clustering on intermediate scales ($\sim 0.1 < r < 10$ Mpc) involves varying parameters associated with a functional form for how many galaxies should occupy a halo of a given mass, and then assuming that the satellite galaxies have the same radial distribution as the underlying dark matter (e.g., Zehavi et al., 2011). However, I showed that simply varying the occupation number of halos was insufficient to match the data as brighter and brighter satellite galaxies were considered. I took the additional step of allowing for flexibility of the satellite galaxy density profile. While the inner slope of the dark matter density profile has an approximate universal r^{-1} logarithmic slope, I set the inner slope of satellite galaxies as $r^{-\gamma}$, where γ was a free parameter. The striking result I found was that for satellite galaxies dimmer than an absolute r-band magnitude of -20 the radial profile of satellite galaxies is well described by the dark matter distribution. However, brighter satellite galaxies have radial profiles with significantly steeper inner slopes than r^{-1}. I found inner logarithmic slopes ranging from -1.6 to -2.1. Our results suggest that the processes that govern the spatial distribution of galaxies, once they have merged into larger halos, must be luminosity dependent, such that luminous galaxies become poor tracers of the underlying dark matter.

Galaxy formation/evolution is extremely complex, and the aim of this work was to shed light on fundamental physical processes by means of the spatial clustering of galaxies. Many open questions remain, yet as galaxy surveys only continue to improve, we will rapidly approach a more comprehensive understanding of how galaxies form

and evolve.

References

Abazajian, K. N., J. K. Adelman-McCarthy, M. A. Agüeros, S. S. Allam, C. Allende Prieto, D. An, K. S. J. Anderson, S. F. Anderson, J. Annis, N. A. Bahcall, & et al., 2009: The Seventh Data Release of the Sloan Digital Sky Survey. ApJS, **182**, 543–558.

Abe, F., I. A. Bond, B. S. Carter, R. J. Dodd, M. Fujimoto, J. B. Hearnshaw, M. Honda, J. Jugaku, S. Kabe, P. M. Kilmartin, B. S. Koribalski, M. Kobayashi, K. Masuda, Y. Matsubara, M. Miyamoto, Y. Muraki, T. Nakamura, G. R. Nankivell, S. Noda, G. S. Pennycook, L. Z. Pipe, N. J. Rattenbury, M. Reid, N. J. Rumsey, T. Saito, H. Sato, S. Sato, M. Sekiguchi, D. J. Sullivan, T. Sumi, Y. Watase, T. Yanagisawa, P. C. M. Yock, & M. Yoshizawa, 1999: Observation of the Halo of the Edge-On Galaxy IC 5249. AJ, **118**, 261–272.

Aguerri, J. A. L., N. Castro-Rodríguez, N. Napolitano, M. Arnaboldi, & O. Gerhard, 2006: Diffuse light in Hickson compact groups: the dynamically young system HCG 44. A&A, **457**, 771–778.

Almeida, C., C. M. Baugh, D. A. Wake, C. G. Lacey, A. J. Benson, R. G. Bower, & K. Pimbblet, 2008: Luminous red galaxies in hierarchical cosmologies. MNRAS, **386**, 2145–2160.

Bailin, J., E. F. Bell, S. N. Chappell, D. J. Radburn-Smith, & R. S. de Jong, 2011: The Resolved Stellar Halo of NGC 253. ApJ, **736**, 24–+.

Baugh, C. M., 1996: The real-space correlation function measured from the APM Galaxy Survey. MNRAS, **280**, 267–275.

Behroozi, P. S., C. Conroy, & R. H. Wechsler, 2010: A Comprehensive Analysis of Uncertainties Affecting the Stellar Mass-Halo Mass Relation for $0 < z < 4$. ApJ, **717**, 379–403.

Behroozi, P. S., R. H. Wechsler, & H.-Y. Wu, 2011: The Rockstar Phase-Space Temporal Halo Finder and the Velocity Offsets of Cluster Cores. *ArXiv e-prints*.

Bell, E. F. & R. S. de Jong, 2001: Stellar Mass-to-Light Ratios and the Tully-Fisher Relation. ApJ, **550**, 212–229.

Benson, A. J., 2005: Orbital parameters of infalling dark matter substructures. MNRAS, **358**, 551–562.

—, 2010: Galaxy formation theory. Phys. Rep., **495**, 33–86.

Berlind, A. A. & D. H. Weinberg, 2002: The Halo Occupation Distribution: Toward an Empirical Determination of the Relation between Galaxies and Mass. ApJ, **575**, 587–616.

Berlind, A. A., D. H. Weinberg, A. J. Benson, C. M. Baugh, S. Cole, R. Davé, C. S. Frenk, A. Jenkins, N. Katz, & C. G. Lacey, 2003: The Halo Occupation Distribution and the Physics of Galaxy Formation. ApJ, **593**, 1–25.

Bernstein, G. M., R. C. Nichol, J. A. Tyson, M. P. Ulmer, & D. Wittman, 1995: The Luminosity Function of the Coma Cluster Core for $-25 < M/R < -9.4$. AJ, **110**, 1507–+.

Berrier, J. C., J. S. Bullock, E. J. Barton, H. D. Guenther, A. R. Zentner, & R. H. Wechsler, 2006: Close Galaxy Counts as a Probe of Hierarchical Structure Formation. ApJ, **652**, 56–70.

Binney, J. & S. Tremaine, 2008: *Galactic Dynamics: Second Edition*. Princeton University Press.

Blake, C., A. Collister, & O. Lahav, 2008: Halo-model signatures from 380000 Sloan Digital Sky Survey luminous red galaxies with photometric redshifts. MNRAS, **385**, 1257–1269.

Blanton, M. R., D. W. Hogg, N. A. Bahcall, I. K. Baldry, J. Brinkmann, I. Csabai, D. Eisenstein, M. Fukugita, J. E. Gunn, Ž. Ivezić, D. Q. Lamb, R. H. Lupton, J. Loveday, J. A. Munn, R. C. Nichol, S. Okamura, D. J. Schlegel, K. Shimasaku, M. A. Strauss, M. S. Vogeley, & D. H. Weinberg, 2003: The Broadband Optical Properties of Galaxies with Redshifts $0.02 < z < 0.22$. ApJ, **594**, 186–207.

Blanton, M. R., D. J. Schlegel, M. A. Strauss, J. Brinkmann, D. Finkbeiner, M. Fukugita, J. E. Gunn, D. W. Hogg, Ž. Ivezić, G. R. Knapp, R. H. Lupton, J. A. Munn, D. P. Schneider, M. Tegmark, & I. Zehavi, 2005: New York University Value-Added Galaxy Catalog: A Galaxy Catalog Based on New Public Surveys. AJ, **129**, 2562–2578.

Blumenthal, G. R., S. M. Faber, R. Flores, & J. R. Primack, 1986: Contraction of dark matter galactic halos due to baryonic infall. ApJ, **301**, 27–34.

Blumenthal, G. R., S. M. Faber, J. R. Primack, & M. J. Rees, 1984: Formation of galaxies and large-scale structure with cold dark matter. Nature, **311**, 517–525.

Bond, J. R., S. Cole, G. Efstathiou, & N. Kaiser, 1991: Excursion set mass functions for hierarchical Gaussian fluctuations. ApJ, **379**, 440–460.

Bower, R. G., A. J. Benson, R. Malbon, J. C. Helly, C. S. Frenk, C. M. Baugh, S. Cole, & C. G. Lacey, 2006: Breaking the hierarchy of galaxy formation. MNRAS, **370**, 645–655.

Boylan-Kolchin, M., J. S. Bullock, & M. Kaplinghat, 2011a: The Milky Way's bright satellites as an apparent failure of LCDM. *ArXiv e-prints*.

—, 2011b: Too big to fail? The puzzling darkness of massive Milky Way subhaloes. MNRAS, **415**, L40–L44.

Boylan-Kolchin, M., V. Springel, S. D. M. White, & A. Jenkins, 2010: There's no place like home? Statistics of Milky Way-mass dark matter haloes. MNRAS, **406**, 896–912.

Bryan, G. L. & M. L. Norman, 1998: Statistical Properties of X-Ray Clusters: Analytic and Numerical Comparisons. ApJ, **495**, 80.

Bullock, J. S., T. S. Kolatt, Y. Sigad, R. S. Somerville, A. V. Kravtsov, A. A. Klypin, J. R. Primack, & A. Dekel, 2001: Profiles of dark haloes: evolution, scatter and environment. MNRAS, **321**, 559–575.

Busha, M. T., R. H. Wechsler, P. S. Behroozi, B. F. Gerke, A. A. Klypin, & J. R. Primack, 2010: Statistics of Satellite Galaxies Around Milky Way-Like Hosts. *ArXiv e-prints*.

Byrd, G. & M. Valtonen, 1990: Tidal generation of active spirals and S0 galaxies by rich clusters. ApJ, **350**, 89–94.

Calcáneo-Roldán, C., B. Moore, J. Bland-Hawthorn, D. Malin, & E. M. Sadler, 2000: Galaxy destruction and diffuse light in clusters. MNRAS, **314**, 324–333.

Carlberg, R. G., M. Sullivan, & D. Le Borgne, 2009: Dwarf Galaxy Clustering and Missing Satellites. ApJ, **694**, 1131–1138.

Carroll, S. M., W. H. Press, & E. L. Turner, 1992: The cosmological constant. ARA&A, **30**, 499–542.

Castro-Rodríguez, N., J. A. L. Aguerri, M. Arnaboldi, O. Gerhard, K. C. Freeman, N. R. Napolitano, & M. Capaccioli, 2003: Narrow band survey for intragroup light in the Leo HI cloud. Constraints on the galaxy background contamination in imaging surveys for intracluster planetary nebulae. A&A, **405**, 803–812.

Chandrasekhar, S., 1943: Dynamical Friction. I. General Considerations: the Coefficient of Dynamical Friction. ApJ, **97**, 255–+.

Chapman, S. C., R. Ibata, G. F. Lewis, A. M. N. Ferguson, M. Irwin, A. McConnachie, & N. Tanvir, 2006: A Kinematically Selected, Metal-poor Stellar Halo in the Outskirts of M31. ApJ, **653**, 255–266.

Chen, J., 2009: The galaxy cross-correlation function as a probe of the spatial distribution of galactic satellites. A&A, **494**, 867–877.

Chiba, M. & T. C. Beers, 2000: Kinematics of Metal-poor Stars in the Galaxy. III. Formation of the Stellar Halo and Thick Disk as Revealed from a Large Sample of Nonkinematically Selected Stars. AJ, **119**, 2843–2865.

Coil, A. L., J. A. Newman, M. C. Cooper, M. Davis, S. M. Faber, D. C. Koo, & C. N. A. Willmer, 2006: The DEEP2 Galaxy Redshift Survey: Clustering of Galaxies as a Function of Luminosity at z = 1. ApJ, **644**, 671–677.

Colín, P., A. A. Klypin, A. V. Kravtsov, & A. M. Khokhlov, 1999: Evolution of Bias in Different Cosmological Models. ApJ, **523**, 32–53.

Colless, M., G. Dalton, S. Maddox, W. Sutherland, P. Norberg, S. Cole, J. Bland-Hawthorn, T. Bridges, R. Cannon, C. Collins, W. Couch, N. Cross, K. Deeley, R. De Propris, S. P. Driver, G. Efstathiou, R. S. Ellis, C. S. Frenk, K. Glazebrook, C. Jackson, O. Lahav, I. Lewis, S. Lumsden, D. Madgwick, J. A. Peacock, B. A. Peterson, I. Price, M. Seaborne, & K. Taylor, 2001: The 2dF Galaxy Redshift Survey: spectra and redshifts. MNRAS, **328**, 1039–1063.

Conroy, C. & R. H. Wechsler, 2009: Connecting Galaxies, Halos, and Star Formation Rates Across Cosmic Time. ApJ, **696**, 620–635.

Conroy, C., R. H. Wechsler, & A. V. Kravtsov, 2006: Modeling Luminosity-dependent Galaxy Clustering through Cosmic Time. ApJ, **647**, 201–214.

—, 2007: The Hierarchical Build-Up of Massive Galaxies and the Intracluster Light since z = 1. ApJ, **668**, 826–838.

Cooray, A. & R. Sheth, 2002: Halo models of large scale structure. Phys. Rep., **372**, 1–129.

da Costa, L. N., P. S. Pellegrini, W. L. W. Sargent, J. Tonry, M. Davis, A. Meiksin, D. W. Latham, J. W. Menzies, & I. A. Coulson, 1988: The Southern Sky Redshift Survey. ApJ, **327**, 544–560.

Da Rocha, C. & C. Mendes de Oliveira, 2005: Intragroup diffuse light in compact groups of galaxies: HCG 79, 88 and 95. MNRAS, **364**, 1069–1081.

Da Rocha, C., B. L. Ziegler, & C. Mendes de Oliveira, 2008: Intragroup diffuse light in compact groups of galaxies - II. HCG 15, 35 and 51. MNRAS, **388**, 1433–1443.

Davis, M., J. Huchra, D. W. Latham, & J. Tonry, 1982: A survey of galaxy redshifts. II - The large scale space distribution. ApJ, **253**, 423–445.

Davis, M. & P. J. E. Peebles, 1983: A survey of galaxy redshifts. V - The two-point position and velocity correlations. ApJ, **267**, 465–482.

de Lapparent, V., M. J. Geller, & J. P. Huchra, 1988: The mean density and two-point correlation function for the CfA redshift survey slices. ApJ, **332**, 44–56.

De Lucia, G., G. Kauffmann, V. Springel, S. D. M. White, B. Lanzoni, F. Stoehr, G. Tormen, & N. Yoshida, 2004: Substructures in cold dark matter haloes. MNRAS, **348**, 333–344.

Del Popolo, A., 2010: On the universality of density profiles. MNRAS, **408**, 1808–1817.

Del Popolo, A. & P. Kroupa, 2009: Density profiles of dark matter haloes on galactic and cluster scales. A&A, **502**, 733–747.

Diemand, J., M. Kuhlen, & P. Madau, 2007: Formation and Evolution of Galaxy Dark Matter Halos and Their Substructure. ApJ, **667**, 859–877.

Diemand, J., B. Moore, & J. Stadel, 2004: Convergence and scatter of cluster density profiles. MNRAS, **353**, 624–632.

Dohm-Palmer, R. C., A. Helmi, H. Morrison, M. Mateo, E. W. Olszewski, P. Harding, K. C. Freeman, J. Norris, & S. A. Shectman, 2001: Mapping the Galactic Halo. V. Sagittarius Dwarf Spheroidal Tidal Debris 60deg from the Main Body. ApJ, **555**, L37–L40.

Dunkley, J., M. Bucher, P. G. Ferreira, K. Moodley, & C. Skordis, 2005: Fast and reliable Markov chain Monte Carlo technique for cosmological parameter estimation. MNRAS, **356**, 925–936.

Einasto, J., 1965: Influence of the atmospheric and instrumental dispersion on the brightness distribution in a galaxy. *Trudy Inst. Astrofiz. Alma-Ata 51, 87*.

Eisenstein, D. J., I. Zehavi, D. W. Hogg, R. Scoccimarro, M. R. Blanton, R. C. Nichol, R. Scranton, H.-J. Seo, M. Tegmark, Z. Zheng, S. F. Anderson, J. Annis, N. Bahcall, J. Brinkmann, S. Burles, F. J. Castander, A. Connolly, I. Csabai, M. Doi, M. Fukugita, J. A. Frieman, K. Glazebrook, J. E. Gunn, J. S. Hendry, G. Hennessy, Z. Ivezić, S. Kent, G. R. Knapp, H. Lin, Y.-S. Loh, R. H. Lupton, B. Margon, T. A. McKay, A. Meiksin, J. A. Munn, A. Pope, M. W. Richmond, D. Schlegel, D. P. Schneider, K. Shimasaku, C. Stoughton, M. A. Strauss, M. SubbaRao, A. S. Szalay, I. Szapudi, D. L. Tucker, B. Yanny, & D. G. York, 2005: Detection of the Baryon Acoustic Peak in the Large-Scale Correlation Function of SDSS Luminous Red Galaxies. ApJ, **633**, 560–574.

Eke, V. R., S. Cole, & C. S. Frenk, 1996: Cluster evolution as a diagnostic for Omega. MNRAS, **282**, 263–280.

El-Zant, A., I. Shlosman, & Y. Hoffman, 2001: Dark Halos: The Flattening of the Density Cusp by Dynamical Friction. ApJ, **560**, 636–643.

Faltenbacher, A. & W. G. Mathews, 2005: On the dynamics of the satellite galaxies in NGC 5044. MNRAS, **362**, 498–504.

Feldmeier, J. J., 2006: Intracluster Planetary Nebulae. In M. J. Barlow & R. H. Méndez, ed., *Planetary Nebulae in our Galaxy and Beyond*, vol. 234 of *IAU Symposium*, pp. 33–40.

Feldmeier, J. J., P. R. Durrell, R. Ciardullo, & G. H. Jacoby, 2001: A Search for Intra-group Planetary Nebulae in the M 81 Group. *ArXiv Astrophysics e-prints*.

Fry, J. N., 1996: The Evolution of Bias. ApJ, **461**, L65+.

Fukushige, T., A. Kawai, & J. Makino, 2004: Structure of Dark Matter Halos from Hierarchical Clustering. III. Shallowing of the Inner Cusp. ApJ, **606**, 625–634.

Gallagher, J. S., III & J. P. Ostriker, 1972: A Note on Mass Loss during Collisions between Galaxies a nd the Formation of Giant Systems. AJ, **77**, 288–+.

Gan, J., X. Kang, F. C. van den Bosch, & J. Hou, 2010: An improved model for the dynamical evolution of dark matter subhaloes. MNRAS, **408**, 2201–2212.

Gao, L., G. De Lucia, S. D. M. White, & A. Jenkins, 2004: Galaxies and subhaloes in ΛCDM galaxy clusters. MNRAS, **352**, L1–L5.

Gao, L., J. F. Navarro, S. Cole, C. S. Frenk, S. D. M. White, V. Springel, A. Jenkins, & A. F. Neto, 2008: The redshift dependence of the structure of massive Λ cold dark matter haloes. MNRAS, **387**, 536–544.

Ghigna, S., B. Moore, F. Governato, G. Lake, T. Quinn, & J. Stadel, 1998: Dark matter haloes within clusters. MNRAS, **300**, 146–162.

—, 2000: Density Profiles and Substructure of Dark Matter Halos: Converging Results at Ultra-High Numerical Resolution. ApJ, **544**, 616–628.

Giocoli, C., L. Pieri, G. Tormen, & J. Moreno, 2009: A merger tree with microsolar mass resolution: application to γ-ray emission from subhalo population. MNRAS, **395**, 1620–1630.

Giocoli, C., G. Tormen, & F. C. van den Bosch, 2008: The population of dark matter subhaloes: mass functions and average mass-loss rates. MNRAS, **386**, 2135–2144.

Gnedin, O. Y., 2003: Dynamical Evolution of Galaxies in Clusters. ApJ, **589**, 752–769.

Gnedin, O. Y., A. V. Kravtsov, A. A. Klypin, & D. Nagai, 2004: Response of Dark Matter Halos to Condensation of Baryons: Cosmological Simulations and Improved Adiabatic Contraction Model. ApJ, **616**, 16–26.

Gonzalez, A. H., D. Zaritsky, & A. I. Zabludoff, 2007: A Census of Baryons in Galaxy Clusters and Groups. ApJ, **666**, 147–155.

Gott, J. R., III, M. Jurić, D. Schlegel, F. Hoyle, M. Vogeley, M. Tegmark, N. Bahcall, & J. Brinkmann, 2005: A Map of the Universe. ApJ, **624**, 463–484.

Gott, J. R., III & E. L. Turner, 1979: An extension of the galaxy covariance function to small scales. ApJ, **232**, L79–L81.

Graham, A. W., D. Merritt, B. Moore, J. Diemand, & B. Terzić, 2006: Empirical Models for Dark Matter Halos. II. Inner Profile Slopes, Dynamical Profiles, and ρ/σ^3. AJ, **132**, 2701–2710.

Guhathakurta, P., J. C. Ostheimer, K. M. Gilbert, R. M. Rich, S. R. Majewski, J. S. Kalirai, D. B. Reitzel, & R. J. Patterson, 2005: Discovery of an extended halo of metal-poor stars in the Andromeda spiral galaxy. *ArXiv Astrophysics e-prints*.

Gunn, J. E., 1977: Massive galactic halos. I - Formation and evolution. ApJ, **218**, 592–598.

Guo, Q., S. Cole, V. Eke, & C. Frenk, 2012: Satellite Galaxy Number Density Profiles in the Sloan Digital Sky Survey. *ArXiv e-prints*.

Guo, Q., S. White, C. Li, & M. Boylan-Kolchin, 2010: How do galaxies populate dark matter haloes? MNRAS, **404**, 1111–1120.

Gustafsson, M., M. Fairbairn, & J. Sommer-Larsen, 2006: Baryonic pinching of galactic dark matter halos. Phys. Rev. D, **74(12)**, 123522–+.

Hamilton, A. J. S., 1993: Toward Better Ways to Measure the Galaxy Correlation Function. ApJ, **417**, 19–+.

Hamilton, A. J. S. & M. Tegmark, 2002: The real-space power spectrum of the PSCz survey from 0.01 to $300hMpc^{-1}$. MNRAS, **330**, 506–530.

Hashimoto, Y., Y. Funato, & J. Makino, 2003: To Circularize or Not To Circularize?-Orbital Evolution of Satellite Galaxies. ApJ, **582**, 196–201.

Hauser, M. G. & P. J. E. Peebles, 1973: Statistical Analysis of Catalogs of Extragalactic Objects. 11. the Abell Catalog of Rich Clusters. ApJ, **185**, 757–786.

Hayashi, E., J. F. Navarro, J. E. Taylor, J. Stadel, & T. Quinn, 2003: The Structural Evolution of Substructure. ApJ, **584**, 541–558.

Hermit, S., B. X. Santiago, O. Lahav, M. A. Strauss, M. Davis, A. Dressler, & J. P. Huchra, 1996: The two-point correlation function and morphological segregation in the Optical Redshift Survey. MNRAS, **283**, 709–720.

Hogg, D. W., D. J. Eisenstein, M. R. Blanton, N. A. Bahcall, J. Brinkmann, J. E. Gunn, & D. P. Schneider, 2005: Cosmic Homogeneity Demonstrated with Luminous Red Galaxies. ApJ, **624**, 54–58.

Hood, M., T. Smecker-Hane, M. Teig, A. M. N. Ferguson, & M. J. Irwin, 2007: Kinematics of the Stellar Populations of M33. In A. Vallenari, R. Tantalo, L. Portinari, & A. Moretti, ed., *From Stars to Galaxies: Building the Pieces to Build Up the Universe*, vol. 374 of *Astronomical Society of the Pacific Conference Series*, pp. 281–+.

Hubble, E., 1929: A Relation between Distance and Radial Velocity among Extra-Galactic Nebulae. *Proceedings of the National Academy of Science*, **15**, 168–173.

Huchra, J., M. Davis, D. Latham, & J. Tonry, 1983: A survey of galaxy redshifts. IV - The data. ApJS, **52**, 89–119.

Ibata, R., M. Irwin, G. F. Lewis, & A. Stolte, 2001: Galactic Halo Substructure in the Sloan Digital Sky Survey: The Ancient Tidal Stream from the Sagittarius Dwarf Galaxy. ApJ, **547**, L133–L136.

Irwin, M. J., A. M. N. Ferguson, R. A. Ibata, G. F. Lewis, & N. R. Tanvir, 2005: A Minor-Axis Surface Brightness Profile for M31. ApJ, **628**, L105–L108.

Ivezić, Ž., J. Goldston, K. Finlator, G. R. Knapp, B. Yanny, T. A. McKay, S. Amrose, K. Krisciunas, B. Willman, S. Anderson, C. Schaber, D. Erb, C. Logan, C. Stubbs, B. Chen, E. Neilsen, A. Uomoto, J. R. Pier, X. Fan, J. E. Gunn, R. H. Lupton, C. M. Rockosi, D. Schlegel, M. A. Strauss, J. Annis, J. Brinkmann, I. Csabai, M. Doi, M. Fukugita, G. S. Hennessy, R. B. Hindsley, B. Margon, J. A. Munn, H. J. Newberg, D. P. Schneider, J. A. Smith, G. P. Szokoly, A. R. Thakar, M. S. Vogeley, P. Waddell, N. Yasuda, & D. G. York, 2000: Candidate RR Lyrae Stars Found in Sloan Digital Sky Survey Commissioning Data. AJ, **120**, 963–977.

Jenkins, A., C. S. Frenk, F. R. Pearce, P. A. Thomas, J. M. Colberg, S. D. M. White, H. M. P. Couchman, J. A. Peacock, G. Efstathiou, & A. H. Nelson, 1998: Evolution of Structure in Cold Dark Matter Universes. ApJ, **499**, 20–+.

Jenkins, A., C. S. Frenk, S. D. M. White, J. M. Colberg, S. Cole, A. E. Evrard, H. M. P. Couchman, & N. Yoshida, 2001: The mass function of dark matter haloes. MNRAS, **321**, 372–384.

Jiang, T., D. W. Hogg, & M. R. Blanton, 2011: Galaxy growth by merging in the nearby universe. *ArXiv e-prints*.

Jing, Y. P., G. Börner, & Y. Suto, 2002: Spatial Correlation Functions and the Pairwise Peculiar Velocity Dispersion of Galaxies in the Point Source Catalog Redshift Survey: Implications for the Galaxy Biasing in Cold Dark Matter Models. ApJ, **564**, 15–22.

Jing, Y. P., H. J. Mo, & G. Boerner, 1998: Spatial Correlation Function and Pairwise Velocity Dispersion of Galaxies: Cold Dark Matter Models versus the Las Campanas Survey. ApJ, **494**, 1–+.

Johansson, P. H., T. Naab, & J. P. Ostriker, 2009: Gravitational Heating Helps Make Massive Galaxies Red and Dead. ApJ, **697**, L38–L43.

Kaiser, N., 1987: Clustering in real space and in redshift space. MNRAS, **227**, 1–21.

Kalirai, J. S., K. M. Gilbert, P. Guhathakurta, S. R. Majewski, J. C. Ostheimer, R. M. Rich, M. C. Cooper, D. B. Reitzel, & R. J. Patterson, 2006: The Metal-poor Halo of the Andromeda Spiral Galaxy (M31)1,. ApJ, **648**, 389–404.

Kazantzidis, S., L. Mayer, C. Mastropietro, J. Diemand, J. Stadel, & B. Moore, 2004: Density Profiles of Cold Dark Matter Substructure: Implications for the Missing-Satellites Problem. ApJ, **608**, 663–679.

Kitzbichler, M. G. & S. D. M. White, 2008: A calibration of the relation between the abundance of close galaxy pairs and the rate of galaxy mergers. MNRAS, **391**, 1489–1498.

Klypin, A., S. Gottlöber, A. V. Kravtsov, & A. M. Khokhlov, 1999a: Galaxies in N-Body Simulations: Overcoming the Overmerging Problem. ApJ, **516**, 530–551.

Klypin, A., A. V. Kravtsov, O. Valenzuela, & F. Prada, 1999b: Where Are the Missing Galactic Satellites? ApJ, **522**, 82–92.

Klypin, A. A., S. Trujillo-Gomez, & J. Primack, 2011: Dark Matter Halos in the Standard Cosmological Model: Results from the Bolshoi Simulation. ApJ, **740**, 102.

Komatsu, E., K. M. Smith, J. Dunkley, C. L. Bennett, B. Gold, G. Hinshaw, N. Jarosik, D. Larson, M. R. Nolta, L. Page, D. N. Spergel, M. Halpern, R. S. Hill, A. Kogut, M. Limon, S. S. Meyer, N. Odegard, G. S. Tucker, J. L. Weiland, E. Wollack, & E. L. Wright, 2011: Seven-year Wilkinson Microwave Anisotropy Probe (WMAP) Observations: Cosmological Interpretation. ApJS, **192**, 18.

Koushiappas, S. M., A. R. Zentner, & A. V. Kravtsov, 2010: The distribution of annihilation luminosities in dark matter substructure. *ArXiv e-prints*.

Kravtsov, A. V., A. A. Berlind, R. H. Wechsler, A. A. Klypin, S. Gottlöber, B. Allgood, & J. R. Primack, 2004a: The Dark Side of the Halo Occupation Distribution. ApJ, **609**, 35–49.

Kravtsov, A. V., O. Y. Gnedin, & A. A. Klypin, 2004b: The Tumultuous Lives of Galactic Dwarfs and the Missing Satellites Problem. ApJ, **609**, 482–497.

Kravtsov, A. V. & A. A. Klypin, 1999: The Origin and Evolution of Halo Bias in Linear and Nonlinear Regimes. ApJ, **520**, 437–453.

Krick, J. E., R. A. Bernstein, & K. A. Pimbblet, 2006: Diffuse Optical Light in Galaxy Clusters. I. Abell 3888. AJ, **131**, 168–184.

Lacey, C. & S. Cole, 1993: Merger rates in hierarchical models of galaxy formation. MNRAS, **262**, 627–649.

—, 1994: Merger Rates in Hierarchical Models of Galaxy Formation - Part Two - Comparison with N-Body Simulations. MNRAS, **271**, 676–+.

Landy, S. D. & A. S. Szalay, 1993: Bias and variance of angular correlation functions. ApJ, **412**, 64–71.

Law, D. R., K. V. Johnston, & S. R. Majewski, 2005: A Two Micron All-Sky Survey View of the Sagittarius Dwarf Galaxy. IV. Modeling the Sagittarius Tidal Tails. ApJ, **619**, 807–823.

Leauthaud, A., M. R. George, P. S. Behroozi, K. Bundy, J. Tinker, R. H. Wechsler, C. Conroy, A. Finoguenov, & M. Tanaka, 2011: The integrated stellar content of dark matter halos. *ArXiv e-prints*.

Lee, K., M. Giavalisco, O. Y. Gnedin, R. S. Somerville, H. C. Ferguson, M. Dickinson, & M. Ouchi, 2006: The Large-Scale and Small-Scale Clustering of Lyman Break Galaxies at $3.5 <= z <= 5.5$ from the GOODS Survey. ApJ, **642**, 63–80.

Lequeux, J., F. Combes, M. Dantel-Fort, J. Cuillandre, B. Fort, & Y. Mellier, 1998: NGC 5907 revisited: a stellar halo formed by cannibalism? A&A, **334**, L9–L12.

Li, C. & S. D. M. White, 2009: Autocorrelations of stellar light and mass in the low-redshift Universe. *ArXiv e-prints*.

—, 2010: Autocorrelations of stellar light and mass in the low-redshift Universe. MNRAS, **407**, 515–519.

Lin, Y. & J. J. Mohr, 2004: K-band Properties of Galaxy Clusters and Groups: Brightest Cluster Galaxies and Intracluster Light. ApJ, **617**, 879–895.

Ludlow, A. D., J. F. Navarro, V. Springel, M. Vogelsberger, J. Wang, S. D. M. White, A. Jenkins, & C. S. Frenk, 2010: Secondary infall and the pseudo-phase-space density profiles of cold dark matter haloes. MNRAS, **406**, 137–146.

Lupton, R., J. E. Gunn, Z. Ivezić, G. R. Knapp, & S. Kent, 2001: The SDSS Imaging Pipelines. In Harnden, F. R., Jr., F. A. Primini, & H. E. Payne, eds., *Astronomical Data Analysis Software and Systems X*, vol. 238 of *Astronomical Society of the Pacific Conference Series*, pp. 269–+.

Macciò, A. V., A. A. Dutton, & F. C. van den Bosch, 2008: Concentration, spin and shape of dark matter haloes as a function of the cosmological model: WMAP1, WMAP3 and WMAP5 results. MNRAS, **391**, 1940–1954.

Maddox, S. J., G. Efstathiou, W. J. Sutherland, & J. Loveday, 1990: The APM galaxy survey. I - APM measurements and star-galaxy separation. MNRAS, **243**, 692–712.

Magliocchetti, M. & C. Porciani, 2003: The halo distribution of 2dF galaxies. MNRAS, **346**, 186–198.

Mandelbaum, R., U. Seljak, R. J. Cool, M. Blanton, C. M. Hirata, & J. Brinkmann, 2006: Density profiles of galaxy groups and clusters from SDSS galaxy-galaxy weak lensing. MNRAS, **372**, 758–776.

Mandelbaum, R., U. Seljak, & C. M. Hirata, 2008: A halo mass – concentration relation from weak lensing. *J. Cosmology Astroparticle Phys.*, **8**, 6–+.

Marzke, R. O., M. J. Geller, L. N. da Costa, & J. P. Huchra, 1995: Pairwise Velocities of Galaxies in the CfA and SSRS2 Redshift Surveys. AJ, **110**, 477–+.

Masjedi, M., D. W. Hogg, & M. R. Blanton, 2008: The Growth of Luminous Red Galaxies by Merging. ApJ, **679**, 260–268.

Masjedi, M., D. W. Hogg, R. J. Cool, D. J. Eisenstein, M. R. Blanton, I. Zehavi, A. A. Berlind, E. F. Bell, D. P. Schneider, M. S. Warren, & J. Brinkmann, 2006: Very Small Scale Clustering and Merger Rate of Luminous Red Galaxies. ApJ, **644**, 54–60.

McBride, C. K., A. J. Connolly, J. P. Gardner, R. Scranton, R. Scoccimarro, A. A. Berlind, F. Marín, & D. P. Schneider, 2011: Three-point Correlation Functions of SDSS Galaxies: Constraining Galaxy-mass Bias. ApJ, **739**, 85.

McConnachie, A. W., S. C. Chapman, R. A. Ibata, A. M. N. Ferguson, M. J. Irwin, G. F. Lewis, N. R. Tanvir, & N. Martin, 2006: The Stellar Halo and Outer Disk of M33. ApJ, **647**, L25–L28.

McGee, S. L. & M. L. Balogh, 2010: Constraints on intragroup stellar mass from hostless Type Ia supernovae. MNRAS, **403**, L79–L83.

Melnick, J., J. Hoessel, & S. D. M. White, 1977: Photoelectric surface photometry of the Coma cluster. MNRAS, **180**, 207–218.

Merritt, D., 1983: Relaxation and tidal stripping in rich clusters of galaxies. I. Evolution of the mass distribution. ApJ, **264**, 24–48.

Mihos, J. C., P. Harding, J. Feldmeier, & H. Morrison, 2005: Diffuse Light in the Virgo Cluster. ApJ, **631**, L41–L44.

Moore, B., S. Ghigna, F. Governato, G. Lake, T. Quinn, J. Stadel, & P. Tozzi, 1999: Dark Matter Substructure within Galactic Halos. ApJ, **524**, L19–L22.

More, S., F. C. van den Bosch, M. Cacciato, H. J. Mo, X. Yang, & R. Li, 2009: Satellite kinematics - II. The halo mass-luminosity relation of central galaxies in SDSS. MNRAS, **392**, 801–816.

Morrison, H. L., 1993: The local density of halo giants. AJ, **106**, 578–590.

Morrison, H. L., M. Mateo, E. W. Olszewski, P. Harding, R. C. Dohm-Palmer, K. C. Freeman, J. E. Norris, & M. Morita, 2000: Mapping the Galactic Halo. I. The "Spaghetti" Survey. AJ, **119**, 2254–2273.

Morrison, H. L., E. D. Miller, P. Harding, D. R. Stinebring, & T. A. Boroson, 1997: Stellar Populations in Edge-On Galaxies From Deep CCD Surface Photometry.II. One-Dimensional FITS of NGC 891. AJ, **113**, 2061–2074.

Moster, B. P., R. S. Somerville, C. Maulbetsch, F. C. van den Bosch, A. V. Macciò, T. Naab, & L. Oser, 2010: Constraints on the Relationship between Stellar Mass and Halo Mass at Low and High Redshift. ApJ, **710**, 903–923.

Murante, G., M. Arnaboldi, O. Gerhard, S. Borgani, L. M. Cheng, A. Diaferio, K. Dolag, L. Moscardini, G. Tormen, L. Tornatore, & P. Tozzi, 2004: The Diffuse Light in Simulations of Galaxy Clusters. ApJ, **607**, L83–L86.

Nagai, D. & A. V. Kravtsov, 2005: The Radial Distribution of Galaxies in Λ Cold Dark Matter Clusters. ApJ, **618**, 557–568.

Navarro, J. F., C. S. Frenk, & S. D. M. White, 1997: A Universal Density Profile from Hierarchical Clustering. ApJ, **490**, 493–+.

Navarro, J. F., A. Ludlow, V. Springel, J. Wang, M. Vogelsberger, S. D. M. White, A. Jenkins, C. S. Frenk, & A. Helmi, 2010: The diversity and similarity of simulated cold dark matter haloes. MNRAS, **402**, 21–34.

Neistein, E., C. Li, S. Khochfar, S. M. Weinmann, F. Shankar, & M. Boylan-Kolchin, 2011: A tale of two populations: the stellar mass of central and satellite galaxies. *ArXiv e-prints*.

Newberg, H. J., B. Yanny, C. Rockosi, E. K. Grebel, H.-W. Rix, J. Brinkmann, I. Csabai, G. Hennessy, R. B. Hindsley, R. Ibata, Z. Ivezić, D. Lamb, E. T. Nash, M. Odenkirchen, H. A. Rave, D. P. Schneider, J. A. Smith, A. Stolte, & D. G. York, 2002: The Ghost of Sagittarius and Lumps in the Halo of the Milky Way. ApJ, **569**, 245–274.

Nierenberg, A. M., M. W. Auger, T. Treu, P. J. Marshall, & C. D. Fassnacht, 2011: Luminous Satellites of Early-type Galaxies. I. Spatial Distribution. ApJ, **731**, 44–+.

Norberg, P., C. M. Baugh, E. Hawkins, S. Maddox, D. Madgwick, O. Lahav, S. Cole, C. S. Frenk, I. Baldry, J. Bland-Hawthorn, T. Bridges, R. Cannon, M. Colless, C. Collins, W. Couch, G. Dalton, R. De Propris, S. P. Driver, G. Efstathiou, R. S. Ellis, K. Glazebrook, C. Jackson, I. Lewis, S. Lumsden, J. A. Peacock, B. A. Peterson, W. Sutherland, & K. Taylor, 2002: The 2dF Galaxy Redshift Survey: the dependence of galaxy clustering on luminosity and spectral type. MNRAS, **332**, 827–838.

Oguri, M. & J. Lee, 2004: A realistic model for spatial and mass distributions of dark halo substructures: An analytic approach. MNRAS, **355**, 120–128.

Ouchi, M., T. Hamana, K. Shimasaku, T. Yamada, M. Akiyama, N. Kashikawa, M. Yoshida, K. Aoki, M. Iye, T. Saito, T. Sasaki, C. Simpson, & M. Yoshida, 2005: Definitive Identification of the Transition between Small- and Large-Scale Clustering for Lyman Break Galaxies. ApJ, **635**, L117–L120.

Peñarrubia, J. & A. J. Benson, 2005: Effects of dynamical evolution on the distribution of substructures. MNRAS, **364**, 977–989.

Peacock, J. A., S. Cole, P. Norberg, C. M. Baugh, J. Bland-Hawthorn, T. Bridges, R. D. Cannon, M. Colless, C. Collins, W. Couch, G. Dalton, K. Deeley, R. De Propris, S. P. Driver, G. Efstathiou, R. S. Ellis, C. S. Frenk, K. Glazebrook, C. Jackson, O. Lahav, I. Lewis, S. Lumsden, S. Maddox, W. J. Percival, B. A. Peterson, I. Price, W. Sutherland, & K. Taylor, 2001: A measurement of the cosmological mass density from clustering in the 2dF Galaxy Redshift Survey. Nature, **410**, 169–173.

Peacock, J. A. & R. E. Smith, 2000: Halo occupation numbers and galaxy bias. MNRAS, **318**, 1144–1156.

Peebles, P. J. E., 1973: Statistical Analysis of Catalogs of Extragalactic Objects. I. Theory. ApJ, **185**, 413–440.

—, 1974: The Nature of the Distribution of Galaxies. A&A, **32**, 197–+.

Peebles, P. J. E. & M. G. Hauser, 1974: Statistical Analysis of Catalogs of Extragalactic Objects. III. The Shane-Wirtanen and Zwicky Catalogs. ApJS, **28**, 19–+.

Percival, W. J., B. A. Reid, D. J. Eisenstein, N. A. Bahcall, T. Budavari, M. Fukugita, J. E. Gunn, Z. Ivezic, G. R. Knapp, R. G. Kron, J. Loveday, R. H. Lupton, T. A. McKay, A. Meiksin, R. C. Nichol, A. C. Pope, D. J. Schlegel, D. P. Schneider, D. N. Spergel, C. Stoughton, M. A. Strauss, A. S. Szalay, M. Tegmark, D. H. Weinberg, D. G. York, & I. Zehavi, 2009: Baryon Acoustic Oscillations in the Sloan Digital Sky Survey Data Release 7 Galaxy Sample. *ArXiv e-prints*.

Perlmutter, S., G. Aldering, P. Nugent, G. Goldhaber, & R. Knop, 1999: Physical and Standard Candle Properties of Type Ia Supernovae from a Large, Homogeneous, Nearby Sample. In *NOAO Proposal ID #1999A-0116*, pp. 116–+.

Pierini, D., S. Zibetti, F. Braglia, H. Böhringer, A. Finoguenov, P. D. Lynam, & Y. Zhang, 2008: Diffuse stellar emission in X-ray luminous galaxy clusters at z ˜ 0.3. I. Is the diffuse optical light boosted and rejuvenated in merging clusters? A&A, **483**, 727–739.

Prada, F., A. A. Klypin, A. J. Cuesta, J. E. Betancort-Rijo, & J. Primack, 2011: Halo concentrations in the standard LCDM cosmology. *ArXiv e-prints*.

Press, W. H. & P. Schechter, 1974: Formation of Galaxies and Clusters of Galaxies by Self-Similar Gravitational Condensation. ApJ, **187**, 425–438.

Purcell, C. W., J. S. Bullock, E. J. Tollerud, M. Rocha, & S. Chakrabarti, 2011: The Sagittarius impact as an architect of spirality and outer rings in the Milky Way. Nature, **477**, 301–303.

Purcell, C. W., J. S. Bullock, & A. R. Zentner, 2007: Shredded Galaxies as the Source of Diffuse Intrahalo Light on Varying Scales. ApJ, **666**, 20–33.

—, 2008: The metallicity of diffuse intrahalo light. MNRAS, **391**, 550–558.

Reed, D., F. Governato, L. Verde, J. Gardner, T. Quinn, J. Stadel, D. Merritt, & G. Lake, 2005: Evolution of the density profiles of dark matter haloes. MNRAS, **357**, 82–96.

Reid, B. A., W. J. Percival, D. J. Eisenstein, L. Verde, D. N. Spergel, R. A. Skibba, N. A. Bahcall, T. Budavari, M. Fukugita, J. R. Gott, J. E. Gunn, Z. Ivezic, G. R. Knapp, R. G. Kron, R. H. Lupton, T. A. McKay, A. Meiksin, R. C. Nichol, A. C. Pope, D. J. Schlegel, D. P. Schneider, M. A. Strauss, C. Stoughton, A. S. Szalay, M. Tegmark, D. H. Weinberg, D. G. York, & I. Zehavi, 2009: Cosmological Constraints from the Clustering of the Sloan Digital Sky Survey DR7 Luminous Red Galaxies. *ArXiv e-prints*.

Riess, A. G., A. V. Filippenko, P. Challis, A. Clocchiatti, A. Diercks, P. M. Garnavich, R. L. Gilliland, C. J. Hogan, S. Jha, R. P. Kirshner, B. Leibundgut, M. M. Phillips, D. Reiss, B. P. Schmidt, R. A. Schommer, R. C. Smith, J. Spyromilio, C. Stubbs, N. B. Suntzeff, & J. Tonry, 1998: Observational Evidence from Supernovae for an Accelerating Universe and a Cosmological Constant. AJ, **116**, 1009–1038.

Robertson, B. E., A. V. Kravtsov, J. Tinker, & A. R. Zentner, 2009: Collapse Barriers and Halo Abundance: Testing the Excursion Set Ansatz. ApJ, **696**, 636–652.

Romano-Díaz, E., I. Shlosman, C. Heller, & Y. Hoffman, 2009: Dissecting Galaxy Formation. I. Comparison Between Pure Dark Matter and Baryonic Models. ApJ, **702**, 1250–1267.

Romano-Díaz, E., I. Shlosman, Y. Hoffman, & C. Heller, 2008: Erasing Dark Matter Cusps in Cosmological Galactic Halos with Baryons. ApJ, **685**, L105–L108.

Ross, A. J., W. J. Percival, & R. J. Brunner, 2010: Evolution of the clustering of photometrically selected SDSS galaxies. MNRAS, **407**, 420–434.

Rudick, C. S., J. C. Mihos, L. H. Frey, & C. K. McBride, 2009: Tidal Streams of Intracluster Light. ApJ, **699**, 1518–1529.

Rudick, C. S., J. C. Mihos, & C. K. McBride, 2011: The Quantity of Intracluster Light: Comparing Theoretical and Observational Measurement Techniques using Simulated Clusters. ApJ, **732**, 48–+.

Ryden, B. S. & J. E. Gunn, 1987: Galaxy formation by gravitational collapse. ApJ, **318**, 15–31.

Sackett, P. D., H. L. Morrisoni, P. Harding, & T. A. Boroson, 1994: A faint luminous halo that may trace the dark matter around spiral galaxy NGC5907. Nature, **370**, 441–443.

Santiago, B. X., M. A. Strauss, O. Lahav, M. Davis, A. Dressler, & J. P. Huchra, 1995: The Optical Redshift Survey: Sample Selection and the Galaxy Distribution. ApJ, **446**, 457–+.

Saunders, W., W. J. Sutherland, S. J. Maddox, O. Keeble, S. J. Oliver, M. Rowan-Robinson, R. G. McMahon, G. P. Efstathiou, H. Tadros, S. D. M. White, C. S. Frenk, A. Carramiñana, & M. R. S. Hawkins, 2000: The PSCz catalogue. MNRAS, **317**, 55–63.

Schulz, A. E., R. Mandelbaum, & N. Padmanabhan, 2010: Testing adiabatic contraction with Sloan Digital Sky Survey elliptical galaxies. MNRAS, **408**, 1463–1475.

Scoccimarro, R., R. K. Sheth, L. Hui, & B. Jain, 2001: How Many Galaxies Fit in a Halo? Constraints on Galaxy Formation Efficiency from Spatial Clustering. ApJ, **546**, 20–34.

Seigar, M. S., A. W. Graham, & H. Jerjen, 2007: Intracluster light and the extended stellar envelopes of cD galaxies: an analytical description. MNRAS, **378**, 1575–1588.

Shectman, S. A., S. D. Landy, A. Oemler, D. L. Tucker, H. Lin, R. P. Kirshner, & P. L. Schechter, 1996: The Las Campanas Redshift Survey. ApJ, **470**, 172–+.

Shen, S., H. J. Mo, S. D. M. White, M. R. Blanton, G. Kauffmann, W. Voges, J. Brinkmann, & I. Csabai, 2003: The size distribution of galaxies in the Sloan Digital Sky Survey. MNRAS, **343**, 978–994.

Sheth, R. K., A. Diaferio, L. Hui, & R. Scoccimarro, 2001: On the streaming motions of haloes and galaxies. MNRAS, **326**, 463–472.

Siegel, M. H., S. R. Majewski, I. N. Reid, & I. B. Thompson, 2002: Star Counts Redivivus. IV. Density Laws through Photometric Parallaxes. ApJ, **578**, 151–175.

Simha, V., D. Weinberg, R. Dave, M. Fardal, N. Katz, & B. D. Oppenheimer, 2010: Testing Subhalo Abundance Matching in Cosmological Smoothed Particle Hydrodynamics Simulations. *ArXiv e-prints*.

Smith, R. E., J. A. Peacock, A. Jenkins, S. D. M. White, C. S. Frenk, F. R. Pearce, P. A. Thomas, G. Efstathiou, & H. M. P. Couchman, 2003: Stable clustering, the halo model and non-linear cosmological power spectra. MNRAS, **341**, 1311–1332.

Somerville, R. S. & T. S. Kolatt, 1999: How to plant a merger tree. MNRAS, **305**, 1–14.

Sommer-Larsen, J., 2006: Properties of intra-group stars and galaxies in galaxy groups: 'normal' versus 'fossil' groups. MNRAS, **369**, 958–968.

Sommer-Larsen, J. & M. Limousin, 2009: Moderate Steepening of Galaxy Cluster Dark Matter Profiles by Baryonic Pinching. *ArXiv e-prints*.

Springel, V., C. S. Frenk, & S. D. M. White, 2006: The large-scale structure of the Universe. Nature, **440**, 1137–1144.

Springel, V., S. D. M. White, A. Jenkins, C. S. Frenk, N. Yoshida, L. Gao, J. Navarro, R. Thacker, D. Croton, J. Helly, J. A. Peacock, S. Cole, P. Thomas, H. Couchman, A. Evrard, J. Colberg, & F. Pearce, 2005: Simulations of the formation, evolution and clustering of galaxies and quasars. Nature, **435**, 629–636.

Stadel, J., D. Potter, B. Moore, J. Diemand, P. Madau, M. Zemp, M. Kuhlen, & V. Quilis, 2009: Quantifying the heart of darkness with GHALO - a multibillion particle simulation of a galactic halo. MNRAS, **398**, L21–L25.

Stewart, K. R., J. S. Bullock, E. J. Barton, & R. H. Wechsler, 2009: Galaxy Mergers and Dark Matter Halo Mergers in ΛCDM: Mass, Redshift, and Mass-Ratio Dependence. ApJ, **702**, 1005–1015.

Strauss, M. A., D. H. Weinberg, R. H. Lupton, V. K. Narayanan, J. Annis, M. Bernardi, M. Blanton, S. Burles, A. J. Connolly, J. Dalcanton, M. Doi, D. Eisenstein, J. A. Frieman, M. Fukugita, J. E. Gunn, Ž. Ivezić, S. Kent, R. S. J. Kim, G. R. Knapp, R. G. Kron, J. A. Munn, H. J. Newberg, R. C. Nichol, S. Okamura, T. R. Quinn, M. W. Richmond, D. J. Schlegel, K. Shimasaku, M. SubbaRao, A. S. Szalay, D. Vanden Berk, M. S. Vogeley, B. Yanny, N. Yasuda, D. G. York, & I. Zehavi, 2002: Spectroscopic Target Selection in the Sloan Digital Sky Survey: The Main Galaxy Sample. AJ, **124**, 1810–1824.

Tasitsiomi, A., A. V. Kravtsov, R. H. Wechsler, & J. R. Primack, 2004: Modeling Galaxy-Mass Correlations in Dissipationless Simulations. ApJ, **614**, 533–546.

Taylor, J. E. & A. Babul, 2004: The evolution of substructure in galaxy, group and cluster haloes - I. Basic dynamics. MNRAS, **348**, 811–830.

—, 2005a: The evolution of substructure in galaxy, group and cluster haloes - II. Global properties. MNRAS, **364**, 515–534.

—, 2005b: The evolution of substructure in galaxy, group and cluster haloes - III. Comparison with simulations. MNRAS, **364**, 535–551.

Tegmark, M., M. A. Strauss, M. R. Blanton, K. Abazajian, S. Dodelson, H. Sandvik, X. Wang, D. H. Weinberg, I. Zehavi, N. A. Bahcall, F. Hoyle, D. Schlegel, R. Scoccimarro, M. S. Vogeley, A. Berlind, T. Budavari, A. Connolly, D. J. Eisenstein, D. Finkbeiner, J. A. Frieman, J. E. Gunn, L. Hui, B. Jain, D. Johnston, S. Kent, H. Lin, R. Nakajima, R. C. Nichol, J. P. Ostriker, A. Pope, R. Scranton, U. Seljak, R. K. Sheth, A. Stebbins, A. S. Szalay, I. Szapudi, Y. Xu, J. Annis, J. Brinkmann, S. Burles, F. J. Castander, I. Csabai, J. Loveday, M. Doi, M. Fukugita, B. Gillespie, G. Hennessy, D. W. Hogg, Ž. Ivezić, G. R. Knapp, D. Q. Lamb, B. C. Lee, R. H. Lupton, T. A. McKay, P. Kunszt, J. A. Munn, L. O'Connell, J. Peoples, J. R. Pier, M. Richmond, C. Rockosi, D. P. Schneider, C. Stoughton, D. L. Tucker, D. E. vanden Berk, B. Yanny, & D. G. York, 2004: Cosmological parameters from SDSS and WMAP. Phys. Rev. D, **69(10)**, 103501–+.

Thuan, T. X. & J. Kormendy, 1977: Photographic measurements of the diffuse light in the Coma cluster. PASP, **89**, 466–473.

Tinker, J., A. V. Kravtsov, A. Klypin, K. Abazajian, M. Warren, G. Yepes, S. Gottlöber, & D. E. Holz, 2008: Toward a Halo Mass Function for Precision Cosmology: The Limits of Universality. ApJ, **688**, 709–728.

Tinker, J. L., 2007: Redshift-space distortions with the halo occupation distribution - II. Analytic model. MNRAS, **374**, 477–492.

Tinker, J. L., D. H. Weinberg, Z. Zheng, & I. Zehavi, 2005: On the Mass-to-Light Ratio of Large-Scale Structure. ApJ, **631**, 41–58.

Tissera, P. B., S. D. M. White, S. Pedrosa, & C. Scannapieco, 2010: Dark matter response to galaxy formation. MNRAS, **406**, 922–935.

Toledo, I., J. Melnick, F. Selman, H. Quintana, E. Giraud, & P. Zelaya, 2011: Diffuse intracluster light at intermediate redshifts: intracluster light observations in an X-ray cluster at z= 0.29. MNRAS, **414**, 602–614.

Totsuji, H. & T. Kihara, 1969: The Correlation Function for the Distribution of Galaxies. PASJ, **21**, 221–+.

Tucker, D. L., A. Oemler, Jr., R. P. Kirshner, H. Lin, S. A. Shectman, S. D. Landy, P. L. Schechter, V. Muller, S. Gottlober, & J. Einasto, 1997: The Las Campanas Redshift Survey galaxy-galaxy autocorrelation function. MNRAS, **285**, L5–L9.

Uson, J. M., S. P. Boughn, & J. R. Kuhn, 1991: Diffuse light in dense clusters of galaxies. I - R-band observations of Abell 2029. ApJ, **369**, 46–53.

Vale, A. & J. P. Ostriker, 2004: Linking halo mass to galaxy luminosity. MNRAS, **353**, 189–200.

—, 2006: The non-parametric model for linking galaxy luminosity with halo/subhalo mass. MNRAS, **371**, 1173–1187.

van den Bosch, F. C., G. Tormen, & C. Giocoli, 2005: The mass function and average mass-loss rate of dark matter subhaloes. MNRAS, **359**, 1029–1040.

van den Bosch, F. C., X. Yang, H. J. Mo, S. M. Weinmann, A. V. Macciò, S. More, M. Cacciato, R. Skibba, & X. Kang, 2007: Towards a concordant model of halo occupation statistics. MNRAS, **376**, 841–860.

Vogelsberger, M., J. Zavala, & A. Loeb, 2012: Subhaloes in Self-Interacting Galactic Dark Matter Haloes. *ArXiv e-prints*.

Wake, D. A., K. E. Whitaker, I. Labbé, P. G. van Dokkum, M. Franx, R. Quadri, G. Brammer, M. Kriek, B. F. Lundgren, D. Marchesini, & A. Muzzin, 2011: Galaxy Clustering in the NEWFIRM Medium Band Survey: The Relationship Between Stellar Mass and Dark Matter Halo Mass at $1 < z < 2$. ApJ, **728**, 46–+.

Wang, L. & Y. P. Jing, 2010: Modelling galaxy stellar mass evolution from z ˜ 0.8 to today. MNRAS, **402**, 1796–1806.

Wang, L., C. Li, G. Kauffmann, & G. De Lucia, 2006: Modelling galaxy clustering in a high-resolution simulation of structure formation. MNRAS, **371**, 537–547.

Warren, M. S., K. Abazajian, D. E. Holz, & L. Teodoro, 2006: Precision Determination of the Mass Function of Dark Matter Halos. ApJ, **646**, 881–885.

Watson, D. F., A. A. Berlind, C. K. McBride, D. W. Hogg, & T. Jiang, 2011a: The Extreme Small Scales: Do Satellite Galaxies Trace Dark Matter? *Submitted to ApJ*.

Watson, D. F., A. A. Berlind, C. K. McBride, & M. Masjedi, 2010: Modeling the Very Small Scale Clustering of Luminous Red Galaxies. ApJ, **709**, 115–119.

Watson, D. F., A. A. Berlind, & A. R. Zentner, 2011b: A Cosmic Coincidence: The Power-law Galaxy Correlation Function. ApJ, **738**, 22–+.

—, 2011c: Constraining Satellite Galaxy Stellar Mass Loss and Predicting Intrahlo Light I: Theoretical Framework and Luminosity Dependence. *Submitted to ApJ*.

Wechsler, R. H., J. S. Bullock, J. R. Primack, A. V. Kravtsov, & A. Dekel, 2002: Concentrations of Dark Halos from Their Assembly Histories. ApJ, **568**, 52–70.

Weil, M. L., J. Bland-Hawthorn, & D. F. Malin, 1997: Diffuse Stellar Light at 100 Kiloparsec Scales in M87. ApJ, **490**, 664–+.

Weinberg, D. H., S. Colombi, R. Davé, & N. Katz, 2008: Baryon Dynamics, Dark Matter Substructure, and Galaxies. ApJ, **678**, 6–21.

Wetterer, C. J. & J. T. McGraw, 1996: RR Lyrae Variable Star Distribution in the Galactic Halo. AJ, **112**, 1046–+.

Wetzel, A. R., J. L. Tinker, & C. Conroy, 2011: Galaxy evolution in groups and clusters: star formation rates, red sequence fractions, and the persistent bimodality. *ArXiv e-prints*.

Wetzel, A. R. & M. White, 2010: What determines satellite galaxy disruption? MNRAS, **403**, 1072–1088.

White, P. M., G. Bothun, M. A. Guerrero, M. J. West, & W. A. Barkhouse, 2003: Extraordinary Diffuse Light in Hickson Compact Group 90. ApJ, **585**, 739–749.

White, S. D. M. & M. J. Rees, 1978: Core condensation in heavy halos - A two-stage theory for galaxy formation and clustering. MNRAS, **183**, 341–358.

Willman, B., F. Governato, J. Wadsley, & T. Quinn, 2004: The origin and properties of intracluster stars in a rich cluster. MNRAS, **355**, 159–168.

Yang, X., H. J. Mo, & F. C. van den Bosch, 2003: Constraining galaxy formation and cosmology with the conditional luminosity function of galaxies. MNRAS, **339**, 1057–1080.

—, 2008: Galaxy Groups in the SDSS DR4. II. Halo Occupation Statistics. ApJ, **676**, 248–261.

Yang, X., H. J. Mo, F. C. van den Bosch, Y. Zhang, & J. Han, 2011: Evolution of the Galaxy - Dark Matter Connection and the Assembly of Galaxies in Dark Matter Halos. *ArXiv e-prints*.

Yanny, B., H. J. Newberg, S. Kent, S. A. Laurent-Muehleisen, J. R. Pier, G. T. Richards, C. Stoughton, J. E. Anderson, Jr., J. Annis, J. Brinkmann, B. Chen, I. Csabai, M. Doi, M. Fukugita, G. S. Hennessy, Ž. Ivezić, G. R. Knapp, R. Lupton, J. A. Munn, T. Nash, C. M. Rockosi, D. P. Schneider, J. A. Smith, & D. G. York, 2000: Identification of A-colored Stars and Structure in the Halo of the Milky Way from Sloan Digital Sky Survey Commissioning Data. ApJ, **540**, 825–841.

York, D. G. et al., 2000: The Sloan Digital Sky Survey: Technical Summary. AJ, **120**, 1579–1587.

Zappacosta, L., D. A. Buote, F. Gastaldello, P. J. Humphrey, J. Bullock, F. Brighenti, & W. Mathews, 2006: The Absence of Adiabatic Contraction of the Radial Dark Matter Profile in the Galaxy Cluster A2589. ApJ, **650**, 777–790.

Zehavi, I., D. J. Eisenstein, R. C. Nichol, M. R. Blanton, D. W. Hogg, J. Brinkmann, J. Loveday, A. Meiksin, D. P. Schneider, & M. Tegmark, 2005a: The Intermediate-Scale Clustering of Luminous Red Galaxies. ApJ, **621**, 22–31.

Zehavi, I., D. H. Weinberg, Z. Zheng, A. A. Berlind, J. A. Frieman, R. Scoccimarro, R. K. Sheth, M. R. Blanton, M. Tegmark, H. J. Mo, N. A. Bahcall, J. Brinkmann, S. Burles, I. Csabai, M. Fukugita, J. E. Gunn, D. Q. Lamb, J. Loveday, R. H. Lupton, A. Meiksin, J. A. Munn, R. C. Nichol, D. Schlegel, D. P. Schneider, M. SubbaRao, A. S. Szalay, A. Uomoto, & D. G. York, 2004: On Departures from a Power Law in the Galaxy Correlation Function. ApJ, **608**, 16–24.

Zehavi, I., Z. Zheng, D. H. Weinberg, M. R. Blanton, N. A. Bahcall, A. A. Berlind, J. Brinkmann, J. A. Frieman, J. E. Gunn, R. H. Lupton, R. C. Nichol, W. J. Percival, D. P. Schneider, R. A. Skibba, M. A. Strauss, M. Tegmark, & D. G. York, 2011: Galaxy Clustering in the Completed SDSS Redshift Survey: The Dependence on Color and Luminosity. ApJ, **736**, 59.

Zehavi, I., Z. Zheng, D. H. Weinberg, J. A. Frieman, A. A. Berlind, M. R. Blanton, R. Scoccimarro, R. K. Sheth, M. A. Strauss, I. Kayo, Y. Suto, M. Fukugita, O. Nakamura, N. A. Bahcall, J. Brinkmann, J. E. Gunn, G. S. Hennessy, Ž. Ivezić, G. R. Knapp, J. Loveday, A. Meiksin, D. J. Schlegel, D. P. Schneider, I. Szapudi, M. Tegmark, M. S. Vogeley, & D. G. York, 2005b: The Luminosity and Color Dependence of the Galaxy Correlation Function. ApJ, **630**, 1–27.

Zehavi, I. et al., 2002: Galaxy Clustering in Early Sloan Digital Sky Survey Redshift Data. ApJ, **571**, 172–190.

Zentner, A. R., 2007: The Excursion Set Theory of Halo Mass Functions, Halo Clustering, and Halo Growth. *International Journal of Modern Physics D*, **16**, 763–815.

Zentner, A. R., A. A. Berlind, J. S. Bullock, A. V. Kravtsov, & R. H. Wechsler, 2005: The Physics of Galaxy Clustering. I. A Model for Subhalo Populations. ApJ, **624**, 505–525.

Zentner, A. R. & J. S. Bullock, 2003: Halo Substructure and the Power Spectrum. ApJ, **598**, 49–72.

Zheng, Z., 2004: Interpreting the Observed Clustering of Red Galaxies at z ˜ 3. ApJ, **610**, 61–68.

Zheng, Z., A. A. Berlind, D. H. Weinberg, A. J. Benson, C. M. Baugh, S. Cole, R. Davé, C. S. Frenk, N. Katz, & C. G. Lacey, 2005: Theoretical Models of the Halo Occupation Distribution: Separating Central and Satellite Galaxies. ApJ, **633**, 791–809.

Zheng, Z., A. L. Coil, & I. Zehavi, 2007: Galaxy Evolution from Halo Occupation Distribution Modeling of DEEP2 and SDSS Galaxy Clustering. ApJ, **667**, 760–779.

Zheng, Z., I. Zehavi, D. J. Eisenstein, D. H. Weinberg, & Y. P. Jing, 2009: Halo Occupation Distribution Modeling of Clustering of Luminous Red Galaxies. ApJ, **707**, 554–572.

Zibetti, S. & A. M. N. Ferguson, 2004: A faint red stellar halo around an edge-on disc galaxy in the Hubble Ultra Deep Field. MNRAS, **352**, L6–L10.

Zibetti, S., S. D. M. White, D. P. Schneider, & J. Brinkmann, 2005: Intergalactic stars in z˜ 0.25 galaxy clusters: systematic properties from stacking of Sloan Digital Sky Survey imaging data. MNRAS, **358**, 949–967.